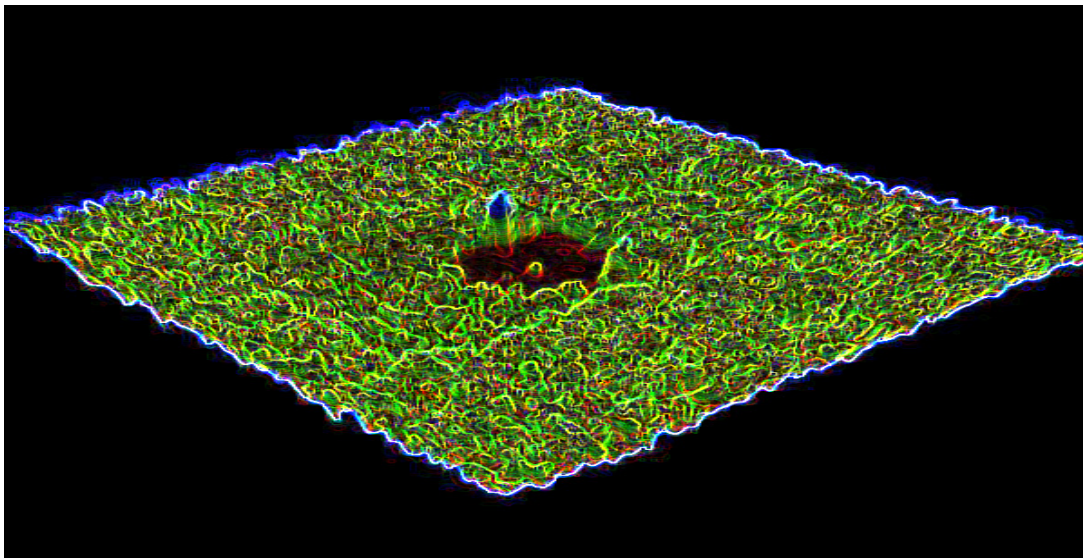


Nanobiotechnology: Tools for Proteomics

–

Molecular Organization and Manipulation of Proteins and Protein Complexes in Nanodimensions



Dissertation

**zur Erlangung des Doktorgrades
der Naturwissenschaften**

vorgelegt beim Fachbereich

Chemische und Pharmazeutische Wissenschaften (FB 14)

der Johann Wolfgang Goethe-Universität am Main

von

Ali Tinazli

aus Bad Homburg v. d. H.

Vom Fachbereich Chemische und Pharmazeutische Wissenschaften (FB 14)
der Johann Wolfgang Goethe-Universität als Dissertation angenommen.

Dekan: Prof. Dr. H. Schwalbe

Gutachter: Prof. Dr. R. Tampé
Prof. Dr. E. Bamberg
Prof. Dr. H.-J. Butt

Prüfungskommission: Prof. Dr. R. Tampé
Prof. Dr. E. Bamberg
Prof. Dr. B. Kolbesen
Prof. Dr. B. Ludwig

Datum des Druckes: 14. Februar 2007

Datum der Disputation: 02. Juli 2007

Note: sehr gut „summa cum laude“

Publications & Patents

1. R. Gamsjäger, B. Wimmer, H. Kahr, **A. Tinazli**, S. Pićurić, S. Lata, R. Tampé, Y. Maulet, H. J. Gruber, P. Hinterdorfer, and C. Romanin, **Oriented binding of the His₆-tagged carboxyl-tail of the L-type Ca²⁺ channel 1-subunit to a new NTA-functionalized self-assembled monolayer.** 2004, *Langmuir*, 20, 5885-5890.
2. S. Hutschenreiter, **A. Tinazli**, K. Model, and R. Tampé, **Two-substrate association with the 20S proteasome at single-molecule level.** 2004, *EMBO J.*, 23, 2488-2497.
3. **A. Tinazli** & R. Tampé, **Small is beautiful – Bioforschung in der Nanowelt.** 2004, *Forschung Frankfurt*, 3-4, 10-14.
4. **A. Tinazli**, J. Tang, R. Valiokas, S. Pićurić, S. Lata, J. Piehler, B. Liedberg, and R. Tampé, **High-affinity chelator thiols for switchable and oriented immobilization of histidine-tagged proteins: a generic platform for protein chip technologies.** 2005, *Chem. Eur. J.*, 11, 5249-5259.
5. G. Klenkar, R. Valiokas, I. Lundström, **A. Tinazli**, R. Tampé, J. Piehler, and B. Liedberg, **Piezo dispensed microarray of multivalent chelating thiols for dissecting complex protein-protein interactions.** 2006, *Anal. Chem.*, 78, 3643-3650.
6. K. Schulze, A. Mulder, **A. Tinazli**, and R. Tampé, **Activity control of the 20S proteasome complex by synthetic gatekeepers.** 2006, *Angew. Chem. Int. Ed. Engl.*, 45, 5702-5205.
7. R. Valiokas, G. Klenkar, **A. Tinazli**, R. Tampé, B. Liedberg, and J. Piehler, **Differential protein assembly on micropatterned surfaces with tailored molecular and surface multivalency.** 2006, *ChemBioChem*, 7, 1325-1329.
8. F. Kienberger, H. Artelsmaier, **A. Tinazli**, C. Rankl, R. Tampé, H. Gruber, P. Hinterdorfer, D. Blaas, **AFM-based nanochip for the detection and characterization of viruses.** 2006, patent No. A961/2006.
9. C. D. Hahn, C. Leitner, T. Weinbrenner, R. Schlapak, **A. Tinazli**, R. Tampé, B. Lackner, C. Steindl, P. Hinterdorfer, H. J. Gruber, and M. Hölzl, **Self-assembled monolayers with latent aldehydes for protein immobilization.** 2007, *Bioconjug. Chem.*, 18, 247-253.
10. C. D. Hahn, **A. Tinazli**, M. Hölzl, C. Leitner, P. J. Winklehner, F. Frederix, B. Lackner, N. Müller, C. Klampfl, F. Kienberger, P. Hinterdorfer, R. Tampé, and H. J. Gruber, **Pragmatic studies on protein-resistant gold surfaces.** 2007, *Chemical Monthly*, 01/2007 online first article.
11. C.Q. Scheckhuber, N. Erjavec, **A. Tinazli**, T. Nyström, and H. D. Osiewacz, **Reducing mitochondrial fission by deleting *Dnm1* increases the health span in two fungal ageing models.** 2007, *Nature Cell Biol.*, 9, 99-105.
12. **A. Tinazli**, J. Piehler, M. Beuttler, R. Guckenberger, and R. Tampé, **Native protein nanolithography that can write, read and erase.** 2007, *Nature Nanotech.*, 2, 220-225.

13. M. Hölzl, **A. Tinazli**, C. Leitner, C. D. Hahn, B. Lackner, R. Tampé, and H. J. Gruber **Protein-resistant SAMs on gold with latent aldehyde functions**. 2007, *Langmuir*, 23, 5571-5577.
14. K. Thelen, T. Wolfram, B. Maier, S. Jährling, **A. Tinazli**, J. Piehler, J. P. Spatz, and G. E. Pollerberg **Cell adhesion molecule DM-GRASP presented in different nanopatterns to neurons regulates attachment and neurite growth**. 2007, *submitted*.
15. F. Kienberger, H. Artelsmair, **A. Tinazli**, R. Schlapak, G. Kada, J. Wruss, C. Rankl, S. Howorka, R. Tampé, D. Blaas, H. Gruber, and P. Hinterdorfer, **Nanochip for the detection and characterization of single virus particles**. 2007, *submitted*.
16. A. Turchanin, **A. Tinazli**, M. El-Desawy, R. Tampé, and A. Götzhäuser, **E-beam nanolithography meets molecular self-assembly and chemical biology – a new route for protein chip fabrication**. 2007, *in preparation*.
17. T. Hoang, **A. Tinazli**, R. Tampé, and M. Karas, **Protein chips for purification and analysis of phosphopeptides by mass spectrometry**. 2007, *in preparation*.
18. **A. Tinazli**, K. Buchholz, A. Kleefen, R. Tampé, and M. Tornow, **SOI nanopored cavities for lipid membrane investigations**. 2007, *in preparation*.

Lectures & Posters

09/2006	Department of Medicine, J. W. Goethe University, Frankfurt am Main, Germany (oral)
08/2006	Faculty of Chemistry, Heinrich Heine University Düsseldorf, Germany (oral)
07/2006	Faculty of Chemistry, Philipps University Marburg, Germany (oral)
06/2006	Fujirebio Inc., Tokyo, Japan (oral)
03/2006	Interdisciplinary Nanoscience Center (iNano), University of Aarhus, Denmark (oral)
02/2006	VIII. Annual Linz Winter Workshop, Linz, Austria (oral)
02/2006	DECHEMA status seminar chip technologies, Frankfurt am Main, Germany (poster)
11/2005	2nd Nanotechnology forum Hesse, Hanau, Germany (poster)
11/2005	Invited speaker at the faculty celebration of the J. W. Goethe University, Frankfurt am Main, Germany (oral)
09/2005	Chemical Nanotechnology Talks VI, Frankfurt am Main, Germany (poster)
09/2005	International Summer School Hirschegg 2005, Austria (oral)
07/2005	Bio-Image Summer School “Visualization, Manipulation and Modeling of Single Biomolecules”, Paris, France (poster)
05/2005	3rd International Workshop to Develop a Global Nanotechnology Network, Saarbrücken, Germany (poster)

05/2005	Bielefeld Institute for BioPhysics and Nanoscience, University of Bielefeld, Germany (oral)
04/2005	Faculty of Biology, Ruhr University Bochum, Germany (oral)
04/2005	NanoBionics III – from Molecules to Applications, Marburg, Germany (poster); <i>Presentation was awarded with the 1st Prize.</i>
02/2005	VII. Annual Linz Winter Workshop, Austria (oral)
11/2004	1st Nanotechnology forum Hesse, Hanau, Germany (poster)
09/2004	International Summer School Hirschegg 2004, Austria (oral)
09/2004	MESA+ Institute for Nanotechnology, University of Twente, The Netherlands (oral)
09/2004	Faculty of Chemistry, Philipps University Marburg, Germany (oral)
02/2004	Applied Biosystems – Applera Deutschland GmbH, Darmstadt, Germany (oral)
10/2003	1st BMBF-Symposium Nanobiotechnology, Hannover, Germany (poster)
09/2003	Scanning Probe Microscopy and Organic Materials XII, Mainz, Germany (oral)
09/2003	International Summer School Hirschegg 2003, Austria (oral)
09/2003	Faculty of Chemistry, Philipps University Marburg, Germany (oral)
02/2003	DECHEMA status seminar chip technologies, Frankfurt am Main, Germany
02/2003	V. Annual Linz Winter Workshop, Austria (poster)
12/2002	Max-Planck-Institute of Biochemistry, Martinsried, Germany (oral)
09/2002	3rd International Symposium on Physics, Chemistry and Biology with Single Molecules, Tutzing, Germany
09/2002	International Summer School Hirschegg 2002, Austria (oral)

Grants

The results of this Ph.D. thesis contributed significantly to successfully approved research grants from the “Bundesministerium für Bildung und Forschung” (BMBF):

- Einschritt-Fabrikation von Biochip Nanotemplaten: Molekulare Gasphasenabscheidung zur Funktionalisierung nanostrukturierter Oberflächen (BMBF)
- MultiplexLAB on NanoChip: Multiplexes elektrisches, mechanisches und optisches Auslesen von biologischen Membranprozessen an Silizium-Nanoporenchips (BMBF)

Acknowledgment

This work was enabled by a fruitful atmosphere at the interface of biology, chemistry, and physics. First of all, I want to thank my “Doktorvater” Prof. Dr. **Robert Tampé** for his continuous challenging, motivation, and teaching of science. He always supported me in the best way and provided me a stimulating scientific environment which gave me the freedom to operate as independent as possible. I also appreciated his special support for one of my favourite music style: Robert always encouraged me to play-back Black Metal (e.g. *Khold*) at Christmas parties and other occasions of public joy.

Special thanks appertain to Prof. Dr. **Jacob Piehler**. He was always open for discussing experimental or conceptual issues. Furthermore, he had this kind of humor which enabled an autocatalytic feedback loop of laughter at different occasions (e.g. “*RNA squirrels*” in Marburg).

Another very important fundament for this Ph.D. was the ability to evaporate gold. Herefore I am very grateful to Prof. Dr. **Ernst Bamberg** and Prof. Dr. **Klaus Fendler** at the Max Planck Institute for Biophysics for providing access to the gold evaporation facility and scientific discussion.

Gold chemistry is not trivial and requires an in-depth expertise on surface chemistry and related aspects. Dr. **Ramūnas Valiokas** and Prof. Dr. **Bo Liedberg** taught me everything, which is essential for successful gold functionalization during a very boosting period at the University of Linköping in Sweden. Beside the scientific aspects of our collaboration I especially appreciated that Ramūnas shared my enthusiasm for South Park (“*Ok, Mr. Mackey?*”).

Another crucial fundament for my Ph.D. work was provided by Dr. **Michael Kappl** and Prof. Dr. **Hans-Jürgen Butt** at the Max Planck Institute for Polymer Research in Mainz. They introduced me into the amazing world of atomic force microscopy and were always available for valuable discussions.

Dr. **Reinhard Guckenberger** (alias “*Guckus*”) and Dipl.-Phys. **Mirjam Beuttler** at the Max Planck Institute for Biochemistry in Martinsried enriched this work from the physical point of view and pedaled with me during a foggy and cold November evening in 2005 to the “*Erdinger Weissbräu*” in Großhadern.

I thank Prof. Dr. **Marc Tornow** and Dr. **Karin Buchholz** at the Walter Schottky Institute of the TU Munich for accessing the wide field of silicon chip fabrication and μ TAS. We learned a lot about fluorescence, biomimetic membranes, and silicon substrates and I am looking forward for the future advances of this challenging project.

One of the best examples for self-organization of scientists was my collaboration with Dr. **Andrey Turchanin** and Prof. Dr. **Armin Götzhäuser** at the University of Bielefeld in “Ost-Westfalen”. Andrey and I decided to try something new with chemical e-beam lithography and multivalent chelators. So, we met occasionally just for fun in Bielefeld, performed experiments, and merged successfully physics with biology.

My longest collaboration was conducted with the Institute of Biophysics in Linz (“*Tu felix Austria*”). Prof. Dr. **Hermann Gruber**, Prof. Dr. **Peter Hinterdorfer**, and Prof. Dr. **Christoph Romanin** enabled a

trustful cooperation with successful and productive scientific exchange. Some of my Austrian cooperation friends kidnapped me once to the Alps and convinced me, that vegetarian food can really be very tasty.

Tribute should be paid to my practical and diploma students. **Srdjan Pićurić** was the first one and we initiated together the “King Midas Chip” project at the very early stage of my Ph.D. Despite the challenging situation of becoming experts in a totally new field without knowing anything (“*Work harder, faster, longer!*”) we really had a lot of fun (“*Somehow!*”). Together with **Tatjana Hofmann**, we established chemical force microscopy in our lab – 4 weeks were enough for the first successful AFM scan (18th September 2003) and a bottle of champagne sponsored by Robert. **Alexander Kleefen** shared not only my ardor for South Park (“*Everyone & everything is marclar on Marclar and their marclar is not our marclar!*”), but he also contributed with really very good science! **Andrea Mädler** and **Heike Staudt** supported me in frame of a practical course during characterization of our new SPR chips with very low unspecific binding and “*Nicht-Lustig*” Cartoons.

Gerhard Spatz-Kümbel is a real Hesse guy (“*Offebäscher!*”) and a great man! He provided me chemical materials and joyful lunch conversations. **Christine Le Gal** supported me always in administrative tasks. Furthermore, I could share with her some kind of French humor (“*Y voit rien*” vs. “*Ivoirien*”). I am grateful to Dr. **Jilin Tang** for her continuous commitment during her post-doc period and the kind introduction to Chinese culture and way of life (“Do never cry, even if a knife is stabbed into your stomach!”). Dr. **Alart Mulder** is not only an amazing Dutch surface chemist who opened good discussions, he also was quite susceptible to my special sense of humor (*remember the belt in Austria and the RNA squirrels in Marburg!*). Dr. **Silke Hutschenreiter**, Dipl.-Chem. **Katrin Schulze** and Dipl.-Ing. **Annett Reichel** were great “Doktorschwestern”. Katrin had a very good sense for “normal behavior” (“*Nein, Ali, tu das nicht!*”). In addition they shared their precious proteins with me. Dr. **Joachim Koch** and Dr. **Rupert Abele** were some kind of “Großer Bruder” for me and really supportive in every issue. However, I videotaped Joachim once and he is a great actor (“*Hallo Muddi!*”). Rupert brought to me this kind of German dialect, which I can use very well in my new hometown Überlingen in Baden-Württemberg (“*Wir können alles, ausser Hochdeutsch!*”). Dr. **Martynas Gavutis** was the other crazy guy beside me, who spent his Saturday nights in the lab. However, we enjoyed always our “*midnight conversations*” about “*cultural activities*”. Dr. **Suman Lata**, the freezing entity, ate up always my tasty *Chicken Biryani* and compensated these actions with a very beautiful Indian saying: “*Knowledge is the only thing, which adds to, when you share it.*”

The most important persons in my life were my mother and father **Nursen** and **Ismail Tinazli**. They supported me always at any level and taught me to think in a differentiated manner. The mistress of MS Word **Sevda Özalp** entered my life in a rainy day in 2002 and is my sunshine since this moment. After a few years of deep friendship, she decided to become Sevda Tinazli (9th December 2005) and is my partner in wisdom (“*Siehe Tibet-Ausstellung in der Villa Hügel.*”). Together we explored the “*Ruhrpott*” and I am very grateful for her never-ending patience, especially, when I spent the weekend in the lab.

*Die Wissenschaft ist nichts Abstraktes, sondern als Produkt menschlicher Arbeit
auch in ihrem Werdegang eng verknüpft mit der Eigenart und dem Schicksal
der Menschen, die sich ihr widmen.*

EMIL FISCHER

0 Table of Contents

Handle stets so, daß die Anzahl der Wahlmöglichkeiten größer wird!

HEINZ VON FÖRSTER

0	Table of Contents	10
1	Introduction: Biology meets Nanotechnology	14
1.1	From Genomics to Proteomics.....	14
1.2	Concepts of Protein Immobilization	15
1.3	Surface Design of Protein Chips	17
1.3.1	Lipid Bilayers.....	18
1.3.2	Self-Assembled Monolayers	20
1.3.3	Functionalized Glass Substrates.....	23
1.4	Nanotechnology	24
1.5	Fabrication of Protein Arrays with Lithographic Techniques	28
1.5.1	Microcontact Printing	29
1.5.2	E-Beam Nanolithography	31
1.5.3	Scanning Probe-related Nanolithography	32
1.6	Aim of the Ph.D. Thesis.....	34
1.6.1	Surface Architecture and Chemistry for a Generic Protein Chip Platform.....	35
1.6.2	A Novel Lithographic Technology for Fabrication of Protein Nanoarrays	35
1.6.3	Parallel Array Generation by Chemical E-Beam Nanolithography.....	35
1.6.4	Microcavities for Organization of Membrane Proteins	36
2	Theoretical Background of Methodologies	37
2.1	Atomic Force Microscopy	37
2.2	Confocal Laser Scanning Microscopy	39
2.3	Surface Plasmon Resonance	41
2.4	Surface Sensitive Analytics	44
2.4.1	Contact Angle Goniometry	44
2.4.2	Ellipsometry	45

2.4.3	Infrared Reflection-Absorption Spectroscopy	45
2.4.4	X-Ray Photoelectron Spectroscopy	46
2.5	MALDI Mass Spectrometry.....	46
3	Materials.....	49
3.1	Chemicals.....	49
3.2	Buffers and Solutions.....	50
3.2.1	Cell Culture	50
3.2.2	Chromatography.....	50
3.2.3	Protein Immobilization	51
3.3	Media	51
3.3.1	LB Medium.....	51
3.3.2	Agarose Plates.....	51
3.4	Plasmids and Strains	51
3.4.1	pRSET5a and 6a.....	51
3.4.2	<i>E. coli</i> BL21(DE3).....	52
3.5	Equipment.....	52
3.5.1	General Equipment	52
3.5.2	Centrifuges and Rotors.....	53
3.5.3	Columns	53
3.5.4	Supplementary Materials	53
4	Methods.....	54
4.1	Biological Methods.....	54
4.1.1	Transformation.....	54
4.1.2	Cryostocks.....	54
4.1.3	Cell Culture	54
4.2	Biochemical Methods	55
4.2.1	Purification of His-tagged Proteasomes.....	55
4.2.2	Vesicle Preparation and Formation of Biomimetic Lipid Bilayers.....	56
4.2.3	Protein Immobilization	57

4.3	Biophysical Methods.....	57
4.3.1	Atomic Force Microscopy	57
4.3.2	Chemical Force Microscopy	58
4.3.3	Surface Plasmon Resonance	58
4.3.4	Confocal Laser Scanning Fluorescence Microscopy	58
4.4	Surface Chemical Methods	59
4.4.1	Fabrication of Gold Chips.....	59
4.4.2	Surface Functionalization of Gold Chips.....	60
4.4.3	Microcontact Printing	60
4.4.4	Coupling of tris-NTA Modules to Amino Biphenyl SAMs.....	60
4.5	Surface Physical Methods.....	61
4.5.1	Contact Angle Goniometry	61
4.5.2	Ellipsometry	61
4.5.3	Infrared Reflection-Absorption Spectroscopy	61
4.5.4	X-Ray Photoelectron Spectroscopy	61
5	Results & Discussion	63
5.1	Development of a Generic Platform for Protein Chip Technologies.....	63
5.1.1	Synthesis of Multivalent Chelator Thiols	63
5.1.2	Formation of Self-Assembled Monolayers with Multivalent Chelator Thiols	64
5.1.3	Switchability of His-tag Recognition.....	68
5.1.4	Protein Immobilization Proofing Specificity, Activity, and Reversibility.....	69
5.1.5	Patterned Protein Arrays on Multivalent Chelator SAMs	73
5.1.6	Purification on a Chip – One-step Enrichment and Analysis	74
5.1.7	Uniform Orientation of Protein Complexes Monitored at Single-Molecule Level ...	76
5.1.8	Conclusions.....	78
5.2	Write, Read and Erase – Native Protein Nanolithography	79
5.2.1	Concept of Native Protein Nanolithography.....	79
5.2.2	Reversible Patterning of Protein Monolayers by Contact Oscillation Mode.....	79
5.2.3	Control of the Orientation of Protein Complexes on Rewritable Protein Chips.....	82

5.2.4	Bioactive Protein Nanoarrays down to 50 nm	84
5.2.5	Conclusions	86
5.3	High-Affinity Protein Chip Fabrication by Chemical E-Beam Nanolithography	87
5.3.1	Coupling of Multivalent Chelators to Biphenyl SAMs	87
5.3.2	Surface Physical Monitoring and Characterization of Multivalent Chelator Biphenyl SAMs	89
5.3.3	Protein Capturing on E-Beam-modified Biochips followed <i>in situ</i>	90
5.3.4	Conclusions	91
5.4	Nanostructured Silicon Chips for Analysis of Membrane Protein Function at Single Molecule Level	92
5.4.1	The Microcavity Concept	92
5.4.2	Membrane Formation on Silicon Substrates	93
5.4.3	FRAP-based Verification of Lipid Bilayer Formation	94
5.4.4	Dual-Color Studies on Membrane Formation at Microcavities	96
5.4.5	Membranes Formation at Microcavities of Optimized SOI Chips	98
5.4.6	Immobilization of His-tagged Proteins on Chelator Lipid Membranes	99
5.4.7	Conclusions	100
6	Summary, Conclusions & Perspectives	103
6.1	English Version	103
6.2	German Version – Ausführliche Zusammenfassung	105
7	Synopsis of Collaborations	110
8	References	111
9	Curriculum Vitae	123

1 Introduction: Biology meets Nanotechnology

*Und es ist das ewig Eine,
das sich vielfach offenbart:
klein das Große, groß das Kleine,
alles nach der eignen Art;
immer wechselnd, fest sich haltend,
nah und fern und fern und nah,
so gestaltend, umgestaltend –
Zum Erstaunen bin ich da.*

JOHANN WOLFGANG GOETHE

*Der Körper eines Einhorns ist völlig frei von Gift
und stößt alles Giftige ab. Wenn man eine lebende
Spinne in einen Ring setzt, der von einem Hautstreifen
des Einhorns gebildet wird, dann kommt die Spinne
nicht aus diesem Kreis heraus. Wenn dieser Ring aber
aus irgendeinem giftigen Stoff gebildet wird, kann die
Spinne die Linie ohne Schwierigkeiten überschreiten,
denn sie entspricht ihrer eigenen Natur.*

BASILIVS VALENTINUS

(Curreus Triumphalis Antimonii, Ed. J. THÖLDE, 1604)

1.1 From Genomics to Proteomics

Unravelling of the human genome at the beginning of this millennium^{1, 2} provided both, access to a huge “biological database” and the realization that genetic information solely is not sufficient for a complete comprehension of biological processes and applications in molecular medicine³. The study of the innumerable products of the estimated 20,000-25,000 human genes⁴ will determine research in life sciences for the next 20 years and launched the post-genomic era. After decades of dominion of molecular genetics the necessity to perform a campaign of dimensions similar to the “human genome project” (HUGO)⁵ but at protein level became obvious. Hence, proteomics superseded genomics and projects as “human proteome analysis” (HUPO) were initiated a few years ago⁶. Systematic approaches to explore the plethora of protein-protein interactions and myriads of dynamic protein networks are at the forefront of biological sciences now.

Many applications in medicine, environmental analysis, and the chemical industry require sensitive methods for sensing small organic molecules. Our sense of smell and taste are designed to perform exactly this task, and the immune system recognizes millions of different molecules. Recognition of small molecules is a specialty of biomolecules, so they provide an attractive approach to the creation of specific sensors. Two components are needed: the recognition element and some mechanism for read-out once the recognition element has found its target. Often, the recognition element may be taken unchanged from the biological source. The challenge is to design a suitable interface to a macroscale read-out device⁷.

Multiplexed, highly parallel biosensor and protein chip technologies deliver promising tools for this challenge even down to single molecule detection⁸⁻¹². Thus there is strong interest in targeting functional biomolecules at controlled positions on surfaces to produce biological arrays for analysis. Key advantages of nanoarray assays are the extremely small amounts of material and short diffusion times required¹³. Various sophisticated technologies were applied for creation of micro- and nanometer-sized molecular patterns in order to organize proteins. Current state-of-the-

art strategies of protein capturing, surface architectures for protein chips, and nanolithographic techniques will be discussed in the next chapters.

1.2 Concepts of Protein Immobilization

Solid-phase-based assays are becoming more and more important in functional proteomics and medical diagnostics. An often underestimated key problem, however, is the immobilization of proteins on solid substrates, while maintaining their function. Whereas DNA molecules are exceptional robust and easy to immobilize in a functional manner – as seen in the triumph of DNA chip technology^{14, 15} – proteins are highly sensitive and chemical heterogeneous entities, and denature rapidly *in vitro* (e.g. at solid interfaces, a process which is hardly understood). Nevertheless, solid-phase chip technologies require the immobilization of proteins in their native states. Structure and function of the protein should not be distressed by the immobilization process. Biological studies often require uniformly oriented immobilization of proteins. Simple physisorption is usually unspecific and will result mostly in the unfolding and inactivation of proteins. Covalent binding of the protein to a reactive surface through surface-accessible residues often lacks regiospecificity and hence correct orientation of the immobilized protein. Such standard protein coupling strategies are depicted in Table 1. Additionally, the reactive site of a protein can be blocked by the immobilization procedure, resulting in reduced activity of the protein¹⁶.

Table 1: Various methods of coupling proteins to chip surfaces.

Functional side group on peptide	Available surface functionalization	Type of binding
-COOH	Amine	electrostatic covalent amide (after activation)
-NH ₂	carboxylic acid, active ester	electrostatic covalent amide
-SH	Maleimide	covalent thioether
-OH	Epoxy	covalent ether

To circumvent these problems, surface capture agents, modified with a tag for specific interaction with the surface, can be used to immobilize proteins. This strategy is based on the established capture agent/fusion protein pairs that have been developed for purification in affinity chromatography. Many fusion proteins with popular tags – such as glutathione S-transferase¹⁷⁻¹⁹,

maltose-binding protein^{20, 21}, the FLAG peptide^{22, 23}, and the well known oligohistidine²⁴⁻²⁷ – are available, whilst other techniques for selective and covalent immobilization of fusion proteins have been reported recently²⁸⁻³⁰. These approaches have the common feature that the protein of interest is fused to a protein trapped irreversibly by its pseudosubstrate (suicide substrate) on the chip surface. Immobilization by metal ion complexation (IMIC) was first introduced as a protocol for protein separation via metal chelate affinity chromatography (IMAC)³¹. This method is based on the non-covalent binding of a biomolecule by complex formation with metal ions, which are immobilized by chelators like iminodiacetic acid (IDA) or *N*-nitrilotriacetic acid (NTA). Over the last decade, the *N*-nitrilotriacetic acid (NTA)/His₆-tag chelator system³² has become a powerful and universal tool for the one-step isolation and purification of gene products^{26, 33}. The principle and reversible nature of this interaction pair is illustrated in Figure 1.

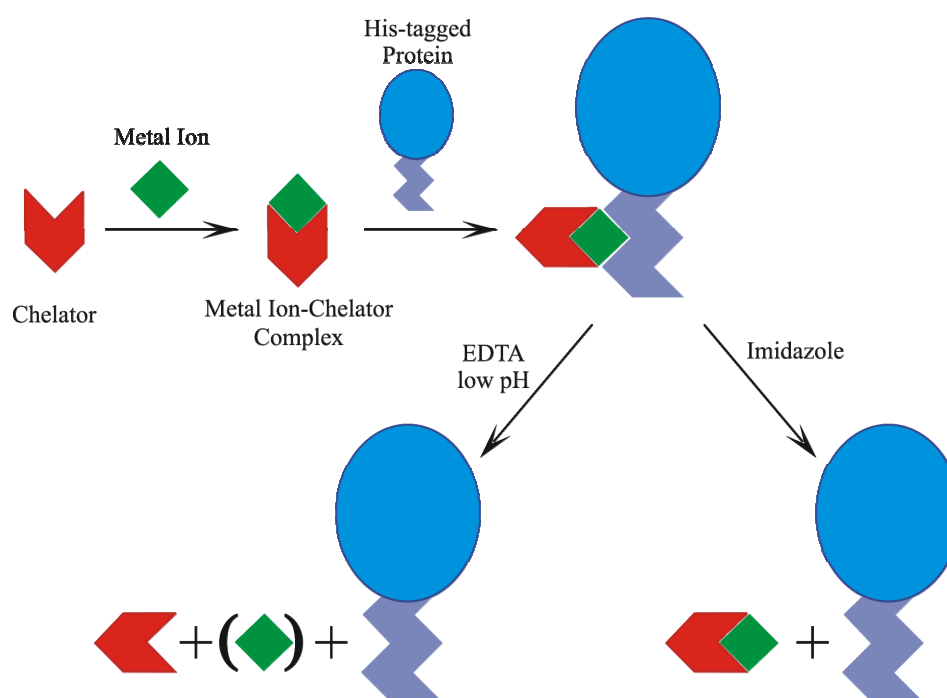


Figure 1: Concept of immobilization by metal ion complexation (IMIC). Addition of divalent metal ions induces the formation of a metal–chelator complex. His-tagged fusion proteins bind to the metal complex and can be removed either by EDTA, imidazole or low pH.

The small and flexible His-tag does usually not impair the functionality of proteins. Additionally, dissociation of the reversible binding can be induced at low pH or by addition of imidazole or EDTA. While such affinity capturing is suitable for protein purification, applications requiring long-term stability on geometrically defined surfaces such as protein arrays and biosensors have been compromised by problems with metal leaching and rapid protein dissociation^{34, 35}. The

chelator lipid concept with NTA-functionalized lipids^{36, 37} gave insights into functional aspects of immobilized proteins³⁸⁻⁴⁰. Evidence for multivalent interactions between the His₆-tag and the NTA groups was found in experiments involving immobilization of His₆-tagged proteins on lipid membranes with chelators at different surface concentrations^{38, 39}. Further, it was concluded that stable binding of His₆-tagged proteins takes place at a specific surface concentration threshold value of NTA lipid. Cumulated NTA clusters with multivalent interaction sites to His₆-tags may thus overcome the limitation of protein dissociation in the conventional NTA/His₆-tag interaction.

Multivalency describes the interactions that take place between a multivalent host and a multivalent guest. The most simple situation occurs when a divalent guest and a divalent host interact to form a 1:1 complex. Multivalent systems are characterized by an intramolecular assembly step following an initial, intermolecular binding event. This makes such systems distinctly different, both thermodynamically and kinetically, from monovalent (between two monovalent entities) and multiply monovalent (between a multivalent and multiple monovalent entities, e.g. binding of oxygen by hemoglobin) systems which lack such intramolecular steps.

An ideal protein chip possesses docking sites that interact stably, specifically, and stoichiometrically (1:1) with proteins. The immobilized proteins should be uniformly oriented, while preserving their function. Furthermore, proteins should be detachable under mild conditions, allowing further analyses and regeneration of the chip. Especially in the case of protein nanoarrays – with only a few immobilized protein individuals on each array spot – as much biofunctionality as possible has to be retained. Hence, only with such an ideal chip architecture bioactive nanoarrays can be employed with optimal performance.

1.3 Surface Design of Protein Chips

In biochip technologies the surface is a transducer between the biomolecules and the analytical device. It is in principle comprised of the solid support (transducer) and the interfacial layer, where the immobilization is performed. In rare cases, the proteins are attached directly onto the support. Usually, for the sake of protein functionality, the surface has to be chemically modified for mimicking a natural environment. The only natural interfaces, which encounter proteins, are lipid bilayers. Hence, they are ideal candidates for the design of artificial, biomimetic interfaces in protein chip technologies.

In 1915 Wolfgang OSTWALD described the subject matter of colloid and surface science as a “world of neglected dimensions.” The reason for such a description stemmed from the unique nature of interfaces and related colloidal phenomena – they could not be readily interpreted based on “classical” atomic or solution theories, and the regions of space involved were beyond the reach of existent experimental techniques. Science has since taken a firm theoretical and experimental hold on the nature of matter at its two extremes: at the molecular, atomic, and subatomic levels, and in the area of bulk materials, including their physical strengths and weaknesses and their chemical and electrical properties. Legions of chemists, physicists, materials scientists, engineers, and others are continuously striving to improve on that knowledge in academic and industrial laboratories around the world. Between those two extremes still lies the world referred to by OSTWALD, and even with the latest advanced techniques for studying the region between phases, a great many mysteries remain to be solved. For that reason, the study of interfaces and colloids can be regarded as entering

the “twilight zone.” That “region” of the physical world represents a bridge not only between chemical and physical phases, but also plays a vital but often unrecognized role in other areas of chemistry, physics, biology, medicine, engineering, and other disciplines⁴¹.

1.3.1 Lipid Bilayers

The cell membrane is the biological interface *per se* and composed of two layers of lipids. Most lipids consist of a hydrophilic headgroup and two hydrophobic tails. A schematic illustration of a cell membrane according to SINGER & NICOLSON^{42, 43} is given in Figure 2. The lipids form a bilayer with a thickness of 3-5 nm, where the headgroups are pointing outward to the aqueous environment and the hydrophobic tails point to each other. Membrane proteins are either incorporated directly into the bilayer or are tethered via long alkyl chains (e.g. farnesyl, geranyl, palmityl, myristyl moieties) or phospholipids as in the case of phosphatidyl inositol-anchored proteins (e.g. DAF). The lipids inside each layer are highly ordered, but have a high lateral mobility. The lateral diffusion coefficient of lipid molecules is in the range of $10^{-12} \text{ m}^2\text{s}^{-1}$, i.e. one lipid molecules passes 2 μm in one second⁴⁴. Therefore the bilayer is sometimes referred to as a two-dimensional liquid crystal.

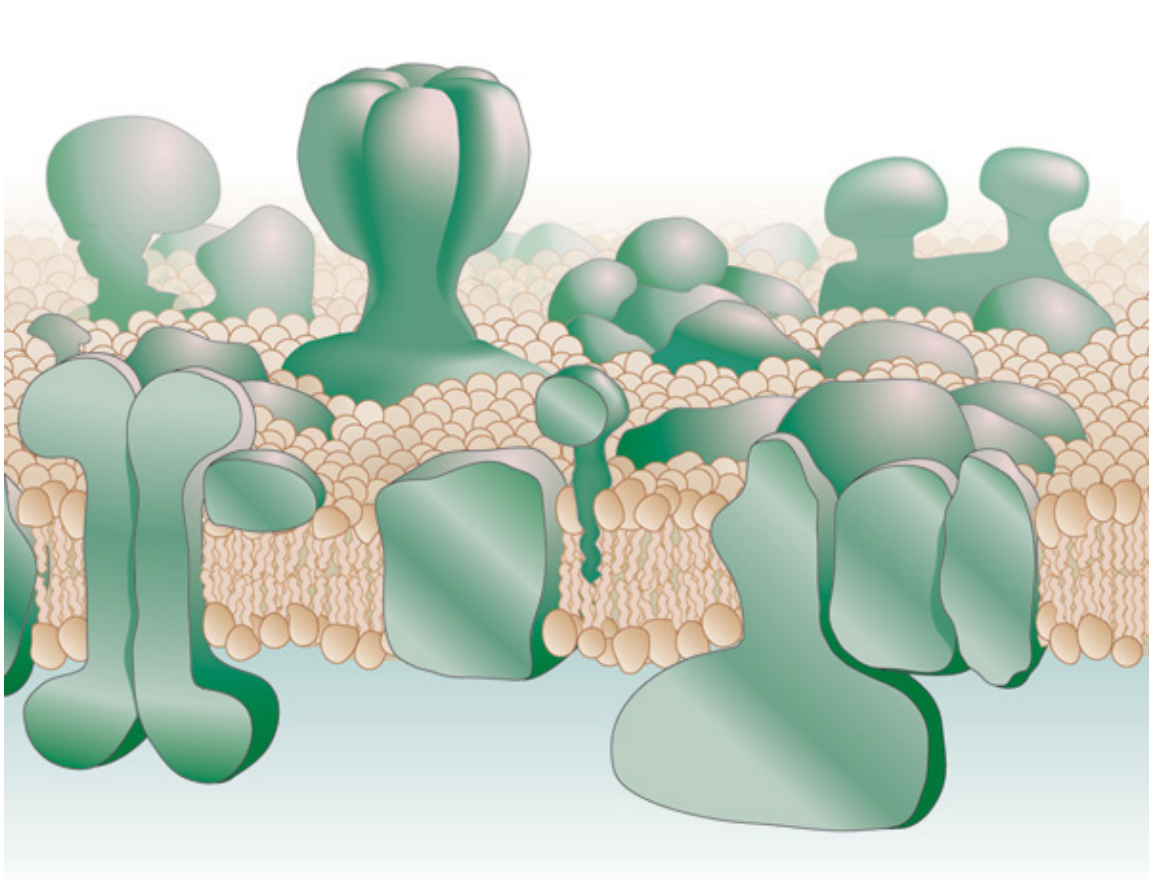


Figure 2: An amended and updated version of the SINGER–NICOLSON 'fluid mosaic model'. Adapted from ^{42, 43}.

A large variety of proteins are incorporated into a lipid bilayer in its natural form. Therefore it is difficult to examine a single type of transmembrane proteins (e.g. ion channels like gramicidin⁴⁵, ABC transporters⁴⁶ or the photosynthetic machinery⁴⁷) in a membrane which is extracted from a cell. For investigations of the transmembrane transport of ions or peptides, it is necessary to have access to both sides of a membrane. This has been accomplished by the patch-clamp technique, which has been introduced by NEHER and SAKMANN⁴⁸. With this technique the inner part of the cell is contacted by a minute glass pipette, which is poked through the membrane. By this the inside can be electrically connected, and the chemical milieu inside the cell can be controlled. By the use of planar patch clamp on chip techniques even whole cells can be studied⁴⁹.

Artificial, biomimetic membranes, with only one or a few selected types of proteins incorporated, are of extremely high interest for both, basic research in biochemistry/biophysics and biotechnological applications (e.g. biosensors). Generation of biomimetic planar lipid bilayers were first reported on painted bilayers by MUELLER in 1962⁵⁰. The artificial membranes are either applied on a solid support or spanned over an aperture. Here, the most problematic issue to be considered is denaturation of the integral proteins if they get in direct contact with the solid support. Many different approaches have been made to prevent this scenario such as supporting the membranes by soft matters as agarose⁵¹, polymer supports⁵², or polymer anchors⁵³. The spanning of artificial membranes over apertures (e.g. of porous materials) of different sizes ranging from 50 nm⁵⁴ to several hundred micrometers⁵⁵⁻⁶⁰ has been shown. The advantage of freely suspended lipid bilayers is the bilateral immersion into the liquid – a scenario which mimicks the natural environment of membrane proteins. Furthermore, both sides can be accessed for fluid exchange and electrical measurement such as ionic currents⁶¹, gating⁶², or combined optical measurement^{63, 64}. Mostly black lipid membranes (BLM)^{65, 66} are used to span apertures⁶⁷ or porous substrates⁵⁶. These membranes were termed according to their black appearance due to interference effects⁶⁵. The lipids are dissolved in a nonpolar solvent and literally painted over the aperture. The disadvantage of BLMs is their instability, as well as the presence of residual solvents which can functionally impair or even denature proteins.

Because of their long hydrocarbon tails, lipids are highly insoluble in water. Self-organization is driven, as in protein folding, by the need to shelter these carbon-rich tails from water. Each lipid has a distinctive *critical micelle concentration*. When placed in water at concentrations greater than the critical concentration, lipids associate to shield the hydrophobic segments from water. The critical concentration is very low and is lower for lipids with longer carbon chains. The shapes of the individual lipid molecules determine the form of the self-organized aggregate. Cylindrical molecules, such as the abundant phospholipids used in cells, form extended lipid bilayers.

Self-organization is a perfect method for creating structures that are flexible, resilient, and self-repairing. Self-organized systems lack the control that is available with self-assembly, but that very lack of defined structures is what is needed in some applications. In natural systems, self-organization is used primarily to create lipid

membranes. In current nanobiotechnology, a number of self-organized forms of lipids and lipid-like molecules are being explored to create novel infrastructures and to create delivery vehicles for nanomedicine⁷.

The most natural way to apply a membrane onto a solid support is probably the vesicle fusion (e.g. in analogy to fusion processes of synaptic vesicles) which was pioneered by MCCONNELL in 1986⁶⁸. Spreading of 25 nm small unilamellar vesicles (SUV) was reported first by BARENHOLZ and colleagues in 1977⁶⁹. Multilamellar vesicles are formed in a suspension of the amphiphilic lipids in a polar solvent, like aqueous buffers. SUVs can be generated from these multilamellar vesicles by sonication and have a diameter of less than 200 nm. As soon as these vesicles come into contact with a solid surface they form a patch of bilayer on the surface. At sufficient amounts of vesicles, a complete membrane bilayer is formed in a self-healing process. Lipid bilayers formed by fusion of SUVs on silicon substrates can be patterned by photolithographic techniques, pre-patterned templates or even electric fields⁷⁰⁻⁷⁹. Membrane proteins can be incorporated either into vesicles before fusion – or proteins are added (e.g. in small vesicles) and incorporated into the bilayer subsequently⁸⁰.

1.3.2 Self-Assembled Monolayers

Self-assembled monolayers (SAMs) are the most widely studied and best developed examples of nonbiological, self-assembling systems^{81, 82}. William ZISMAN is often credited by originating the SAM concept in his 1946 paper⁸³. SAMs are organic assemblies formed by the adsorption of molecular constituents from solution or the gas phase to the surface of solids or in regular arrays on the surface of liquids (in the case of mercury and probably other liquid metals and alloys). The adsorbates organize spontaneously (and sometimes epitaxially) into crystalline (or semicrystalline) structures. SAMs provide a convenient, flexible, and simple system to tailor the interfacial properties of metals, metal oxides, and semiconductors for technological applications.

The molecules or ligands that are able to form SAMs have a chemical functionality, or “headgroup”, with a specific affinity for a substrate; in many cases, the headgroup also has a high affinity for the surface and displaces adsorbed adventitious organic materials from the surface. There are a number of headgroups that bind to specific metals, metal oxides, and semiconductors. However, the most extensively studied and best characterized class of SAMs is derived from the adsorption of alkanethiols on gold⁸⁴⁻⁸⁸ (Figure 3).

Self-assembly is the spontaneous organization of molecules or objects into stable, well-defined structures by noncovalent forces⁸⁹. The key idea in self-assembly is that the final structure is close to or at thermodynamic equilibrium; it therefore tends to form spontaneously and to reject defects. Self-assembly often provides routes to structures having greater order than can be reached in non-self-assembling structures. The final structure is predetermined by the characteristics of the initial subunits: The information that determines the final structure is coded in the structures and properties of the subunits (e.g. shapes and surface functionalities). Self-assembly is ubiquitous in nature⁹⁰: Processes such as folding of proteins and RNAs as well as formation of the DNA

double helix serve as biological illustrations of the potential of self-assembly in microfabrication. Various strategies of self-assembly have been developed and employed to fabricate two- and three-dimensional structures with dimensions ranging from molecular, through mesoscopic, to macroscopic sizes⁹¹⁻⁹⁴.

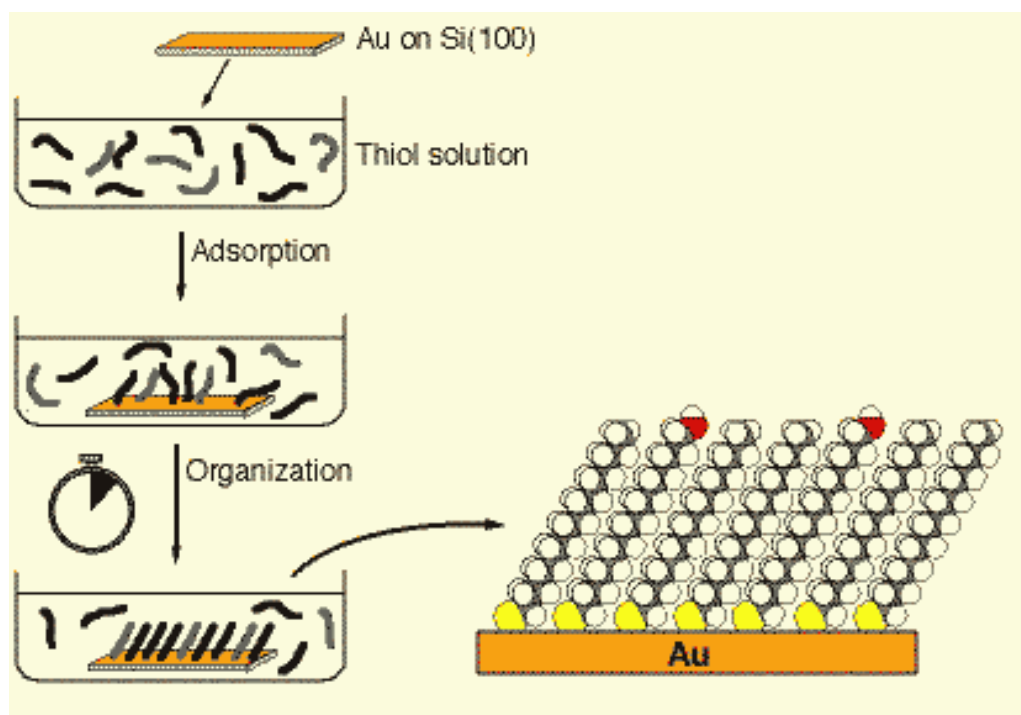


Figure 3: Self-assembly of alkyl thiols on gold substrates. Adapted from ⁹⁵.

Two characteristics of SAMs of alkanethiolates on gold distinguish them from organic assemblies composed from amphiphiles, e.g. fatty acids, on metal oxides. First, thiols build up single highly organized layers at the surface *reproducibly*; and second, ω -functionalized alkanethiols (XC_nSH , where X is $-\text{CH}_3$, $-\text{COOH}$, $-\text{PO}_3^{2-}$, $-\text{OH}$, etc.) form monolayers having the terminal group, X, exposed. Molecular assemblies consisting of fatty acids always minimize the surface energy by building a hydrocarbon-terminated surface, whereas the strong affinity of the thiol group (a “soft” ligand) for gold often makes it possible to form well-defined interfaces that present a wide range of structures, including ones that were polar, electroactive, or biologically relevant⁹⁶. Alkyl thiols chemisorb spontaneously on a gold surface and form adsorbed alkanethiolates $\text{CH}_3(\text{CH}_2)_n\text{S}^-$. Only very small quantities of organic materials are needed to form a SAM ($\sim 10^{14}$ molecules, or ~ 1 nanomole, covers 1 cm^2 of surface). This ensures a broad applicability of this technology, as it can be used with ligands that are scarce, precious, or difficult to synthesize.

The formation of ordered SAMs is a relatively fast process: Highly ordered SAMs of hexadecanethiolate on gold can be prepared by immersing a gold substrate into a solution of

hexadecanethiol in ethanol (1 mM) for several minutes, and formation of SAMs during microcontact printing (c.f.) may occur even in seconds. The ability to form ordered structures rapidly is one of the factors that ultimately determine the success of microcontact printing. This process is assumed to occur with the loss of dihydrogen; the fate of the hydrogen atom is still not established⁸⁵. The product that is formed is probably best understood as a gold(I) thiolate (RSAu) adsorbed on metallic gold [Au(0)]. The C_nS-Au bond is predominantly covalent, and has little polar character. Sulphur atoms bonded to the gold surface bring the alkyl chains into close contact; these contacts freeze out and configurational entropy leads to an ordered structure. For carbon chains of up to approximately 20 atoms, the degree of interaction in a SAM increases with the density of molecules on the surface and the length of the alkyl backbones. Only alkanethiolates with $n > 11$ form the closely packed and essentially two-dimensional organic quasi-crystals supported on gold that characterize this kind of SAMs most useful in surface science and nanotechnology⁹⁷.

The structures and properties of SAMs from alkanethiolates on gold have been examined using a number of surface sensitive techniques⁸². It is generally accepted that sulphur atoms form a $(\sqrt{3} \times \sqrt{3})R30^\circ$ overlayer (R = rotated) on the Au(111) surface (Figure 4).

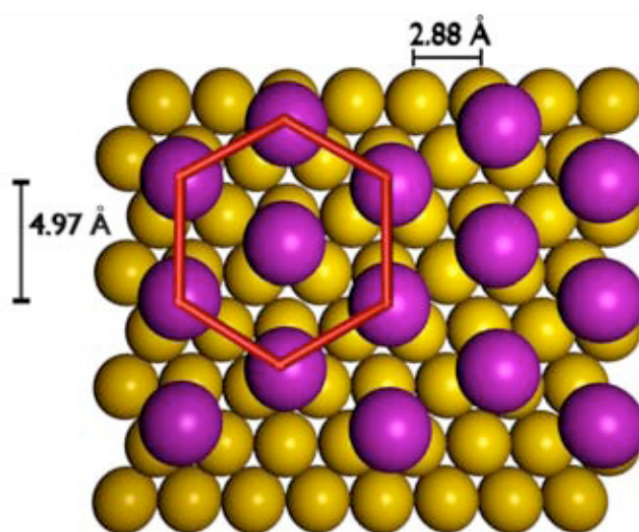


Figure 4: The Au(111) lattice (yellow circles) is shown with a thiolate (purple circles) overlayer in a $(\sqrt{3} \times \sqrt{3})R30^\circ$ arrangement. The distance between sulfur atoms is 4.99 Å. Adapted from ⁹⁸.

Due to their limited lateral resolution, optical and diffraction techniques can only reveal the level of average order in SAMs (i.e. the dominant lattices and their dimensions) over the probed area (typically a few square millimeters). Recent scanning tunnelling microscopy (STM) studies showed that these systems are heterogeneous and structurally complex: The alkyl chains form a

“superlattice” at the surface of the monolayer, meaning a lattice with a symmetry and dimension different from that of the underlying hexagonal lattice formed by sulphur atoms⁹⁷. These results indicate that the order in the top part of a SAM is not dictated solely by the sulphur atoms directly bonded to the gold surface, but also depends strongly on the intermolecular interactions between the alkyl backbones. When alkanethiolates are terminated in head groups other than methyl, it becomes even more complicated to predict and determine the structures of the SAMs⁸⁵.

An alternative and promising strategy towards technology on the nanometer scale is offered by the bottom-up (small-upward) approach, which starts from atom or molecules and builds up to nanostructures. Chemists, by the nature of their discipline, are already at the bottom, because they can manipulate atoms and molecules. They are, therefore, in the ideal position to develop bottom-up strategies for the construction of nanoscale devices and machines. The bottom-up approach to nanotechnology is relatively new. Until a few decades ago, in fact, nanotechnology was not considered an obtainable objective by physicists. The dominant idea, derived from quantum theory, was that atoms are fuzzy entities that “must no longer be regarded as identifiable individuals”, and “form a world of potentialities or possibilities rather than one of things or facts”. From the point of view of quantum theory, molecular structure is not an intrinsic property, but a metaphor. Such ideas, of course, were never shared by chemists who long before had established that atoms are material and reliable building blocks for constructing molecules and that molecules have well defined sizes and shapes⁹⁹.

SAMs of alkanethiolates on gold exhibit many of the features that are most attractive about self-assembling systems: Ease of preparation, density of defects low enough to be useful in many applications, good stability under ambient laboratory conditions, practicality in technological applications, and amenability to control interfacial properties (physical, chemical, electrochemical, and biochemical) of the system. As a result, SAMs are excellent model systems for studies on wetting, adhesion, lubrication, corrosion, nucleation, protein adsorption, and cell attachment^{100, 101}.

1.3.3 Functionalized Glass Substrates

Although self-assembled monolayers of thiols on gold are almost optimal for creating homogeneous and stable layers on solid substrates, they are – due to their lack of transparency and strong quenching effects^{102, 103} – of limited use in optical detection techniques. Hence, glass substrates are the best choice in case of applications with fluorescence read-out. Unfortunately, glass-type surfaces do not allow a selective covalent attachment of defined and oriented monolayers as in the case of gold substrates. However, glass-type surfaces can be chemically modified by silanization¹⁰⁴. Densely ordered assembly of alkyl silane monolayers is generally not obtained by silanization, partially for sterical reason¹⁰⁵, but also because of side reactions leading to oligomerization and formation of multiple layers. Side reactions are particularly critical when using silanes containing functional groups required for immobilization. Thus, silanized surfaces are often heterogeneous and display very strong non-specific adsorption¹⁰⁶, which can only be reduced by attaching layers of hydrophilic polymers with considerable thickness (20-80 nm)¹⁰⁷. These layers reduce non-specific binding, but proportionally interfere with the binding event¹⁰⁷, and can also

affect the sensitivity of the transducer. Polyethylene glycol (PEG) is regarded as a material that resists protein and cell adsorption^{108, 109}. PEGs are non-branched polymers, which have high exclusion volumes due to their conformational entropy, and therefore repel (bio-) polymers including proteins. Thus, surface-attached polymer cushions substantially decrease non-specific adsorption of proteins and other macromolecules to artificial surfaces as initially shown 1982 by MORI et al¹¹⁰. Furthermore, its protein repelling properties make PEG chains suitable for protein immobilization¹¹¹. PIEHLER et al. reported¹¹² a generic approach for effectively shielding glass-type surfaces with ultra-thin layers of functionalized polyethylene glycols (PEG), and at the same time they incorporated functional groups for protein immobilization¹¹³. These ultra-thin PEG layers can be used in a very similar way as alkanethiolates on gold, even though they have very different physico-chemical bases: Alkyl thiol SAMs are formed spontaneously by a very selective reaction, and they are orientedly stabilized by cooperative inter-chain attraction. Conversely, dense PEG layers are forced by a non-selective reaction under extreme conditions (high temperature, high concentration). In aqueous environment, the orientation of the polymer chains in the layer is dominated by inter-chain repulsion due to the high exclusion volume of the PEG chains leading to its excellent protein repelling properties. In applications based on optical read-out (e.g. fluorescence) this type of surface architecture allows optimal signal-to-noise ratios.

1.4 Nanotechnology

The ancient style of technology that led from flint chips to silicon chips handles atoms and molecules in bulk – call it bulk technology. The new technology will handle individual atoms and molecules with control and precision – call it molecular technology. It will change our world in more ways than we can imagine. Microcircuits have parts measured in micrometers – that is, in millionths of a meter – but molecules are measured in nanometers (a thousand times smaller). The terms "nanotechnology" and "molecular technology" can be used interchangeably to describe the new style of technology. Nanotechnology has its origin in many fields – in the realm of quantum physics, in biotechnology, in industrial work on branching polymers, and combinatorial chemistry, in the development of powerful electron microscopes, and later scanning microscopes. None of this work was called nanotechnology at first, and the connections between these various disciplines were not apparent. "Why..." asked Richard FEYNMAN 1959, "... can we not write the entire 24 volumes of the *Encyclopedica Britannica* on the head of a pin?" FEYNMAN anticipated much of what we see developing in nanotechnology today (Figure 5).

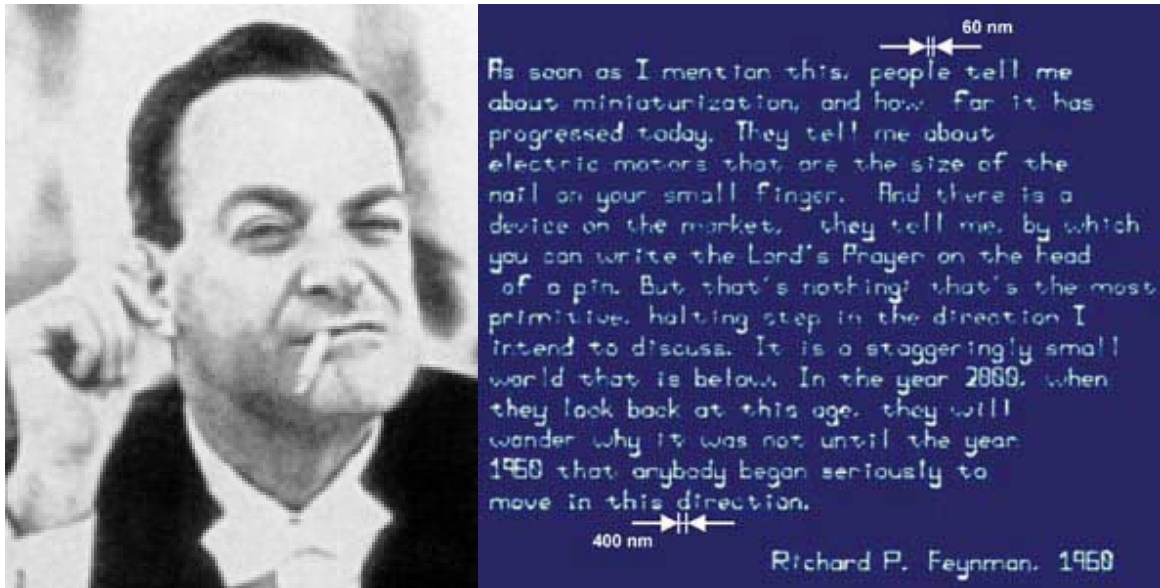


Figure 5: Richard FEYNMAN – the “Father of Nanotechnology” and part of his lecture reproduced using dip-pen nanolithography. Images courtesy of NOBEL Foundation (left) and NanoInk Inc.(right).

The term “nanotechnology” itself was first coined in 1974 by Tokyo Science University professor Norio TANIGUCHI¹¹⁴, who used it to describe the extension of traditional silicon machining down into regions smaller than one micron. The engineers of the new technology will build both nanocircuits and nanomachines. The miniaturization of components for the construction of useful devices and machines is currently pursued by the top-down (large-downward) approach. Figure 6 illustrates this extension of the traditional concept of devices to the molecular level.

This approach, which leads physicists and engineers to manipulate progressively smaller pieces of matter by photolithography and related techniques, has operated outstandingly until now. In 1965 Intel co-founder G. E. MOORE¹¹⁵ predicted that every three years (i) device size would reduce by 33 %, (ii) chip size would increase by 50 %, and (iii) the number of components on a chip would quadruple. This prediction has been fulfilled so far and the potential of laser techniques in the top-down approach to miniaturization has also been exploited for construction of microelectromechanical systems (MEMS).

Nanoscience is the study of phenomena and manipulation of materials at atomic, molecular and macromolecular scales, in order to understand and exploit properties that differ significantly from those on a larger scale. Nanotechnologies are the design, characterisation, production and application of structures, devices and systems by controlling shape and size on a nanometer scale.

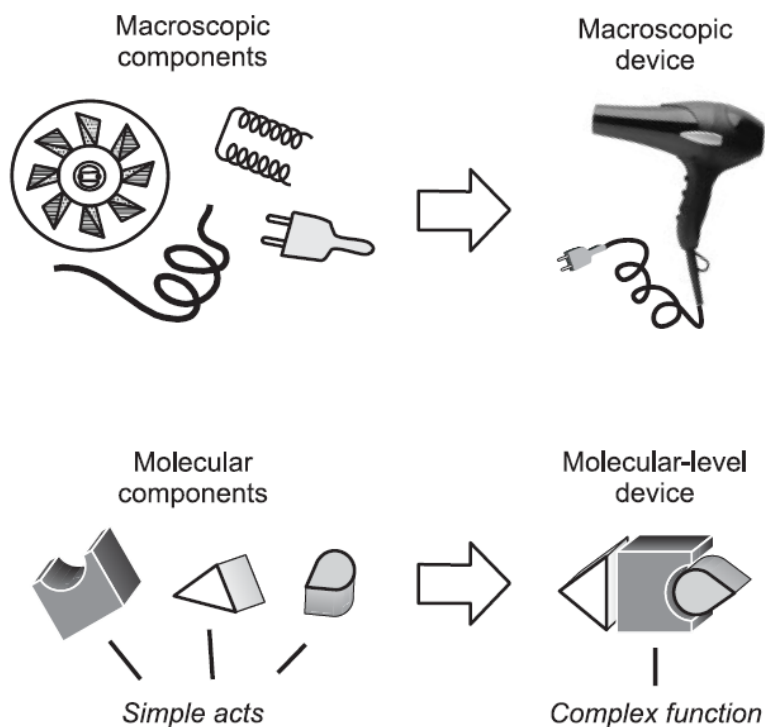


Figure 6: Extension of the concept of the macroscopic device to the molecular level. Adapted from ⁹⁹.

Modern industrial nanotechnology had its origins in the 1930s, in processes used to create silver coatings for photographic film; and chemists have been making polymers, which are large molecules made up of nanoscale subunits, for many decades. However, the earliest known use of nanoparticles is in the ninth century during the Abbasid dynasty. Arab potters used nanoparticles in their glazes so that objects would change colour depending on the viewing angle (the so-called polychrome lustre). Other examples of ancient nanotechnology are the fabulous stained glass fabricated in the Middle Ages, which made use of small gold nanoparticles to create luminous red pigments (Figure 7).

“The current enthusiasm for things “nano” in size has led naturally to a search for connections between these things and biology (the hottest area of science) and technology (where science pays off): if each, individually, is good (so the reasoning goes), the three together must be better. Scientific interest in this intersection of fields is based on the perception that nanotechnology offers biology new tools, and that biology offers nanotechnology access to new types of functional nanosystems – components of the cell – that are unquestionably interesting and possibly useful. Public intersection of “nano” and “bio” is also high, although based in significant part on liberal doses of science-fantasy – “gray goo”, “little submarines”, “the assembler”, and “self-replicating metal-biological hybrids.” ¹¹⁶

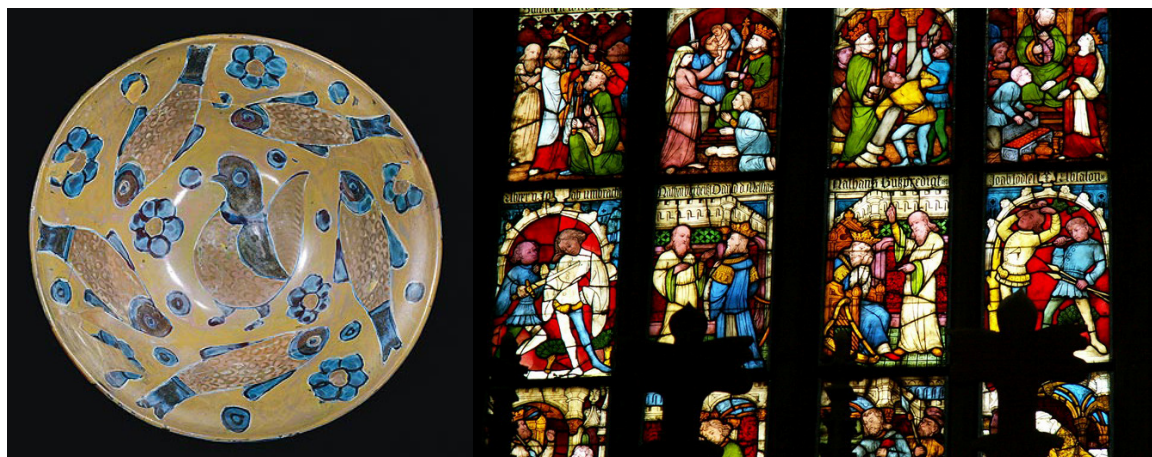


Figure 7: Ancient nanoparticle technology from Africa and Europe.

There are important applications of nanotechnology in biology and biotechnology; biology also provides unparalleled examples of functional nanostructures to excite the imagination of nanotechnologists of all persuasions. When small structures are considered for biological applications, or when small biologically derived structures are determined to have remarkable properties, the size of the system can be “nano” (i.e. 1-100 nm) but also “micro” (i.e. 0.1-1000 μm ; Figure 8). The range of sizes covered by these terms – nanoscale, microscale, and simply “small” – is important: structures vital to the cell have dimensions ranging from those of small molecules to those of millimeter-scale fluidic devices. The promises of nanotechnology are ubiquitous in nature: To make that point, Table 2 lists the use of “nano” as a prefix in words that are often used in the nanotech domain.

Table 2: Proliferation of “Nano” as a prefix. Adapted from ¹¹⁷.

nanoage	nanocrystals	nanomagnetic	nanoscale
nanoarray	nanocube	nanomanipulator	nanoscience
nanoassembly	nanodevice	nanomaterial	nanoscope
nanobacteria	nanodivide	nanomedicine	nanosecond
nanobiologist	nanodomain	nanometer	nanoshell
nanobiomedicine	nanoelectromechanical	nanomicelle	nanostuctured
nanobiotechnology	nanoelectronics	nanoparticle	nanostuctures
nanobot	nanoencapsulation	nanoparticulate	nanoswarm
nanocapsule	nanofabrication	nanophase	nanosystems
nanocassette	nanofibers	nanoplatelates	nanotechnology
nanocatalyst	nanofilter	nanoporous	nanotool
nanocomponent	nanofluidics	nanopowder	nanotube
nanocomposite	nanolayer	nanoproduct	nanotweezers
nanoconnections	nanoliter	nanoreactor	nanowire
nanocosm	nanolithography	nanoreplicator	nanoworks
nanocrystalline	nanomachine	nanorobotics	nanoworld

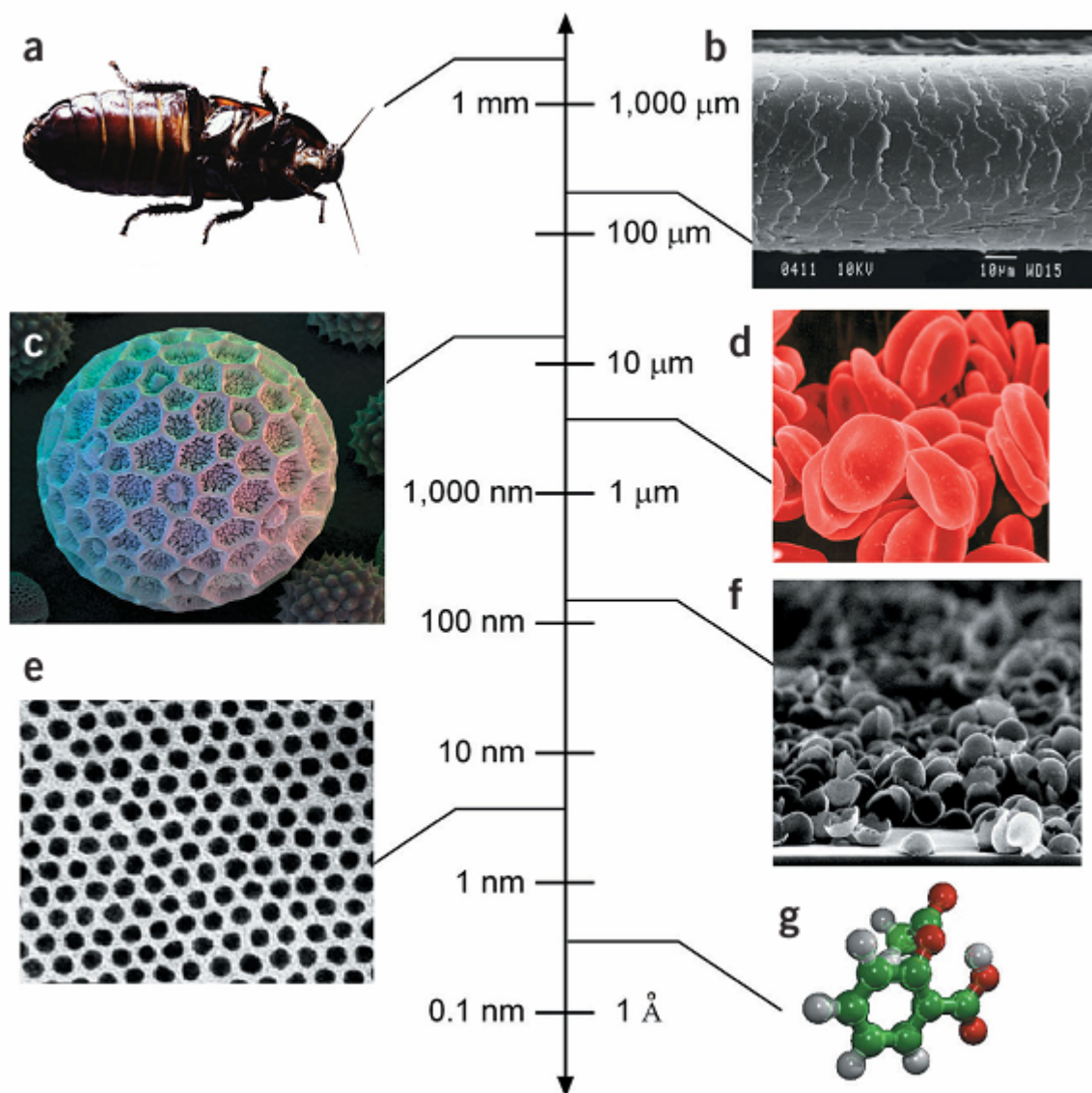


Figure 8: Sizes of representative “small objects”. (a) A cockroach, (b) human hair, (c) *Polygonum* pollen grain, (d) red blood cells, (e) cobalt nanocrystal superlattice, (f) an aggregate of half-shells of palladium (g) aspirin molecule. Adapted from ¹¹⁶.

1.5 Fabrication of Protein Arrays with Lithographic Techniques

As a top-down approach, lithography represents an important surface patterning technique. If we think about the term “lithography” (from the Greek for “stone writing”), most of us probably think in terms of the art world; an ESCHER print is an example of a lithograph. The process was actually invented by a playwright named Alois SENEFELDER in 1798. In its original implementation, an image was painted onto limestone with grease, and the stone was then dipped in ink. The grease would retain the ink while the rest of the stone would repel it. The stone was then pressed onto a piece of paper to create a print (Figure 9)^{118, 119}.

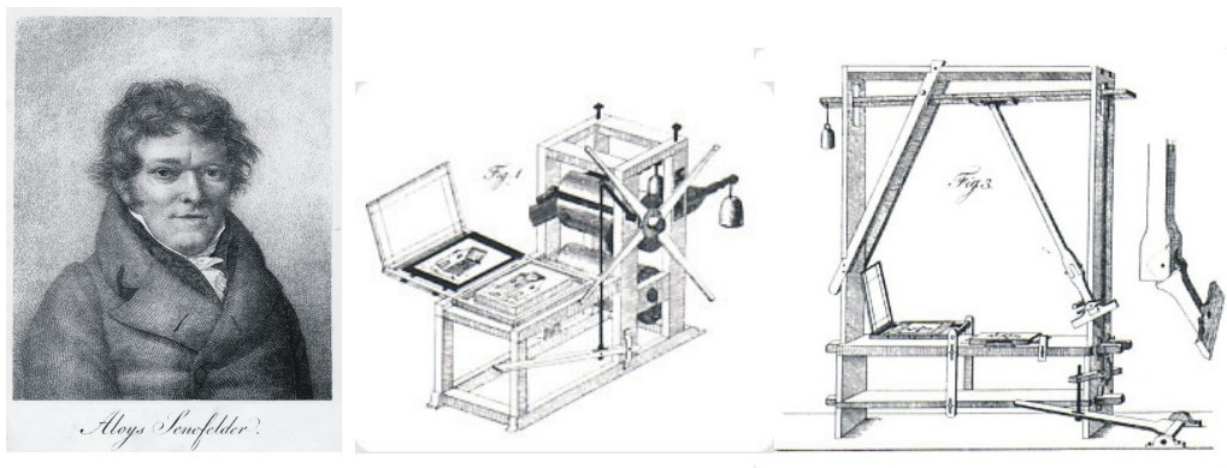


Figure 9: Lithographic stones were introduced by Alois SENEFELDER. Adapted from ¹¹⁸.

Since then, this printing technique has evolved dramatically and is nowadays not only used for printing but also for the (chemical) modification of substrates on a sub-micrometer scale, and is often referred to as:

1.5.1 Microcontact Printing

A method for microscaled stamping of molecules on solid interfaces was originally developed by WHITESIDES and coworkers in Harvard^{120, 121}. The central element in microcontact printing (μ CP) is the stamp. This is a silicone-based elastomer that is microstructured by curing liquid prepolymers of poly(dimethylsiloxane) (PDMS) into a lithographically fabricated master (or mold). Once cured, the stamp is peeled off the mold by hand; bearing an inverted pattern of that of the mold. One mold can be used to replicate many stamps. The relative softness of the stamp, compared to that of a lithographic mask, allows to follow the contours of surfaces onto which it is applied. It is the work of adhesion between the stamp and the substrate that drives the spreading of the initial zones of contact at the expense of an elastic adaptation of the stamp¹²². In μ CP the contact between the elastomer and a substrate occurs at the molecular scale and is termed “conformal”; it ensures the homogeneous transfer of ink from the stamp to the printed areas of the substrate¹²³.

Soft lithography describes a group of novel patterning techniques, such as microcontact printing, microtransfer patterning and liquid embossing, which offer easy, fast, and cheap reproduction of down to sub-micron sized features on large area. These methods can in principle be utilized for depositing or patterning metallic and non-metallic materials even on curved or flexible substrates in a few or just a single simple processing step. The electronics industry, for example, is currently characterized by an enormous price erosion. A strong market pull towards ever decreasing production costs without sacrificing product performance demands fundamentally new, simple, and inexpensive fabrication methods for electronic components and devices. A glance at the flat display market, moreover, reveals the undisputed need for manufacturing processes on ever increasing substrate sizes.

Usually the hydrophobic PDMS stamps are inked with a thiol solution and applied to a gold surface, so that the pattern is transferred by the thiols reacting with the surface (Figure 10). The efficiency of this technique is striking, and even a different thiol solution can be applied to the surface during the next step. Moreover, the easily processed chemical patterns are very suitable for biotechnological applications¹⁰⁰. Instead of simple thiols as an ink, even proteins can be used as stamping material¹²⁴. This deposition is non-specific and self-limiting to a monolayer of proteins if the stamp is rinsed after the inking step.

Stable proteins (exclusively), as for example antibodies, can be inked from an aqueous solution onto a hydrophobic silicon rubber such as PDMS¹²⁵. Hydrophobic polymers in general promote the deposition of proteins from solution through a variety of interactions, and slight or pronounced conformational changes of the protein can accompany this adsorption process. Hydrophobic substrates, as a general rule, have stronger interactions with hydrophobic proteins, and their adsorption process is less influenced by the pH and ionic strength of the solution as well as by the isoelectric point of the protein, as in the case of polar or charged substrates¹²⁶. A number of stable proteins in terms of structure and functions has been microcontact printed, which includes cytochrome c, streptavidin and bovine serum albumin^{124, 127-129}. Due to molecular diffusion accuracy of prints amounts to sub-500 nm patterns. However, the mass transport problem of macromolecules limits routine printing of proteins for industrial applications.

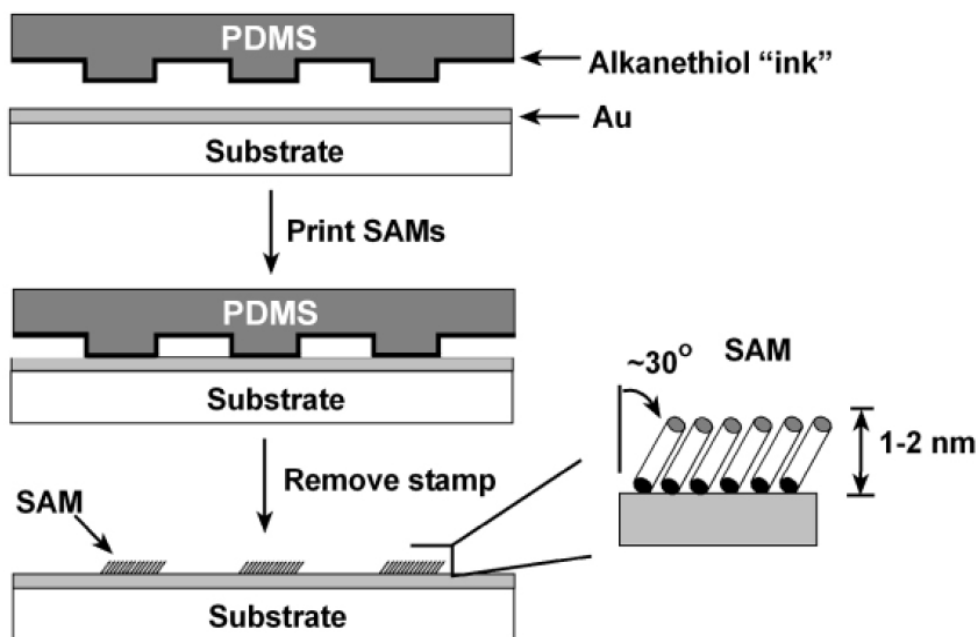


Figure 10: Schematic illustration of a procedure used to pattern SAMs on the gold surface by μ CP. Printed SAMs have same characteristics as formed under conventional conditions (i.e. tilt angle, thickness, etc.). Adapted from ¹³⁰.

1.5.2 E-Beam Nanolithography

Electrons are very precise lithographic tools, as they can be focussed to sub-1 nm areas. The smallest lithographic structures were fabricated with high-energetic focussed electron beams (~ 20 kV) from scanning electron microscopes with dimensions between 5-15 nm. A publication by GÖLZHÄUSER et al. is of particular note because it introduced the possibility for chemical modification and lithography using an electron beam¹³¹. In this work, focused electrons were used to reduce the terminal nitro groups of SAMs to amines. This electron beam-driven reduction to amino functions enabled further derivatization of the surface-bound molecules by subsequent coupling reactions. First, a densely packed monolayer of 4'-nitro-1,1'-biphenyl-4-thiol (NBT) was self-assembled on a gold surface. E-beam writing was used to locally reduce the terminal nitro groups to amino groups¹³², while the aromatic layer was dehydrogenated and cross-linked (Figure 11)¹³³.

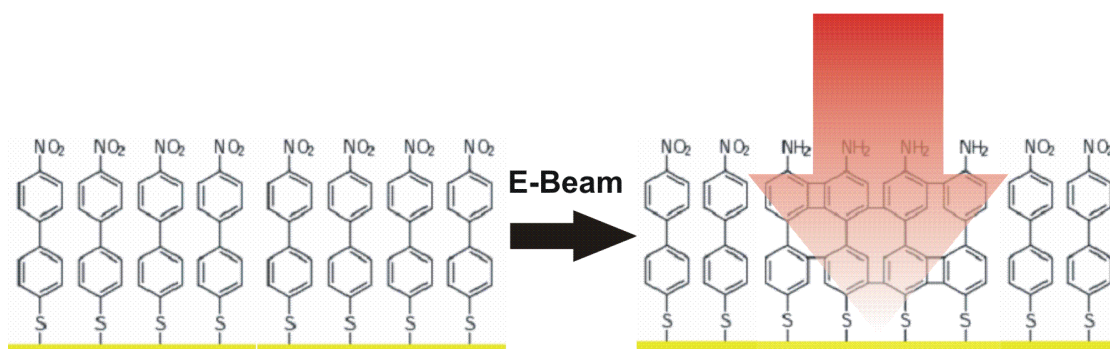


Figure 11: An electron beam converts the terminal nitro groups of a 4'-nitro-1,1'-biphenyl-4-thiol-monolayer to amino groups while the underlying aromatic layer is cross-linked. The cross-linked aminobiphenylthiol region is used for the selective coupling of molecules.

These cross-linked biphenyl SAMs were used as ultrathin (1.2 nm) negative resists for structuring of gold^{133, 134} and silicon substrates¹³⁵, and have such a high stability, that they even could be organized to free-standing nanosheets.¹³⁶ The generated well-ordered templates of amino groups can be used for specific covalent coupling of biomolecules using various spacer molecules¹³⁷. This novel technology enables tethering of molecules at specific sites on nanostructured surfaces down to lateral dimensions of 20 nm^{131, 138, 139}. Chemical e-beam nanolithography is an efficient method for controlled attachment of molecules and molecular complexes at various surfaces (e.g. metals, silicon, indium tin oxide), with manifold potential to future applications in nanobiotechnology. A seminal experiment was covalent coupling of streptavidin to the amino groups of these cross-linked SAMs¹³⁷. The presented technique is well-suited for controlled three-dimensional immobilization of single biomolecules, and the defined assembly of protein complexes.

1.5.3 Scanning Probe-related Nanolithography

Atomic force microscopy (AFM)-based techniques are capable of creating (bio-) molecular patterns with sub-micrometer resolution. AFM has a unique position as nanolithographic technology, because it allows manipulation as well as imaging of the sample. Further, its ability to tailor the chemical composition and structure of a surface on the 1-100 nm length scale is important for researchers studying topics ranging from electronic conduction, to catalysis, to biological recognition in nanoscale systems. This exceptional flexibility of AFM gains more attention and will be the focus of the next section.

One of the tools that has revolutionized nanotechnology, in general, and single molecule biology, in particular, is the atomic force microscope. The AFM has helped create the field of single molecule force spectroscopy. Mechanics has a long tradition of using force-extension data (much like the electrical engineer uses current-voltage data) to probe the inner workings of various materials. It is now possible to apply forces of known magnitude on a macromolecule and study how it deforms under the force. This furnishes structural information and provides insights into the energy landscape the molecule needs to navigate as it undergoes force-induced conformational changes. The energy of deformation associated with such molecules is primarily determined by weak forces such as hydrogen bonds, VAN DER WAALS contacts, and hydration effects. On a more philosophical note, these experiments force us to think in terms of forces and not energy, complementing the traditional views held in molecular biology, and they can lead to many new insights about the relation between structure and function in proteins, polynucleotides, and other macromolecular entities.

At present, the most prominent AFM-based patterning method is the so-called *dip-pen nanolithography* (DPN). The principle of dip-pen nanolithography was first introduced by Hans-Jürgen BUTT¹⁴⁰ and then applied by Chad MIRKIN as a generic patterning technique by chemical surface modification¹⁴¹. Actually this technique looks more like writing with Thomas JEFFERSON's quill pen than it does conventional lithography, except that the quill pen has been shrunk to where its point is a few nanometers at its tip. DPN relies on material being transferred from the AFM tip to the surface. The material can simply be the constituents of the tip itself (i.e. gold), induced by force or current, or it can be physisorbed material. Material on the tip is transferred to the substrate by capillary forces (Figure 12).

DPN inspired scientists from various fields to generate patterns with numerous inks and surfaces. DRAVID et al.¹⁴² have patterned silicon substrates with various dyes, whereas RAYMENT et al.¹⁴³ applied up to fifth-generation dendrimers (G5 DAB, amino terminated) to Si(100) substrates to form several micrometer long lines with diameters down to 100 nm. The effective achievable line widths are highly dependent on the utilized writing speed and temperature¹⁴⁴. Although studies suggested that the transport of material was dependent on a water meniscus between the tip and the substrate^{141, 145}, writing experiments have also been performed at zero relative humidity, which indicates surface diffusion as being a transport factor^{144, 146}. MIRKIN et al. have used DPN to deposit proteins on surfaces to form nanoarrays on gold substrates¹⁴⁷. In this study, solely stable proteins as

IgG or lysozyme were positioned in nanoarrays (islands with diameters of ~ 200 nm), and subsequently coupled with antibodies (anti-IgG).

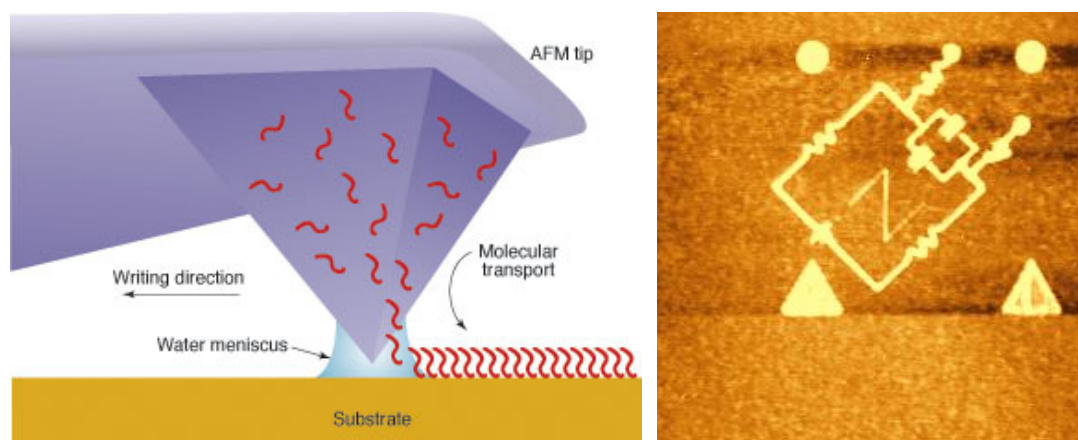


Figure 12: Principle (left)¹⁴⁸ and application (right) of dip-pen nanolithography. Octadecyl thiols were structured with DPN yielding the pattern of an electric circuit. This nanolithographic experiment was performed by Ali TINAZLI at NanoInk Inc. in Skokie (Illinois), the company which commercialized DPN.

Another innovative AFM-based method called *nanoshaving/nanografting*^{149, 150}, can produce nanostructures of SAMs with specific shape, dimension, and composition. This process – invented 1999 by Gang-Yu LIU in Detroit – combines the displacement of molecules within a matrix SAM by an AFM tip, and the use of a self-assembly reaction to fill these revealed sites by a reactive adsorbate. Compared with other methods used to fabricate structured SAMs, nanografting offers higher spatial precision. In best cases generated non-biological nanopatterns have dimensions down to 40 nm. In addition, the resulting nanostructures can be characterized with molecular resolution *in situ* using the same AFM tip. Nanopatterns of thiols that contain chain lengths and terminal groups different from those of the matrix SAM can be generated (Figure 13). The ability to fabricate multiple patterns regiospecifically from desired components opens the possibility for producing selective recognition sites and sensors with orthogonal detection capabilities. Furthermore, nanografting allows fabricated patterns to be altered *in situ* without the need to change masks or repeat entire fabrication processes.

These patterned SAMs produced by nanografting provide new opportunities for pursuing systematic studies of such size-dependent properties as conductivity, nanotribology, and spatially confined surface reactions. Locally confined capturing agents for protein immobilization offer new perspectives for the fabrication of protein nanoarrays. Successful and impressive applications of these sophisticated methods have been demonstrated with biochemical model systems^{147, 151, 152}.

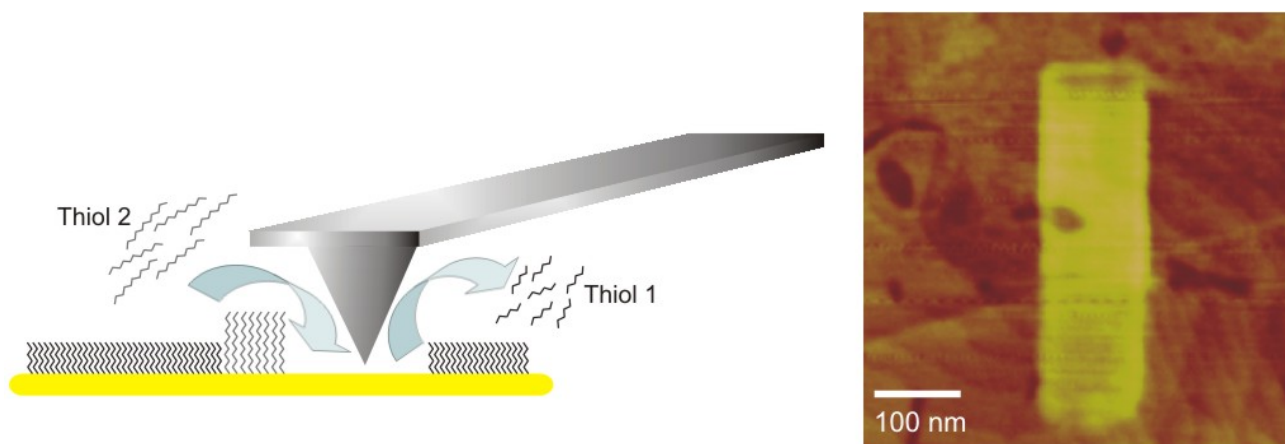


Figure 13: Principle and experiment of nanografting. Hexadecyl thiols (Thiol 1) were replaced locally by matrix thiols (Thiol 2) yielding a differential height pattern in the AFM topographic image. This nanolithographic experiment was performed by Katrin SCHULZE and Ali TINAZLI.

“As nanotechnology moves beyond reliance on proteins, it will grow more ordinary from an engineer’s point of view. Molecules will be assembled like the components of an Erector set, and well-bonded parts will stay put. Just as ordinary tools can build ordinary machines from parts, so molecular tools will bond molecules together to make tiny gears, motors, levers, and casings, and assemble them to make complex machines”¹⁵³.

However, as these methods have their origin in non-biological disciplines they are typically conducted under experimental conditions less suitable for biological applications. Limitations of mass transport, oxidation, dehydration in air, and organic solvents will either impair nanofabrication of protein arrays or even denature proteins. If these techniques are used for biological patterning, an elaborate ambient control system and modification of the AFM tip are often required^{147, 154}. Hence, as shown by recent publications, assays are limited to stable proteins, which are not affected by these experimental conditions and are hardly adapted for general biological applications under native conditions.

Ideally, protein nanoarrays should be generated undisturbed, in a physiological environment, and the protein functionality should be maintained. The procedure must allow precise control of the nanofabrication process, enabling the rapid exchange and adjustment of buffers and solutions. The same AFM tip should be used for imaging, structuring, and read-out including rapid and convenient switching between these modes. Furthermore, proteins or protein complexes should be specifically and uniformly oriented at the nanostructured interface for optimal control of the functionality.

1.6 Aim of the Ph.D. Thesis

Lateral organization of proteins in nanodimensions has to be conducted ideally under physiological conditions, while preserving structure and function of the immobilized protein species

in unique molecular orientation. Only the proteins of interest should be targeted to nanoarrays. Hence, capturing of proteins has to be highly specific and with high affinity preventing dissociation from the functional interface. As the confined space in the nanoarrays has to be used with maximum efficiency, proteins should be immobilized with high density. In respect to technical and economical reasons, recycling of the protein chips should be enabled. These milestones are presented in detail in this chapter.

Although the described ideal conditions in “Concepts of Protein Immobilization” (1.2) as stable, specific, and stoichiometrically defined (1:1) interaction between protein and chip surface appear very specific and hardly to achieve – they are not utopian and allow even the realization of a generic affinity capturing concept of proteins on solid substrates. Based on the classical mono-NTA/His₆-tag interaction pair and the observation of phase segregated chelator lipids, cumulated mono-NTA chelator groups promise high-affinity capturing of any His-tagged protein under physiological conditions due to multivalency effects. Such multivalent chelator species were designed in parallel projects and optimized for generic protein chip technologies.

1.6.1 Surface Architecture and Chemistry for a Generic Protein Chip Platform

A protein chip, suitable for routine use, has presumably to be robust, surviving standard treatments and processes in biochemical and diagnostic laboratories. Self-assembled monolayers of alkyl thiols on gold have high enough stability to resist routine laboratory conditions. Combination of alkyl thiols with multivalent chelators and the development of a generic platform for protein chips, compatible to manifold bioanalytical applications, was one major aspect of this thesis.

1.6.2 A Novel Lithographic Technology for Fabrication of Protein Nanoarrays

Due to its enormous capabilities as a nanoscale imaging, manipulation, and analysis tool, atomic force microscopy is the ideal technology for fabrication of protein nanoarrays. Remarkably, AFM is the only nanotechnological tool for routine use, which can be operated under native conditions, i.e. aqueous solution, physiological ionic strength, pH and temperature. Thus, the invention of novel nanolithographic techniques for nanofabrication of protein arrays under physiological conditions based on AFM was another focus of the current work.

1.6.3 Parallel Array Generation by Chemical E-Beam Nanolithography

An alternative to AFM-based nanolithography is offered by chemical e-beam nanolithography and allows additionally a highly parallel fabrication of protein arrays. Chemical modification of SAMs – as introduced by GÖLZHÄUSER et al.¹³¹ – was combined with the multivalent chelator concept. This enabled us to tailor a protein chip, which benefits from highly

advanced and robust technologies from semiconductor industry with specific and functional high-affinity immobilization of proteins.

1.6.4 Microcavities for Organization of Membrane Proteins

Organization of membrane proteins at interfaces is challenging, as the extramembrane domains should – in order to avoid denaturation – not contact the solid substrate. Hence, silicon-on-insulator (SOI) substrates with microcavities were considered as an innovative chip platform for membrane proteins. A methodology for bridging the nanometer-sized cavity pores with lipid bilayers and a proof of concept with CLSM analysis was realized.

The aim for the design of a nanoscaled protein chip technology involved numerous experimental approaches, steps, and projects merging to *nanobiotechnology*^{7, 155}. The following flow chart (Figure 14) illustrates the strategy and milestones in the presented Ph.D. thesis:

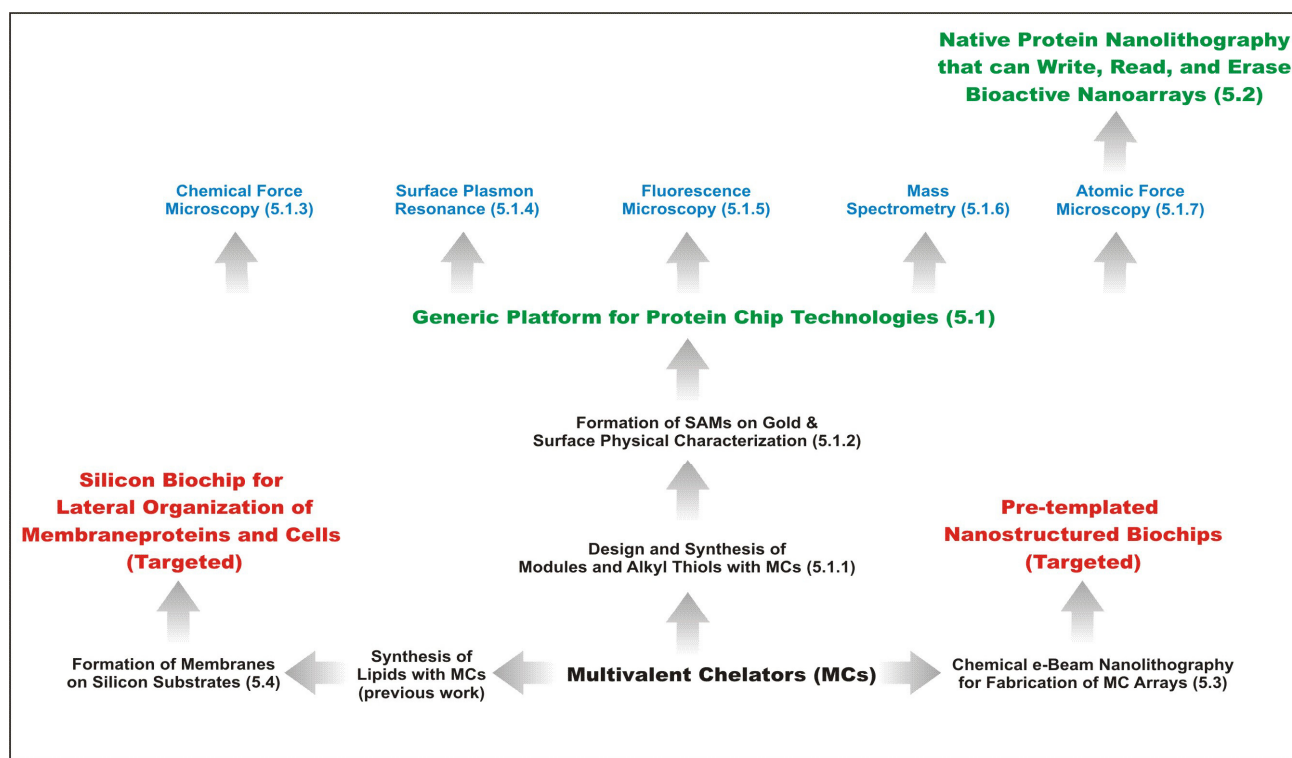


Figure 14: Strategy and milestones for the development of a generic protein chip platform and nanoscaled protein arrays. Black-coloured items are fundamental for the development of the final or targeted technologies. Green highlighted milestones are completed novel concepts. Blue highlighted steps represent ready-to-use novel bioanalytical applications developed as part of the projects. Red highlighted items are targeted technologies and currently at research level. Each step will be presented and discussed in the corresponding Results & Discussion chapter.

2 Theoretical Background of Methodologies

πεπαιδευμένον γάρ ἔστιν ἐπὶ τοσοῦτον τᾶκριβὲς ἐπιζητεῖν καθ' ἕκαστον.

*Es zeichnet einen gebildeten Geist aus, sich mit jenem
Grad an Genauigkeit zufrieden zugeben, den die Natur der Dinge zulässt,
und nicht dort Exaktheit zu suchen, wo nur Annäherung möglich ist.*

ARISTOTELES

This chapter introduces briefly methodologies which were essential for the realization and success of the addressed research projects.

2.1 Atomic Force Microscopy

The atomic force microscope (AFM) is a very high-resolution type of scanning probe microscope. The AFM was invented by BINNIG, QUATE and GERBER in 1986¹⁵⁶, and is one of the foremost tools for imaging, measuring and manipulating matter at the nanoscale.

The AFM consists of a microscale cantilever with a sharp tip (probe) at its end that is used to scan the specimen surface (Figure 15). The cantilever is typically silicon or silicon nitride with a tip radius of curvature in the order of 10 to 30 nanometers. When the tip is brought into proximity of a sample surface, forces between the tip and the sample lead to a deflection of the cantilever according to HOOKE's law. The forces that are measured in AFM include mechanical contact force, VAN DER WAALS forces, capillary forces, chemical bonding, electrostatic forces, magnetic forces, etc. The deflection is measured using a laser spot reflected from the top of the cantilever into an array of photodiodes. If the tip scans at a constant height, there would be a risk that the tip collides with the surface, causing damage. Hence, in most cases a feedback mechanism is employed to adjust a tip-to-sample distance to maintain a constant force between the tip and the sample. Traditionally, the sample is mounted on a piezoelectric tube which can move the sample in the z direction for maintaining a constant force, and the x and y directions for scanning the sample. The resulting x,y,z-map represents the topography of the sample. Resolution of AFM depends strongly on the used tip. Imaging of crystalline substrates at atomic resolution is achieved almost under routine conditions. HEMBACHER et al. reported 2004 imaging of the charge distribution in atoms with closed electron shells¹⁵⁷. Features with a lateral distance of only 77 picometers were revealed.

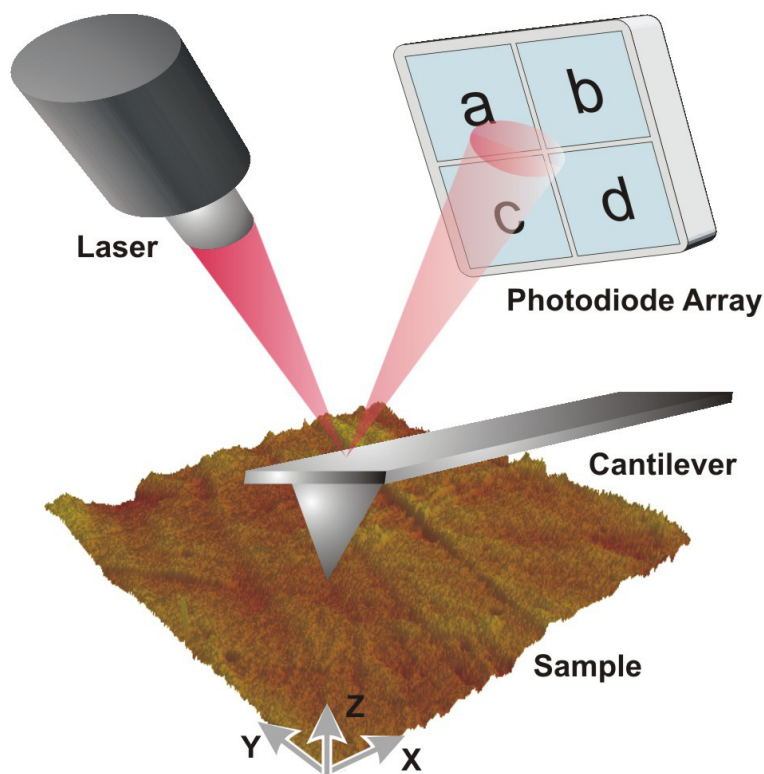


Figure 15: Principle and set-up of an atomic force microscope (AFM).

Depending on the application the AFM can be operated in a number of modes. Most modes applied are the static contact mode and the dynamic Tapping ModeTM. In contact mode operation, the static tip deflection is used as a feedback signal. Because the measurement of a static signal is prone to noise and drift, low stiffness cantilevers are used to boost the deflection signal. However, close to the surface of the sample, attractive forces can be quite strong, causing the tip to 'snap-in' to the surface. The force between the tip and the surface is kept constant during scanning by maintaining a constant deflection.

At ambient conditions, most samples develop a liquid meniscus layer. Hence, capillary forces impair proper scanning and introduce imaging artefacts. TappingModeTM was developed to bypass this problem¹⁵⁸. Here, the cantilever is externally oscillated at its resonance frequency. The oscillation amplitude, phase and resonance frequency are modified by tip-sample interaction forces: These changes in oscillation with respect to the external reference oscillation provide information about the sample properties and it comes in contact with the sample in each cycle. Restoring forces are provided by the cantilever spring to detach the tip from the sample.

The AFM has several advantages over the scanning electron microscope (SEM), which has a similar imaging resolution. Unlike the electron microscope which provides a two-dimensional

projection or a two-dimensional image of a sample, the AFM provides a true three-dimensional surface profile. Additionally, samples viewed by AFM do not require any special treatments (such as metal/carbon coatings) that could irreversibly change or damage the sample. While an electron microscope needs an expensive vacuum environment for proper operation, most AFM modes can work perfectly well in ambient air or even in liquid environment. This makes it possible to study biological macromolecules and even living organisms.

A disadvantage of AFM compared with the scanning electron microscope (SEM) is the image size. The SEM can image an area in the order of millimetres. The AFM can only image a maximum height in the order of micrometers and a maximum scanning area of around 150 by 150 μm . Another inconvenience is that at high resolution, the quality of an image is limited by the radius of curvature of the probe tip, and an incorrect choice of tip for the required resolution can lead to image artefacts. Traditionally the AFM requires several minutes for a typical scan, while an SEM is capable to scan at near real-time (although at relatively low quality) after the chamber is evacuated. The relatively slow scanning rate during AFM imaging often leads to thermal drift in the image, making the AFM microscope less suited for measuring accurate lateral distances. Finally, most AFM images are affected by hysteresis of the piezoelectric material and cross-talk between the (x,y,z) axes that they require software enhancement and filtering.

2.2 Confocal Laser Scanning Microscopy

Confocal laser scanning microscopy (CLSM) is a valuable tool to obtain high resolution images and 3-D reconstructions. The key feature of confocal microscopy is its ability to produce blur-free images of thick specimens at various depths. Images are taken point-by-point and reconstructed with a computer, rather than projected through an eyepiece. The principle for this special kind of microscopy was developed by Marvin MINSKY in 1953¹⁵⁹, but it took another thirty years and the development of lasers as near-ideal point light sources for confocal microscopy to become a standard technique toward the end of the 1980s.

In CLSM, a fluorescent specimen is illuminated by a point laser source, and each volume element is associated with a discrete fluorescence intensity (Figure 16). Here, the size of the focus area, which is crucial for the obtained resolution, is determined by the diffraction limit of the optical system. This is due to the fact that the image of the scanning laser point source is not an infinitely small point but a three-dimensional diffraction pattern. The size of this diffraction pattern and the focal volume is controlled by the numerical aperture of the system's objective lens and the wavelength of the laser light used. This can be seen as the classical resolution limit of conventional

optical microscopes using a so-called wide-field illumination. However, with confocal microscopy it is even possible to overcome this resolution limit of wide-field illuminating techniques as only light generated in a small volume element is detected at a time. Here it is very important to note that the effective volume of light generation is usually smaller than the volume of illumination. The diffraction pattern of detectable light generation is sharper and smaller than the diffraction pattern of illumination. A mixture of emitted fluorescent light as well as reflected laser light from the illuminated spot is then recollecting by the objective lens. A beam splitter separates the light mixture by allowing only the laser light to pass through and reflects the fluorescent light into the detection apparatus. After passing a pinhole, the fluorescent light is detected by a photo-detection device [photomultiplier tube (PMT) or avalanche photodiode], transforming the light signal into an electrical one which is recorded by a computer.

The detector aperture obstructs light that is not coming from the focal point. The out-of-focus points are thus doubly suppressed: Firstly they are not illuminated, and secondly most of their returning light is blocked by the pinhole. With a resolution of 200 nm in the xy-plane and 500 nm in the z-axis CLSM provides an increased resolution compared to conventional microscopy techniques and enables z-stacking of the sample for three-dimensional image reconstruction.

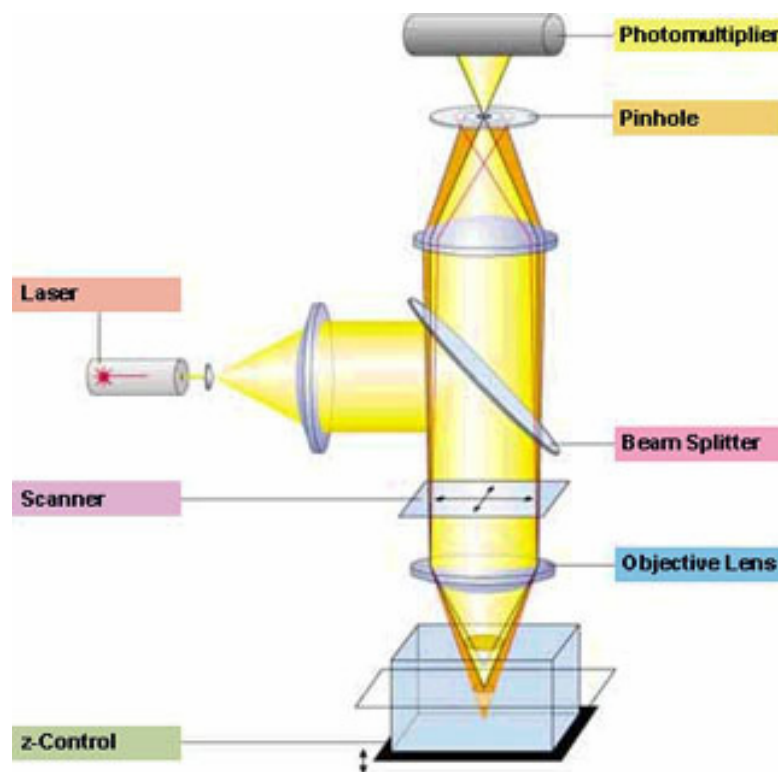


Figure 16: Function principle of a confocal fluorescence laser scanning microscope. Courtesy of Carl Zeiss AG.

The detected light originating from an illuminated volume element within the specimen represents one pixel in the resulting image. As the laser scans over the plane of interest a whole image is obtained pixel by pixel and line by line, while the brightness of a resulting image pixel corresponds to the relative intensity of the detected fluorescent light. The beam is driven across the sample in the horizontal plane using one or more (servo-controlled) scanning mirrors. This scanning method usually has low reaction latency and the scan speed can be varied as slower scans provide a better signal-to-noise ratio resulting in better contrast and higher resolution. Information can be collected from different focal planes by raising or lowering the microscope stage. The computer can generate a three-dimensional picture of a specimen by assembling a stack of these two-dimensional images from successive focal planes.

In addition, confocal microscopy provides a significant improvement in lateral resolution and the capacity for direct, non-invasive serial optical sectioning of intact, thick living specimens with an absolute minimum of sample preparation. As confocal laser scanning microscopy detects fluorescence, a sample usually has to be labelled with fluorescent dyes. However, the actual dye concentration can be very low so that the disturbance of biological systems is kept to a minimum. Some instruments are capable of tracking even single fluorescent molecules.

The resolution limit in confocal microscopy ($xy \sim 200$ nm and z -axis ~ 500 nm) depends not only on the probability of illumination but also on the probability of creating enough detectable photons, hence the actual addressable volume being associated with a generated light intensity is smaller than the illuminated volume. The probability decrease in creating detectable photons affects the signal-to-noise ratio. This can be compensated by using more sensitive photo-detectors or by increasing the intensity of the illuminating laser point source. Increasing the intensity of illumination latter risks excessive bleaching or other damage to the specimen of interest, especially for experiments in which comparison of fluorescence brightness is required.

2.3 Surface Plasmon Resonance

Surface plasmon resonance spectroscopy allows measuring changes in the refractive index at the interface of a conductor and a fluid. Adsorption of biomolecules to a functionalized conductor surface can be studied, as the refractive index of the analytes differs from the refractive index of the bulk solution. The interaction of the immobilized analyte with a soluble ligand can be monitored in real-time, thus revealing kinetic constants.

The resonant interaction between the surface charge oscillation and the electromagnetic field of the light constitutes the surface plasmon. Surface plasmons are collective vibrations of the free

electrons at a conductor surface. The charge fluctuations propagate along the surface of the metal and resemble light waves trapped on the surface (Figure 17). Perpendicularly to the surface an electrical field is induced, which decays exponentially with distance from the surface. The electrical field is assumed to be evanescent according to the bound, non-radiative nature of surface plasmons. In the dielectric medium above the conductor, the decay length of the evanescent field is in the order of half the wavelength of the exciting light, whereas the decay length in the metal is determined by the skin depth. The attenuation of the charge fluctuation (propagation length of the surface plasmon mode) depends on the absorption of the conductor material and on the wavelength of the exciting light.

To excite a plasmon by light the momentum mismatch of surface plasmon mode and photon must be overcome, i. e. the dispersion curves of surface plasmon mode and light must intersect (Figure 18). The problem can be solved by coupling the conductor surface to a medium with a refractive index $n_2 > 1$. The light has to be polarized parallel to the plane of incidence (p-polarized). The surface plasmon resonance instrument is constructed according to the KRETSMANN-RAETHER configuration (Figure 19). In this set-up a laser beam passes through a triangular prism and is directed to the backside of a gold film deposited on a glass slide, i.e. the inserted chip. The incident light is p-polarized by two polarizers. Two flow cells are mounted onto the chip to measure and compare the adsorption of biomolecules. A two-valve system allows the exchange of solutions without introducing air into the cells. A photodiode detects the reflected light.

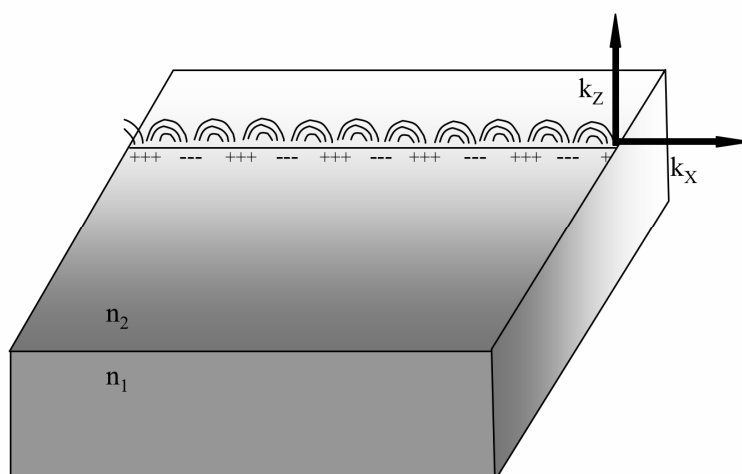


Figure 17: Surface plasmon propagation along a conductor surface. Charges fluctuate at the surface of a conductor with refractive index n_1 coupled to a medium with refractive index $n_2 > 1$. The surface plasmon propagates in x -direction (wave vector k_x), whereby the electrical field decays exponentially in z -direction (wave vector k_z).

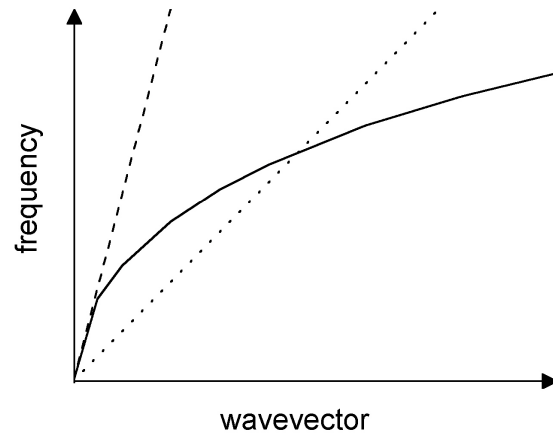


Figure 18: (Anomalous) Dispersion curves of surface plasmons and photons in free space and medium. The dispersion curve for a surface plasmon (bold line), a free space photon (dashed line) and a photon in medium with refractive index $n_2 > 1$ (dotted line) are displayed, whereby the angular frequency of a photon in a medium is $\omega = kx \cdot c/n$ (c : velocity of light, n : refractive index of the medium).

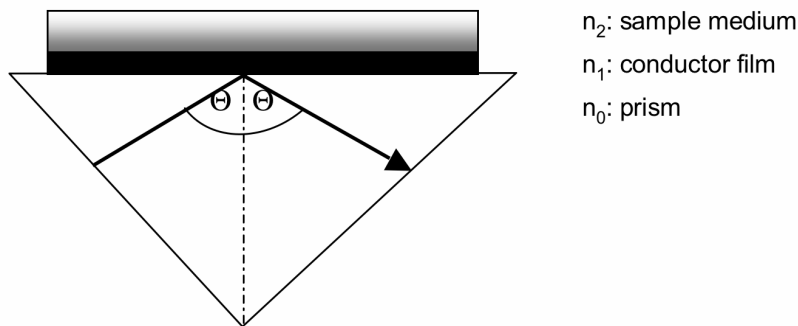


Figure 19: Kretschmann-Raether configuration. *P*-polarized light from a laser passes through a prism and is totally reflected at the interface of a thin conductor film surrounded by sample medium. Reflected light is recorded by a photodiode in dependence on the angle of the incident light.

The reflected intensity is recorded as a function of the angle of incidence θ . Due to energy absorption the minimum θ_{min} indicates the excitation of surface plasmons at the gold-solution interface (Figure 20). Changes in the refractive index at the conductor surface are directly reflected by a shift in the angle θ_{min} as the dispersion relation of surface plasmon is dependent on the refractive index of the medium. Changes in the concentration of a biomolecule in the interfacial region due to physisorption are monitored in the sensorgram as a function of time by measuring θ_{min} . The instrument used for surface plasmon resonance studies, the BIAcore X (BIAcore AB, Uppsala, Sweden) records a shift in θ of 0.1° as 1000 resonance units, which corresponds to a

change in protein concentration at the surface of about 1 ng/mm^2 . (This section was adapted from ¹⁶⁰.)

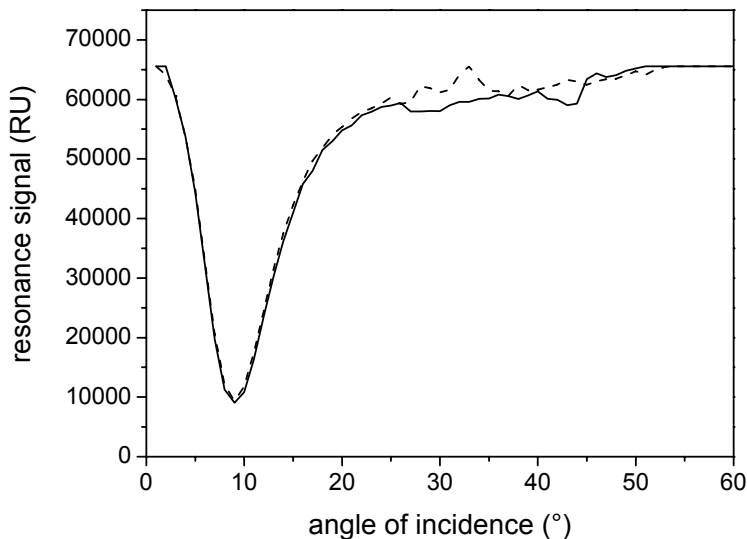


Figure 20: Reflected light intensity in dependence on the angle of the incident light. The intensity of the reflected light is converted into the resonance signal and depicted for both serially connected flow cells (flow cell 1: bold line, flow cell 2: dashed line).

2.4 Surface Sensitive Analytics

All solid materials interact with their surroundings through their surfaces. The physical and chemical composition of these surfaces determines the nature of their interactions. Their surface chemistry will influence such factors as catalytic activity, adhesive properties, wettability, and contact potentials. Surfaces, therefore, influence many crucially important properties of the solid. Following technical sections were adapted from ¹⁶¹.

2.4.1 Contact Angle Goniometry

Contact angle goniometry directly provides information about the macroscopic properties of the surface. The technique is based on probing the surface with a sessile droplet of a liquid and measuring the resulting contact angle θ . The contact angle is related to a surface tension γ of the interface, as given by YOUNG's equation:

$$\gamma_{sv} = \gamma_{sl} + \gamma_{lv} \cos\theta,$$

where γ_{sv} , γ_{sl} , γ_{lv} denote the surface tension at the solid-vapor, the solid-liquid, and the liquid-vapor interfaces, respectively. It can be shown that the free energy of adhesion ΔG_{sl} also is related to the contact angle through

$\Delta G_{sl} = -\gamma_{lv} (1 + \cos\theta)$ (YOUNG-DUPRÉ equation).

In practice, the contact angle analysis of SAMs formally does not include calculations of the energetic parameters of the surface, but rather give a general indication about the exposure of the terminal groups. Another parameter which can be directly obtained by the so-called captive droplet method is the hysteresis. For this purpose, the advancing and receding contact angles (θ_a and θ_r , respectively) are measured upon expanding and reducing the volume of the formed droplet, and a hysteresis $H = \theta_a - \theta_r$ is observed. It is a result of various microscopy parameters of the surface and provides information about the homogeneity and flexibility of the outermost layer of the SAM.

2.4.2 Ellipsometry

Ellipsometry allows the determination of thicknesses of thin organic layers as SAMs. Changes in the state of polarization of elliptically polarized light reflected from the sample surface are measured. The induced phase shift and the relative amplitude change can be related to the optical model of the interface and, by knowing the refractive indices of the substrate and the organic film, the thickness of the film (i.e. SAM) can be determined.

2.4.3 Infrared Reflection-Absorption Spectroscopy

Infrared (IR) spectroscopy provides essential information about the composition of the molecules in terms of constituent groups, their intra- and intermolecular interactions, as well as the orientation of the groups. The normal molecular vibrations in organic compounds occur mainly in the mid IR region (4000-400 cm^{-1}). The vibrations are IR active, if the following selection rule is satisfied:

$$\vec{M}_i = \frac{\partial \vec{\mu}}{\partial Q_i} \neq 0,$$

where $\vec{\mu}$ is the dipole moment, Q_i , the coordinate of the vibrational mode i and \vec{M}_i the transition dipole moment.

FRANCIS and ELLISON developed a special IR method, initially referred to as infrared reflection absorption spectroscopy (IRAS)¹⁶², for investigation of ultrathin organic films on metal substrates. In this set up, the incident angle of the IR beam is high, typically between 80° and 85°. The electric field of the incident beam can be divided into two components that oscillate parallel (p) and perpendicular (s) to the plane of incidence. Upon reflection, the s-vector undergoes a phase shift of 180° for all angles of incidence. Therefore, a standing wave with zero amplitude is formed at the surface by the incident and reflected components of the s-field. Contrary, the incident and reflected components of the p-vector do not diminish, and especially at high angles of incidence,

they combine and form a strong electric field perpendicular to the surface E_{Rp} . A vibrational mode i of a molecule on the surface will be observed in the spectra with an intensity I_i only if the transition dipole moment of the mode has a component perpendicular to the surface because of

$$I_i \propto \left| \frac{\partial \vec{\mu}}{\partial Q_i} \cdot \vec{E} \right|^2.$$

This condition is called the surface selection rule. The intensity I_i is maximal when the molecules are aligned, a situation that can be obtained in SAMs. Therefore, some of the peaks that are normally seen in isotropic bulk IR spectra will appear with low intensities or disappear in IRAS, whereas those satisfying the surface selection rule will show up with increased relative intensities. If the peaks in the spectrum can be assigned to specific molecular vibrations, the structure of the SAM can be studied in detail. Hence, IRAS is a key method in the analysis of SAMs.

2.4.4 X-Ray Photoelectron Spectroscopy

X-ray photoelectron spectroscopy (XPS) allows to obtain the binding energy of electrons emitted from the atoms in the sample. The principle of the measurement is based on the EINSTEIN'S photoelectric relation:

$$E_k = h\nu - (E_b + \phi),$$

Where E_k denotes the measured kinetic energy of a photoemitted electron, removed from the atom by an X-ray photon with energy $h\nu$ and ϕ is the difference between the FERMI level of the solid and vacuum level (the work function of the spectrometer analyzer). At the vacuum level, the electron is free from an interaction with the surface. The equation shows that, by measuring E_k and knowing $h\nu$ and ϕ (a spectrometer constant), it is possible to determine the binding energy E_b . Furthermore, XPS can be used to analyze the chemical composition of the surface, since the core-level electrons from different atoms have distinct E_b values. It is also well-known that the exact value of E_b depends on the chemical environment of the atom. Small variations in E_b , so-called chemical shifts, can be analyzed in order to extract structural information.

2.5 MALDI Mass Spectrometry

Matrix-assisted laser desorption/ionization (MALDI) mass spectrometry determines the molecular mass of molecules by desorption of ions from an organic matrix by means of a laser pulse. The technique was developed by Michael KARAS and Franz HILLENKAMP in the mid eighties^{163, 164}.

The analyte has to be co-crystallized with aromatic compounds, which are excited by UV radiation of a Nd-YAG laser or a nitrogen laser. The excitation energy leads to relaxation into the lattice and transition of molecules into the gas phase. Due to the low laser intensity ($\sim 100 \text{ W/cm}^2$) the analyte molecules stay intact and are protonated by the photoionized matrix. Charged molecules are accelerated in an electrostatic field ($E \sim 1000 \text{ V/mm}$) and are separated during a drift interval because of different velocities according to their mass-to-charge ratio m/z . The time of flight (TOF) is measured for constant acceleration voltage and drift interval:

$$E_{kin} = \frac{1}{2} \cdot m \cdot v^2 = z \cdot e \cdot U$$

$$v = \frac{L}{t}$$

m : molecular mass of the ion

L : fieldless distance

v : ion velocity after acceleration interval

t : time of flight

z : charge factor

$$\frac{m}{z} = \frac{2 \cdot e \cdot U}{L^2} \cdot t^2$$

e : electronic charge

Thus, the mass/charge ratio is proportional to the square of the time of flight and can be calibrated with reference material.

Ion detection is accomplished with an antipolarized conversion dynode, which converts the ion flux into an electron flux (secondary electron multiplier). The analog signal of the secondary electron multiplier is subsequently amplified and digitalized by a transient recorder. With increasing ion mass secondary ions are generated by the dynode leading to temporal dispersion and thus deteriorated resolution. The resolution $R = m/\Delta m$ in MALDI-TOF experiments is determined as full width at half maximum of the peak. The resolution and sensitivity of the detector decreases with higher molecular mass.

Due to uncertainties during desorption and ionization (energetic, spatial, temporal) ions with equivalent charge/mass ratio are heterogeneously distributed with respect to their kinetic energy and also time of flight. To compensate such resolution losses:

- a) The acceleration voltage can be increased. Then the TOF measurement must be more precise.
- b) Ion reflectors can be used. A reflector introduces an antipolarized electrostatic field between two drift intervals. High-energetic ions can survive longer in this “anti-field” and overcome the lag again in the subsequent drift interval. So faster and slower ions with equivalent m/z -ratio are focused at the detector position and give rise to a narrow signal.
- c) Delayed ion extraction can be applied. Accordingly, the electrical field is switched on with a lag to the laser pulse. High-energetic ions move farther away during the lag time and gain lower kinetic

energy than low-energetic ions. So ions with identical m/z -ratio arrive simultaneously at the detector.

Fragmentation of sample molecules can occur either during the ionization (prompt fragmentation) or in the acceleration/drift interval (metastable fragmentation, post source decay). It is induced by collision of analyte molecules with matrix molecules and produces usually a charged fragment ion and a neutral fragment molecule. Fragment ions generated in the acceleration interval gain different kinetic energies and cause noise in the MALDI spectrum. Fragment ions produced in the drift interval cannot be separated from intact molecule ions in a linear MALDI-TOF. But in the reflector mode charged fragments are shifted to lower mass/charge values because the reflector cannot compensate for their decreased kinetic energy. This drawback is overcome by reflectors with variable voltages.

In the MALDI spectrum several species of a molecule are analyzed. The singly charged protein ion $[M^+H]^+$ dominates in the positive ion mode, but also singly protonated dimers $[2M^+H]^+$ and multiply protonated monomers ($[M^+2H]^{2+}$, $[M^+2H]^{3+}$, ...) are visible. The monoisotopic mass is determined from the exact atomic masses of the most frequent isotope of an element. For peptides with molecular masses < 5 kDa the monoisotopic mass is determined, because it gives rise to the most intensive signal. For larger peptides and proteins the average mass is determined due to the highest signal intensity. The average mass is calculated from the average atomic distribution of the elements. Accordingly, the carbon isotopes are mainly responsible for the isotopic pattern of proteins. Due to adduct formation of peptides and proteins with water, matrix molecules and cations, e.g. Na^+ and K^+ , the peaks are broadened.

3 Materials

A market is never saturated with a good product, but it is very quickly saturated with a bad one.

HENRY FORD

3.1 Chemicals

Acetonitrile, p.a.	Fluka
Ammonia, 25% (v/v)	Merck
Ammonium peroxodisulfate	Roth
Ampicillin	Sigma-Aldrich
Atto 565	Atto-Tec
Calcium chloride	Merck
β -Casein, bovine, 90 % (w/w)	Sigma-Aldrich
Chloroform, p.a.	Roth
Chrom, 99.98%	Balzers
Cy5 TM -NHS ester	GE Healthcare
DMF, 99.98%	Fluka
DMSO	Fluka
DTT	Sigma-Aldrich
EDTA solution, 500 mM, pH 8.0	Fluka
EpoTek 377 two-component epoxy glue	Polytec
Ethanol Rotisolv, HPLC Gradient Grade	Roth
Glycerol	Roth
Gold Wire, 1 mm, Premion, 99.9985%	Alfa Aesar
HBS-N buffer, pH 7.5	GE Healthcare
Hellmanex	Hellma
HEPES, p.a.	Roth
His ₁₀ GCGSADAPE	kind gift from Dr. Joachim KOCH
His ₁₀ Maltose binding protein	kind gift from Annett REICHEL
His ₁₀ Maltose-binding protein (Fluorophore-labelled variants)	kind gift from Annett REICHEL
His ₆ Ubiquitin	Sigma-Aldrich
Hydrochloric acid, 37-38 % (v/v)	Roth
Hydrogen peroxide, 30 % (v/v)	Merck
Ifnar2	kind gift from Dr. Jacob PIEHLER
IFN α 2	kind gift from Dr. Jacob PIEHLER
Imidazole	Merck
IPTG	BTS
Isopropanol, p.a.	Roth

Desorption buffer:

50 mM NaP_i, pH 8.0

300 mM NaCl

50 mM EDTA

3.2.2.2 Size exclusion chromatography

10 mM HEPES, pH 7.5

150 mM NaCl

3.2.3 Protein Immobilization

HBS buffer:

10 mM HEPES, pH 7.5

150 mM NaCl

Nickel sulfate solution:

10 mM NiSO₄ in HBS buffer

Imidazole:

1 M imidazole, pH 7.5

EDTA solution:

100 mM Na₂EDTA, pH 8.0

3.3 Media

3.3.1 LB Medium

10 g peptone/L

5 g yeast extract/L

10 g NaCl/L

The medium is autoclaved for 20 min at 121 °C, 2 bars.

3.3.2 Agarose Plates

10 g peptone/L

5 g yeast extract/L

10 g NaCl/L

20 g low melting agarose/L

pH 7.5

The medium is autoclaved for 20 min at 121 °C, 2 bars. When the medium has cooled down to 50 °C, 100 µg/mL sterile ampicillin is added and the petri dishes are filled with 20 mL medium each. After solidification the plates are stored at 4 °C.

3.4 Plasmids and Strains

3.4.1 pRSET5a and 6a

The genes for the two different subunits of the *Thermoplasma acidophilum* proteasome were cloned into the expression vectors pRSET5a and 6a from *E. coli* (4.3 kbp). The plasmid encodes the

proteasomal α - and β -subunit with the His-tag attached to either the N- or C-terminus of the α -subunit or the C-terminus of the β -subunit in tandem under control of the IPTG-inducible T7-promotor. The plasmids were kind gifts from Drs. Erika SEEMÜLLER, Andreas THEß and Wolfgang BAUMEISTER (Max-Planck-Institute of Biochemistry, Martinsried).

3.4.2 *E. coli* BL21(DE3)

$F^- ompT hsd S_B (r_B^- m_B^-) gal dcm$ (DE3)

This strain is protease-deficient, but encodes genomically T7-RNA polymerase. Transformation competent and cryostocks of transformed cells were a kind gift from Dirk SCHAIBLE and Dr. Silke HUTSCHENREITER.

3.5 Equipment

3.5.1 General Equipment

AFM stainless steel sample disks (15 mm)	Plano
Aekta 100 Explorer	GE Healthcare
Autoclave 5075 ELVC	Tuttnauer Systec
Axiovert LSM 510	Zeiss
BIAcore X	GE Healthcare
Cary 50 Bio UV Vis spectrophotometer	Varian
Contact angle goniometer NRL 100	Ramé-Hart
Ellipsometer AutoEL	Rudolph Research
Incubator Kelvitrone t	Heraeus
Infrared spectroscope IFS 66	Bruker Optik
Ino Lab pH meter	WTW
Kern 770 microbalance	Kern
Liposofast extruder	Avestin
Magnetic stirrer	Ikamag Ret
Membrane vacuum pump	Kobe
Mettler PM 400 balance	Mettler
Mettler PM 460 balance	Mettler
Microwave T.D.S.	Samsung
MilliPore Synergy 185 water system	Millipore
MultiMode NanoScope IIIa AFM	Veeco Instruments
Multiprobe XPS spectrometer	Omicron
NP-G gold coated SiN AFM tips	Veeco Instruments
NP-S NanoProbe SiN AFM tips	Veeco Instruments
NTegra AFM	NT-MDT
Oil vacuum pump	AEG

Thermal metal evaporator MED020	Bal-Tec
Thermomixer	Eppendorf
Thermo Spectronic spectrophotometer	Helios
Tweezers, stainless steel	Plano
Vortexer	Bender & Hobein AG
Voyager-DE™ STR Biospectrometry	Applied Biosystems
Weigh glasses	Merck

3.5.2 Centrifuges and Rotors

Eppendorf Centrifuge 5417R	F-45-30-11
Heraeus Sepatech Megafuge 1.0 R	BS4402/A
Sorvall RC 3C Plus	H6000A
Sorvall RC 5B Plus	SS34

3.5.3 Columns

Hi Trap® Chelating HP (1 mL)	GE Healthcare
Superose™ 6 HR10/30 (24 mL)	GE Healthcare

3.5.4 Supplementary Materials

Cuvettes, quartz glass	Hellma
Cuvettes, plastic	Fisher Scientific
Dialysis tube (12-16 kDa MWCO)	Biomol
Eppendorf tubes	Greiner
Filter paper	Whatman
Flow cell IFC5 (2.4 x 0.5 x 0.05 mm, 2 x 0.06 µL)	GE Healthcare
Glass slide D 263	Präzisions Glas & Optik Iserlohn
Gloves, latex	Terumo Teruglove
Gloves, nitril	Servoprax
Microliter™ syringes	Hamilton
Pasteur pipettes	Merck
Pipettes	Abimed
Pipette tips	Greiner
Polycarbonate membranes, pores: 100 nm	Avestin
Spectra Por™ dialysis tube (6-8 kDa MWCO)	Roth
Spin concentrators, Amicon, 30 kDa MWCO	Millipore
Sterile filters	Millipore
Sterile filters, single use	Roth
Test tubes, sterile, 15 and 50 mL	Greiner

4 Methods

Ότι δε λύνεται, κόβεται

Was sich nicht lösen läßt, das zerschneide.

ALEXANDER DER GROBE

4.1 Biological Methods

4.1.1 Transformation

An aliquot of 350 μ L transformation competent *E. coli* cells BL21(DE3) was thawed on ice for 15 min. 100 ng DNA were added to the cell suspension. The transformation sample was incubated on ice for 40 min and heat-shocked at 42 °C for 3 min. After addition of 1 mL LB-Medium (without ampicillin and pre-heated to 37 °C), the cells are incubated on a shaker at 37 °C for 1 h. By plating 100 μ L medium on agarose with 100 μ g ampicillin/mL and overnight incubation at 37 °C, positive transformants were selected.

4.1.2 Cryostocks

4 mL LB medium with 100 μ g ampicillin/mL were inoculated with the transformants from the plate and grown overnight at 37 °C. Cells from 1.5 mL medium were spun down in cryotubes. After discarding the supernatant, the cells were resuspended in 500 μ L of LB medium containing 50 % (v/v) glycerol, snap-frozen, and stored at -80 °C.

4.1.3 Cell Culture

40 mL LB medium with 100 μ g ampicillin/mL were inoculated either with ampicillin-resistant transformants from the agarose plate or a cryostock and grown overnight at 37 °C in a shaker. 1 L LB medium with 100 μ g ampicillin/mL was inoculated with the overnight culture. Cells were grown up to the midlogarithmic phase ($A_{595} = 0.6$) for induction of protein expression with 1 mM IPTG. After 4 h or overnight expression, cells were harvested in the Sorvall RC 3C Plus centrifuge (20 min at 4000 g, 4 °C). The pelleted cells were resuspended in residual LB medium and recentrifuged in the Heraeus Sepatech Megafuge 1.0 R (15 min at 4000 g, 4 °C). The pellet was snap-frozen and stored at -80 °C.

4.2 Biochemical Methods

4.2.1 Purification of His-tagged Proteasomes

4.2.1.1 Cell Lysis

During cell lysis, the protecting outer walls of the cytosol are disrupted to yield the posttranslationally assembled proteasome. Lysozyme hydrolyzes the β -1,4-glycosidic bonds of the peptidoglycane murein, which forms one layer of the cell wall in *E. coli*. Subsequent ultrasonification disrupts the plasma membrane ending up in the cell lysate.

The cell pellet was thawed on ice in 5 mL of lysis buffer and incubated in the presence of a spatula tip lysozyme for 30 min at 4 °C. The cells were lysed by ultrasonification (12 pulses of 15 s at 40 % continuous output of the Branson sonifier). The lysate was cleared from cell debris by centrifugation (37,000 g, 30 min, 4 °C, SS34-rotor).

4.2.1.2 Immobilized Metal Affinity Chromatography (IMAC)

IMAC is applied to separate His-tagged biomolecules via complex formation from the rest of low-affine binders or non-binders. The column material consists of agarose cross-linked with the tridentate ligand iminodiacetate. After loading with transition metal ions like Zn^{2+} , an octahedral complex is formed with molecules, e.g. proteins, bearing two vicinal histidines. The binding specificity is enhanced in the presence of low concentrations of imidazole, which competes with histidines for metal binding sites. His-tagged proteins are eluted in the order of increasing complex stability with an imidazole gradient or a pH gradient.

The supernatant from the centrifugation step was applied to a Hi Trap® metal chelating column at the Aekta system. Previously the column was loaded with 2 mL 100 mM zinc chloride at a flow rate of 200 μ L/min, free metal ions were removed with H_2O and the column was equilibrated with 10 column volumes (CV) of phosphate buffer containing 20 mM imidazole at a flow rate of 3 mL/min. The supernatant (~ 6 mL) was injected in three fractions followed by washing with the double volume of running buffer at a flow rate of 1 mL/min, while the flow through was collected. After washing the column with 10 CV of running buffer, His-tagged proteasomes were eluted at a flow rate of 2 mL/min by applying a step gradient of imidazole (0-20 % B for 10 CV, 35 % B for 3 CV, 35-100 % B for 20 CV). Protein absorption was recorded at 280 nm, 260 nm and 216 nm. The zinc ions were desorbed with the EDTA of the desorption buffer (5 CV) and the column was washed with H_2O (5 CV) before equilibrating it with 20 % ethanol (5 CV) for long term storage.

4.2.1.3 Size Exclusion Chromatography (SEC)

SEC separates molecules according to their molecular mass due to different permeation of analytes in a porous matrix. High-molecular-weight compounds are impeded from diffusing into pores and elute in the void volume V_0 with the solvent. Low-molecular-weight substances move according to their size in the internal pore volume and the inter-bead volume. Thus they are retained on the column and are eluted within a characteristic elution volume V_e .

For separation of contaminating proteins, the obtained fractions from the IMAC were concentrated in Centriplus (MWCO: 30 kDa) to a final volume of 500 μ L in the presence of 2 mM EDTA and loaded at the Aekta system on a Superose™ 6 column pre-equilibrated with 50 mM NaP_i, 150 mM NaCl, pH 7.5 (phosphate buffer) or 10 mM HEPES, 150 mM NaCl, pH 7.5 (HBS buffer) (2 CV). While recording the absorbance at 280 nm, 260 nm and 216 nm, the protein was eluted at a flow rate of 500 μ L/min.

For column calibration 500 μ L of a solution containing 0.5 % (w/v) each of aldolase (158 kDa), katalase (232 kDa), ferritin (445 kDa) and thyroglobulin (669 kDa) in phosphate buffer was supplied after sterile filtration and eluted under the same conditions. For each calibration protein the logarithm of its molecular mass was plotted against the elution volume. The corresponding molecular mass of the His-tagged proteasome was derived from a linear fit.

4.2.1.4 Concentration Determination

The concentration of proteasome solutions were determined as described previously¹⁶⁰. The extinction coefficient of the proteasome was determined, and following formula for direct read-out of the concentration with UV-VIS spectroscopy at A_{280} nm was obtained:

$$\frac{A_{280}}{1 \text{ cm} * 0.630 \frac{l}{g * cm}} \cdot \frac{1}{680.000 \frac{g}{mol}} = \left[\frac{mol}{l} \right]$$

4.2.1.5 Storage

C- and N-terminally His-tagged proteasomes were stored at 4 °C for 8 and 4 weeks, respectively without any loss of activity in HEPES buffer¹⁶⁰. Proteasomes were snap-frozen after addition of 10 % (v/v) glycerol as cryoprotectant and stored at -80 °C.

4.2.2 Vesicle Preparation and Formation of Biomimetic Lipid Bilayers

First, lipid films were prepared by adding 1.99 mmoles SOPC and 0.01 mmoles OG-DHPE in a vial and evaporating the solvent (chloroform) under vacuum at room temperature. Dried lipid films were swollen for 1 h at room temperature in 5 mL HBS buffer yielding a 0.4 mM suspension.

The lipid suspension was either shock frozen and stored at $-80\text{ }^{\circ}\text{C}$ or processed further to form unilamellar vesicles.

Small unilamellar vesicles (SUVs) are obtained by passing liposomes through membrane filters of a defined pore size (100 nm). “Nucleation track” membranes consist of a thin sheet of polymer, e.g. polycarbonate, with straight-sided pore holes. Due to laser irradiation and chemical etching the pores are uniform in diameter. During extrusion liposomes display flexibility in squeezing through the pores. Large liposomes are broken up and decrease in size after resealing. Finally, after multiple passes through the membrane, the average diameter of the rather homogenous liposome population is slightly smaller than the membrane pore diameter and the liposomes are unilamellar.

Lipid extrusion was performed repetitively (19 times) through polycarbonate membranes (100 nm pore diameter) with a LiposoFast Extruder (500 μL -syringes) according to manufacturer’s manual. In order to obtain lipid bilayers, vesicles were fused on silicon chip substrates for 30-60 min. Afterwards, silicon chips with lipid membranes were rinsed in excess volume of deionized water.

4.2.3 Protein Immobilization

Protein chips with (multivalent) metal-chelating surface functionality were first cleaned with 1 M imidazole (pH 7.5) for 15 min. After extensive rinsing with HBS buffer (pH 7.5), metal chelators were activated for protein capturing with a 10 mM NiSO_4 solution. His-tagged proteins were applied for 5-45 min onto the protein chip surface. This chemisorption time depends strongly on the efficiency of the fluidics. In devices with extremely developed fluidics (e.g. BIAcore) short time periods in the range of 5 min are sufficient. In opposite, in AFM experiments longer adsorption times in the range of 30-45 min are required for efficient protein immobilization. Desorption of proteins from the chip surface is achieved by rinsing with 1 M of imidazole and deactivation of chelators occurs by rinsing with 100 mM of EDTA. Again, reaction times depend strongly on the fluidic systems and are in the range of 5-60 min.

4.3 Biophysical Methods

4.3.1 Atomic Force Microscopy

AFM experiments were performed with a Digital Instruments/Veeco NanoScope IIIa SPM MultiMode AFM or an NTegra AFM in a commercial quartz fluid cell. Special care has to be taken to protect the AFM scanner from any liquid exposure. Therefore, the piezo tube was protected always with two layers of nitrile and latex sheets. Operation of the AFM is conducted according to

manufacturer's user manual. If not stated otherwise, NP-S cantilevers with a force constant of 0.06 N/m (Veeco Instruments) were used for all experiments. Imaging was performed in Tapping ModeTM at resonance frequencies of around 9 kHz in HBS buffer at drive amplitudes of 100 to 200 mV. Imaging of the chip surfaces was always performed in HBS buffer.

4.3.2 Chemical Force Microscopy

In chemical force microscopy (CFM), the AFM tip is modified with specific chemical functional groups¹⁶⁵. Hence, the chemically modified tip enables sensing and visualization of chemical properties of the sample surface either with the friction signal in contact mode or the phase lag signal in Tapping ModeTM¹⁶⁶. Both of these signals are proportional to the adhesion between the tip and sample, and can be measured simultaneously with topography.

Gold coated AFM tips were functionalized with a His₁₀-tag peptide (H₁₀GCGSADAPE). The tips were incubated in 20 μ M ethanolic peptide solutions for 5 days at room temperature. Via the thiol group of a single cysteine, the peptides form a monolayer on the gold coated AFM tip. After functionalization, the tips were rinsed gently with ethanol and stored at 4 °C in ethanol until usage.

4.3.3 Surface Plasmon Resonance

Surface plasmon resonance (SPR) measurements were performed on a BIAcore X system at 25 °C, with a flow rate of 10 μ L min⁻¹, if not stated otherwise. HBS buffer was used as running buffer and for all dilutions. Protein immobilization on the chelating SAM surface was carried out by sequential injections of 35 μ L of NiSO₄, followed by injection of 35 μ L of HBS buffer supplemented with imidazole (200 mM), and then followed by addition of His₆-tagged interferon receptor (His₆ ifnar2, 300 nM)¹⁶⁷. To study the activity of His₆ ifnar2 after immobilization, 35 μ L of its ligand IFN α 2 (200 nM) were injected. To determine the amount of unspecific binding, the immobilization protocol was carried out identically, but without addition of nickel ions. In imidazole competition experiments increasing concentrations of imidazole were injected after specific immobilization of His₆ ifnar2 at flow rates of 40 μ L min⁻¹. The surface was rinsed with HBS buffer after each injection. Imidazole (1 M) and EDTA (200 mM) diluted in HBS buffer were used to remove the protein and the Ni²⁺ ions, respectively. Data evaluation was performed using standard analysis software.

4.3.4 Confocal Laser Scanning Fluorescence Microscopy

Patterned chips were imaged by confocal laser scanning fluorescence microscopy (Axiovert LSM 510). During chip handling it was ensured that the chip remained wet all the time. The chips

were mounted into a self-built flow chamber and imaged using a Plan-Neofluor 40x or 63x oil-immersion objective and an inverted microscope set-up. An argon laser (488 nm, 25 mW) was used for excitation of Oregon Green, Atto565, and QuantumDot 655. Fluorescence image data were processed with LSM Zeiss software (Zeiss).

4.4 Surface Chemical Methods

Handling of surfaces and especially surface chemical modification requires a high degree of cleanliness. All tools (e.g. tweezers, glass ware, etc.) were treated 2 x 15 min at 85 °C with standard cleaning solution (SC) 1, which is composed of a 5:1:1 mixture of MilliPore water, hydrogen peroxide (25%), and ammonia (30%). This cleaning step was followed by an extensive rinsing with UV-cleaned MilliPore water. UV-cleaned water, as provided by MilliPore Synergy 185 water system, protects from organic contaminants, which can impair surface chemical reactions.

4.4.1 Fabrication of Gold Chips

4.4.1.1 Gold Evaporation on Glass and Wafer Substrates

Gold surfaces were prepared by evaporation of thin gold films either on glass or standard (100)-silicon wafers. Wafer and glass substrates were cleaned before and after evaporation with SC1 solution for 2 x 15 minutes at 85 °C, followed by extensive rinsing in MilliPore water. Wafer substrates were prepared as published previously¹⁶⁸ and used for contact angle goniometry, ellipsometry, infrared reflection-absorption spectroscopy, and fluorescence microscopy. To perform surface plasmon resonance or mass spectrometry experiments, glass substrates were coated with a 2.5 nm-layer of chromium followed by deposition of a 40 nm or 150 nm thick gold layer in a Bal-Tec Med020 system at a vacuum of 10^{-6} mBar. The specific thickness of the gold layer is due to the application. For SPR semi-transparent gold chips are required, in opposite highly reflective gold layers are required in mass spectrometric experiments. Evaporation of gold on silicon or glass substrates should be performed under (ultra-) high vacuum conditions in order to obtain homogenous gold surfaces.

4.4.1.2 Gold Evaporation on Mica Substrates

For atomic force microscopy, ultraflat gold surfaces were prepared according to the template-stripped gold protocol as previously described¹⁶⁹⁻¹⁷¹. High quality muscovite mica was freshly cleaved and coated with 150-200 nm gold in a Bal-Tec Med020 system at a vacuum of 10^{-5} mBar. Such rather high pressure is fully sufficient for preparation of ultraflat gold surfaces on mica substrates. The temperature in the evaporation chamber was not actively controlled.

1-2 min after evaporation, the chamber was ventilated and the gold-coated mica sheets were glued with EpoTek 377 to AFM stainless steel sample disks. These mica-gold-steel sandwiches were cured at 150 °C for 2 h and equilibrated to room temperature overnight. These chip precursors can be stored in a sealed PETRI dish for several months. Before usage, the mica layer was removed from the gold surface by chemical stripping in tetrahydrofuran (THF) for 10-30 min. The ultraflat gold chips can now be functionalized in thiol solutions.

4.4.2 Surface Functionalization of Gold Chips

Before exposure to the thiol solutions, gold substrates are pre-conditioned in the corresponding organic solvents (e.g. ethanol, acetonitrile, THF). Mixed SAMs with various mixing ratios were formed from solutions of matrix thiol and either mono-NTA thiol or multivalent chelator bis-NTA thiol (20 μM final concentration in acetonitrile or THF, see chapter 5.1 for detailed description). After chemisorption (for 36 h), the SAMs were sonified in acetonitrile or THF, rinsed with ethanol, sonified again in MilliQ water, and stored in MilliQ water at 4 °C if not used immediately.

4.4.3 Microcontact Printing

PDMS stamps were prepared on the same master and under similar conditions as described by ZHOU and colleagues¹⁷². For microcontact printing (μCP) the general protocol developed by DELAMARCHE and co-workers¹⁷³ was used. Briefly, the prepolymer was cured in an oven at 65 °C for around 2 h. Before the imprinting, the stamps were rinsed with ethanol, blown dry with nitrogen gas and inked by applying a droplet (1 $\mu\text{L}/\mu\text{m}^2$ area of the stamp) of ethanolic solution of eicosane thiol (200 μM) for 30 s. The excess liquid was blown away from a stamp with nitrogen gas and the stamp was further dried under stream for another 30 s. Then the stamp was immediately brought into contact with a gold chip for 3-10 s. Afterwards, the chip was soaked in a 20 μM solution of matrix thiol and bis-NTA thiol (97 mol% and 3 mol%, respectively) in acetonitrile. The adsorption time ranged from 3 to 48 h. The prepared chips were washed and loaded with Ni^{2+} ions as described above.

4.4.4 Coupling of tris-NTA Modules to Amino Biphenyl SAMs

A mixture in following sequence was prepared: 1.0 mL Chloroform + 0.03 mL tert-butyl protected *tris*-NTA (10 mM) + 1.0 mL DIC. The mixture was pre-heated at 75 °C for 5-8 min. E-beam treated NBP-SAM chips were put into the glass vial and kept at 75 °C for 30 min. Rinsing 5 times with chloroform was followed by a deprotection in TFA at room temperature for

3-4 h. The chips with deprotected tris-NTA groups were rinsed 10 times with MilliPore water and stored until usage at 4 °C.

4.5 Surface Physical Methods

4.5.1 Contact Angle Goniometry

Contact angles were measured with a Ramé-Hart NRL 100 goniometer without control of the humidity in the ambient, using MilliQ water. Taking the high surface energy of the hydrophilic surfaces into account, only one measurement of the advancing and the receding contact angle was performed per sample.

4.5.2 Ellipsometry

For single-wavelength ellipsometry, average values of the refractive index of the clean gold sample, analyzed prior to the incubation, were used. The refractive index of the substrate and the results of the ellipsometric measurements on the SAMs were taken into a model 'ambient/organic film/gold', assuming an isotropic, transparent organic film¹⁷⁴ with the refractive index of $n = 1.5$ ¹⁷⁵⁻¹⁷⁷. The film thickness was calculated as average at three different spots on at least four samples for each SAM.

4.5.3 Infrared Reflection-Absorption Spectroscopy

The reflection-absorption spectra (IRAS) were recorded at room temperature on a Bruker IFS 66 system, equipped with a grazing angle (85°) infrared reflection accessory and a liquid-nitrogen-cooled MCT detector. The measurement chamber was continuously purged with nitrogen gas during the measurements. The acquisition time was around 10 minutes at 2 cm^{-1} resolution, and three-term BLACKMANN-HARRIS apodization function was applied to the interferograms before FOURIER transformation. SAMs of deuterated hexadecane thiolate ($\text{HS}(\text{CD}_2)_{15}\text{CD}_3$) were used as reference.

4.5.4 X-Ray Photoelectron Spectroscopy

Self-assembled monolayers were analyzed by X-ray photoelectron spectroscopy (XPS) with an Omicron Multiprobe Spectrometer, utilizing Al K_α irradiation. The parameters were optimized to minimize X-ray damage and to obtain an energy resolution of 0.9 eV. Binding energies are referred to the Au $4f_{7/2}$ peak at 84.0 eV. The thickness of the pristine SAMs, as calculated from the attenuation of the Au $4f_{7/2}$ signal using a photoelectron mean free path of 36 Å, was 12.5 ± 0.7 Å, which corresponds to a well ordered, densely packed nitro-biphenyl thiol (NBPT) SAM. Lateral

cross-linking and generation of terminal amino groups in the monolayer were performed by irradiation with 100 eV electrons in high vacuum ($p < 5 \times 10^{-7}$ mbar) at a dose of $\sim 40000 \mu\text{C}/\text{cm}^2$.

5 Results & Discussion

*Quand tu veux construire un bateau,
ne commence pas par rassembler du bois,
couper des planches et distribuer du travail,
mais réveille au sein des hommes le désir de la mer grande et large.*
Antoine de Saint-Exupéry

One major goal of this Ph.D. thesis was the development of a generic protein chip platform suitable for different biophysical techniques. Various biophysical applications of this protein chip platform were established (in part within scientific collaborations) and will be presented in the next chapter (5.1).

The vision at the beginning of these research projects was the invention of a novel lithographic principle for fabrication of bioactive protein nanoarrays. In chapter 5.2 the successful strategy will be discussed. This new tool merges nanotechnology and biochemistry to nanobiotechnology and offers new perspectives in nanosciences and single-molecule biochemistry.

Alternative methodologies for generation of nanopatterned protein chips based on e-beam nanolithography and silicon semi-conductor technologies were explored within the scope of cooperations. The achievements of these side-projects will be demonstrated in chapters 5.3 and 5.4.

5.1 Development of a Generic Platform for Protein Chip Technologies

5.1.1 Synthesis of Multivalent Chelator Thiols

Surfaces of gold in comparison to silicon (oxide) allow a more flexible and convenient chemical, almost defect free modification upon the formation of self-assembled monolayers (SAMs). Oligoethylene glycol (OEG) thiols have been optimized for their anti-adsorptive properties minimizing unspecific protein adsorption¹⁷⁸⁻¹⁸². The triethylene glycol matrix thiol **6** (see Figure 21) operates as a protein-repellent matrix that can be doped with functionalized thiols forming a mixed SAM. In addition to the mono-NTA thiol **9**, a multivalent chelator thiol **12** (bis-NTA thiol) for stable and switchable immobilization of histidine-tagged proteins was introduced. The synthesis of all thiols is modular and based on a 16-mercapto-hexadecanoic acid linked to a triethylene glycol (EG₃) moiety. The question of the optimal alkyl chain length, which determines the chemisorption rate on gold and thus SAM formation, is still controversial⁸². As some kind of literature standard a hexadecane alkyl unit was used for the synthesis. The synthesis was optimized so that a single precursor **3** enables an easy and economic assembly of different compounds, such as the matrix

thiol **6**, the mono-NTA thiol **9**, and bis-NTA thiol **12**. The synthesis of these compounds is outlined in Figure 21. The thiol group of the initial compound 16-mercaptohexadecanoic acid **1** becomes protected by zinc acetate and yields 16-acetylsulfanyl-hexadecanoic acid **2**. This intermediate is coupled to the triethylene glycol (EG₃) moiety via ester bond leading to the precursor **3**. Matrix thiol **6** was synthesized from the precursor **3** by deprotection of the sulfur group with hydrazinium acetate. Coupling of *tert*-butyl-protected mono-NTA **4** or bis-NTA **5** via carbamate linkage and subsequent deprotection of the thiol and carboxyl groups yielding mono-NTA thiol **9** and bis-NTA thiol **12**, respectively.

The deprotection strategy was a critical aspect of the synthesis. At first the thiol group from **7** and **10** is deprotected by hydrazinium acetate yielding **8** and **11**. Because of the possibility that free thiol groups become butylated by the liberated *tert*-butyl moieties from the deprotected NTA groups an efficient strategy for capturing of these *tert*-butyl groups is needed. Eventual deprotection of the thioether bond would require harsh reaction condition and probably degrade the intermediates and thus lower the yield of the final products.

TFA was therefore used for deprotection and EDT as a scavenger for the released *tert*-butyl groups, yielding the final products **9** and **12**. In contrast to other functionalized thiols described, the metal-chelating group is coupled via ester, and not via ether or amide chemistry, yielding a higher efficiency and highly flexible synthesis. The final products (**6**, **9**, **12**) were analyzed by mass spectrometry for their long-term stability in solution and within self-assembled monolayers. Even after 5 days, hydrolysis of the ester bond was not observed. Details on the synthesis and analyses of all products are given in TINAZLI et al. 2005¹⁸³.

5.1.2 Formation of Self-Assembled Monolayers with Multivalent Chelator Thiols

SAMs formed from one component solutions of matrix thiol **6**, mono-NTA thiol **9**, or multivalent bis-NTA thiol **12** in acetonitrile (hereafter referred as SAM **6**, SAM **9** and SAM **12**, respectively) are analyzed by contact angle goniometry and ellipsometry (Figure 22). The contact angles of SAM **6** indicate that the alkyl portion of the molecules being attached to gold, and that the triethylene glycol (EG₃)¹⁸⁴ and NTA portions are exposed to the ambient. The thickness (*d*) of SAM **6** suggests that the all-trans alkyl chains are tilted at approximately 30° to the surface normal corresponding to a theoretical alkyl layer thickness of around 18 Å. Since the average incremental thickness per one EG unit is 3 Å^{185, 186}, the total expected *d* for SAM **6** is 27 Å, a value in good agreement with the experimental results. SAMs **9** and **12** display θ_a values that significantly differ from SAMs terminated by carboxyl groups (typically below 10 deg¹⁷⁵).

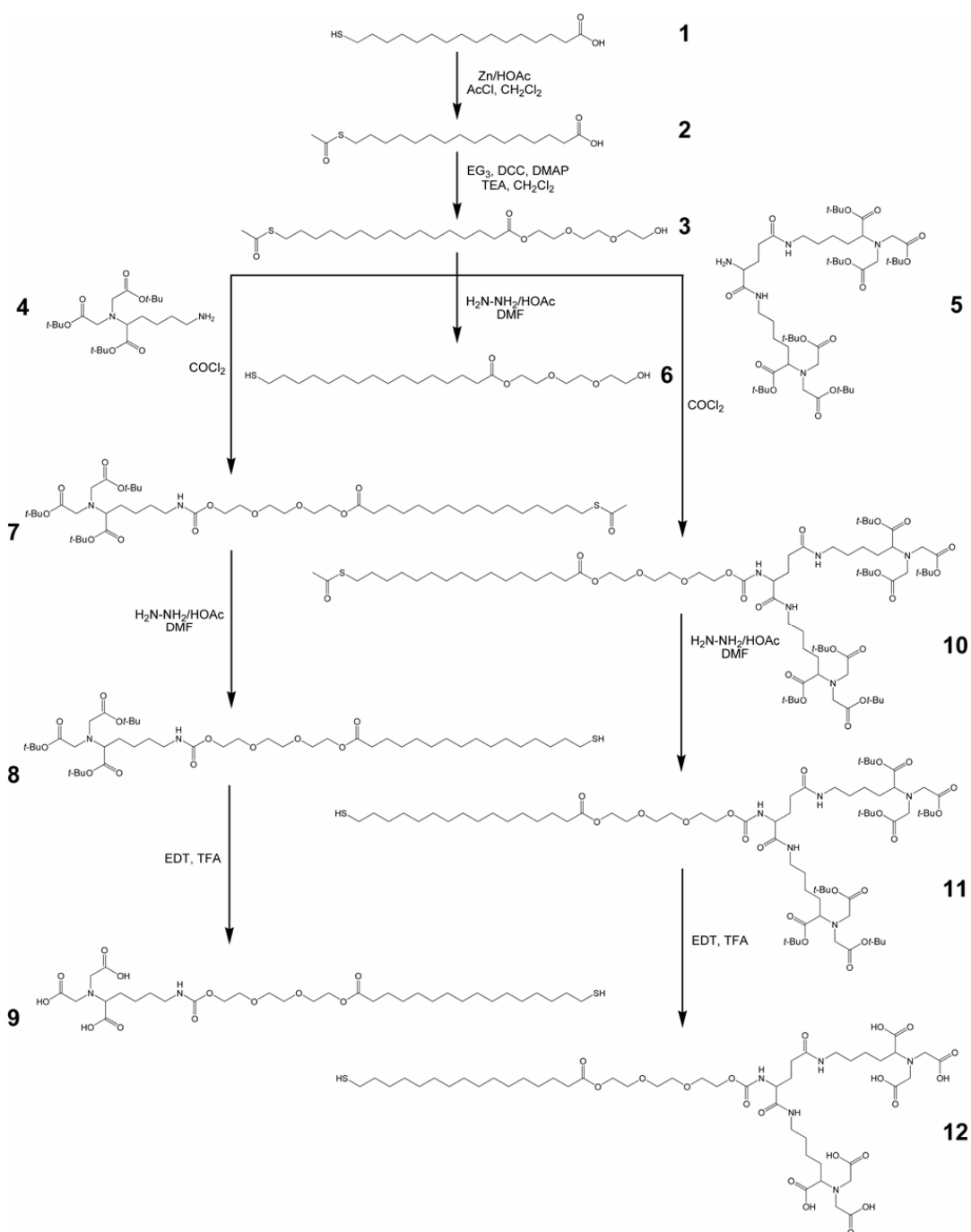


Figure 21: Modular synthesis of mono- and multivalent chelator thiols (9 and 12).

Also, the contact-angle hysteresis is large, suggesting that the surface is heterogeneous, i.e. the pure mono-NTA and bis-NTA SAMs appear to be disordered. Infrared reflection-absorption spectroscopy (IRAS) is used to provide information about the molecular packing and orientation of different groups in the SAMs under investigation.

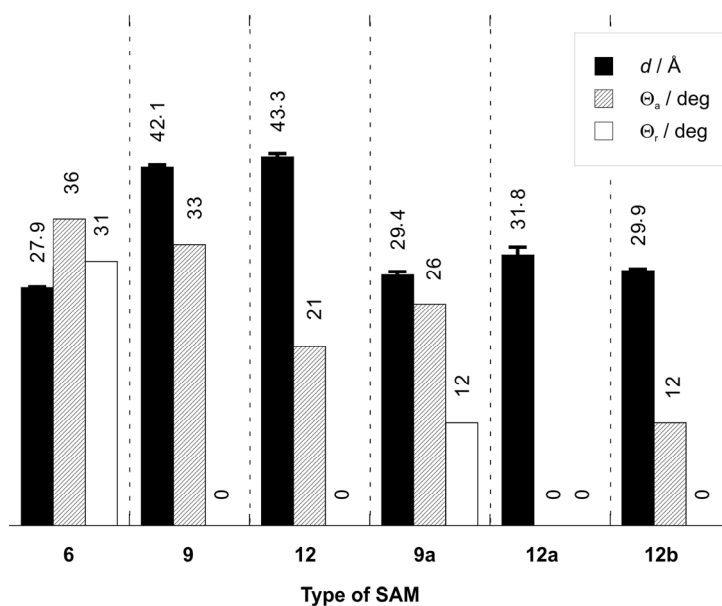


Figure 22: Ellipsometric thickness d and water contact angles (advancing θ_a and receding θ_r) of the investigated self-assembled monolayers (SAMs). Compounds **6**, **9** and **12** were used to form SAMs **6**, **9** and **12**, respectively. Mixed SAMs **9a**, **12a**, and **12b** were formed from mixtures of 3 mol% of compound **9** and 97 mol% of **6** (**9a**), or **12** and **6** (**12a** and **12b**). Acetonitrile was used as a solvent for all the SAMs except for **12b**, which was formed in THF. Value “0” is used to denote contact angles that are $< 10^\circ$.

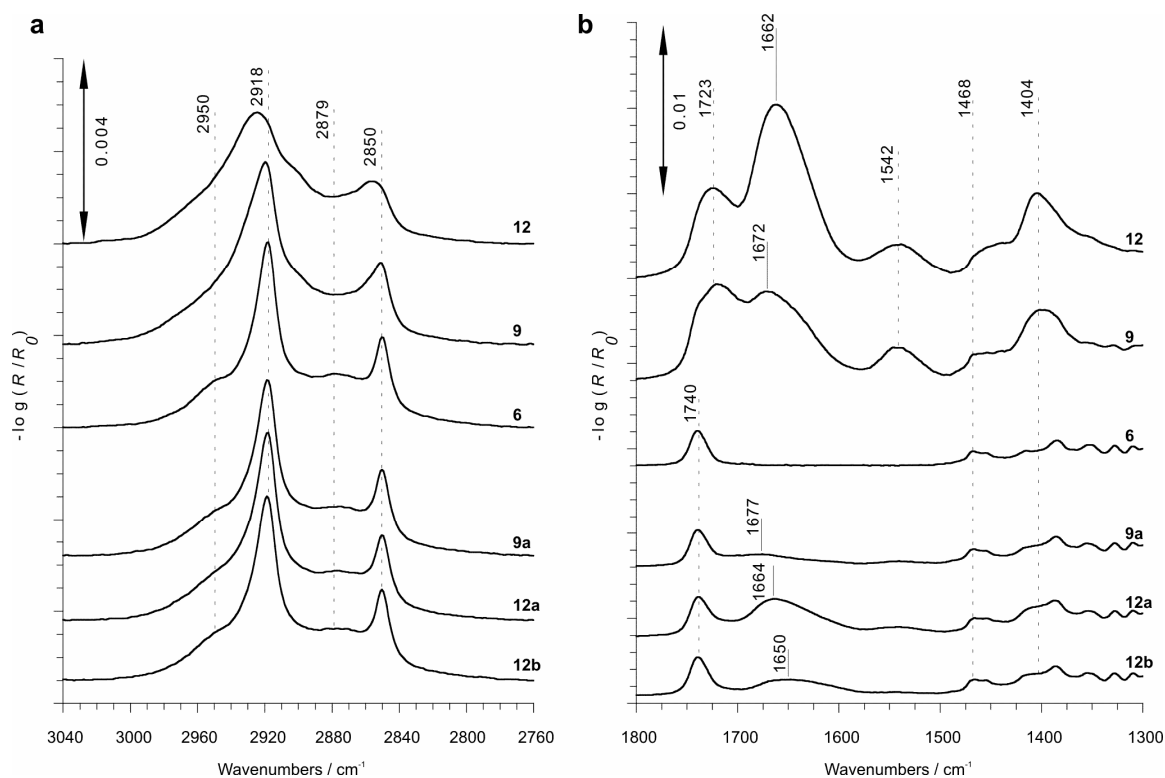


Figure 23: Infrared reflection-absorption spectra of one-component SAMs **6**, **9** and **12** and mixed SAMs **9a**, **12a**, and **12b** showing (a) the CH stretching region (see Figure 22 or text for the description); (b) The fingerprint region.

The CH stretching region indicates that SAM **6** consists of a layer of densely packed, crystalline alkyl chains, as evidenced by the asymmetric (ν_a) and symmetric (ν_s) CH_2 stretches of the alkyl chains at 2918 and 2850 cm^{-1} , respectively (Figure 23a). The CH_2 ν_a and ν_s modes appearing as a shoulder near 2950 cm^{-1} and as broad features in between the sharp alkyl peaks originate from the ethylene glycol tails. A distinctive ν_a peak close to 2890 cm^{-1} is indicative for ethylene glycol tails adopting the helical conformation. The absence of this peak suggests that the EG_3 tails do not adopt a helical conformation. Instead they are more likely adopting an amorphous-like conformation^{187, 188}. The low frequency region of SAM **6** (Figure 23b), which is nearly identical to the previously reported EG_4 -terminated SAM^{184, 187}, contains the ester $\nu(\text{C}=\text{O})$ mode at 1740 cm^{-1} the CH_2 scissors modes at 1468/1455 cm^{-1} ^{184, 189}, as well as other ester and EG_3 related peaks below 1300 cm^{-1} (not shown).

For SAM **9**, the alkyl $\nu_a(\text{CH}_2)$ peak is broadened and shifted upwards to 2920 cm^{-1} , a consequence of an increasing population of gauche defects. Moreover, for the SAM **12**, the ν_a and ν_s modes appear at 2925 and 2856 cm^{-1} , respectively, indicating liquid-like alkyl chains, i.e. the alkyl layer seems to collapse due to the space demanding bis-NTA group. The specific IR signature of the tethered NTA groups^{190, 191} can be found in the fingerprint region (Figure 23b). First of all, a strong carboxyl $\nu(\text{C}=\text{O})$ peak is found at 1723 cm^{-1} ¹⁹². Secondly, a significant fraction of the terminal carboxylic groups is deprotonated, as evidenced by strong peaks at 1672 cm^{-1} (1662 cm^{-1} for **12**) and 1404 cm^{-1} that are due to carboxyl ν_a and ν_s modes, respectively. In the fingerprint region, the amide II band at 1542 cm^{-1} can also be found, while the amide I band overlaps with the much stronger carboxyl ν_a peak discussed above.

Based on the above findings, it is clear that for the specific protein immobilization through the His₆-tag, the chelator groups should be dispersed in an inert two-dimensional “matrix” provided by **6**. In the previous studies on His₆-tag protein immobilization on planar lipid bilayers, 3 mol% concentrations of NTA-lipids gave good results³⁵. Due to their superb properties only SAMs formed from 3 mol% mixtures of **9** or **12** with **6** in acetonitrile and THF that provided an optimal platform for the specific immobilization of histidine-tagged proteins will be discussed.

Mixed SAMs **9a** and **12a** formed from acetonitrile solution of either **9** or **12** (3 mol%) and **6** (97 mol%) are thicker than the SAM **6** (Figure 22). They have lower contact angles with a higher hysteresis than SAM **6**, but most importantly the hysteresis and thereby the heterogeneity is decreased as compared to the single component SAM of **9** and **12**. Moreover, the stable position of the alkyl ν_a and ν_s peaks confirm that the alkyl chains are densely packed in a crystalline, all-trans conformation (Figure 23a). The terminal NTA groups can be easily recognized in the fingerprint

region: the $\nu_a(\text{COO}^-)$ peak appears at 1677 and 1664 cm^{-1} for **9a** and **12a**, respectively. Assuming a similar random orientation of the NTA groups in SAMs **9a** and **12a**, the diagnostic NTA peaks can be used to compare the fraction of NTA moieties in the SAMs. For this purpose, the ester $\nu(\text{C}=\text{O})$ peak is subtracted from the spectra of the mixed SAMs, and the remaining peaks are integrated in the region from 1745 to 1577 cm^{-1} . The integrated peak intensities reveal that in SAM **12a** the total amount of NTA is 3.3 times higher than in SAM **9a**, a significant deviation from the expected factor of 2. To reduce the amount of compound **12** in the mixed SAMs, the solvent was changed from acetonitrile to THF. This effect is confirmed by the reduced thickness values (Figure 22) for SAM **12b** as compared to SAM **12a** (~ 2 Å difference) and by an increase of θ_a . Importantly, the IRAS data show that the change of the solvent does not affect the structure of the alkyl layer (Figure 23a). A slight red shift of the $\nu_a(\text{COO}^-)$ mode (Figure 23b) can be explained by the presence of different counter ions in the samples after drying. The peak integration procedure for SAM **12b** suggests that the total amount of the NTA moieties now is 1.5 times higher than in the case of SAM **9a**. However, it has to be stressed that the IR peak analysis yields only an approximate estimation of the amount of mono- and bis-NTA groups in the SAMs under investigation because of possible differences in peak intensity due to electrostatic interaction and/or orientation effects. Nevertheless, the employed set of the surface analysis techniques clearly shows that SAMs **9a** and **12b** consist of a highly ordered alkyl layer, which, in turn, is covered by an amorphous-like EG_3 layer with sparsely distributed mono- or bis-NTA moieties. The stoichiometric ratios of the constituent functional thiol molecules in these SAMs are very similar and each functional thiol molecule corresponds to one docking site for His₆-tags. Therefore, the well-defined SAMs **9a** and **12b** are used for further investigation.

5.1.3 Switchability of His-tag Recognition

Recognition and capturing of His-tags by the chelating SAMs is metal ion-dependent. Chemically modified AFM tips with His-tag peptides provide an elegant way for the visualization of this dependence. In contrast to conventional AFM – which provides solely topographic information – chemical force microscopy (CFM) functions as a “chemical eye” with nanoscale resolution. Hence, discrimination of His-tag binding or non-binding states of the chelating SAM is enabled by CFM.

By microcontact printing patterns with chelating thiols and non-chelating thiols were prepared. In absence of nickel ions there is no specific interaction between the His-tag peptide modified AFM tip and the chelating SAM (Figure 24). The printed patterns are not detectable (“off”). By addition of nickel ions the interaction is switched on (“on”). Different interaction forces

between AFM tip and chelating/non-chelating surface areas affect a phase lag in TappingMode™, which is visible in the phase image. Complexation of nickel ions by EDTA switches the specific interaction between chelating surface areas and the His-tag peptide at the AFM tip off (“off”) again. Chemical force microscopy is a valuable methodology for convenient affinity mapping of surfaces and especially useful for initial studies of protein chip functionalities without the involvement of proteins.

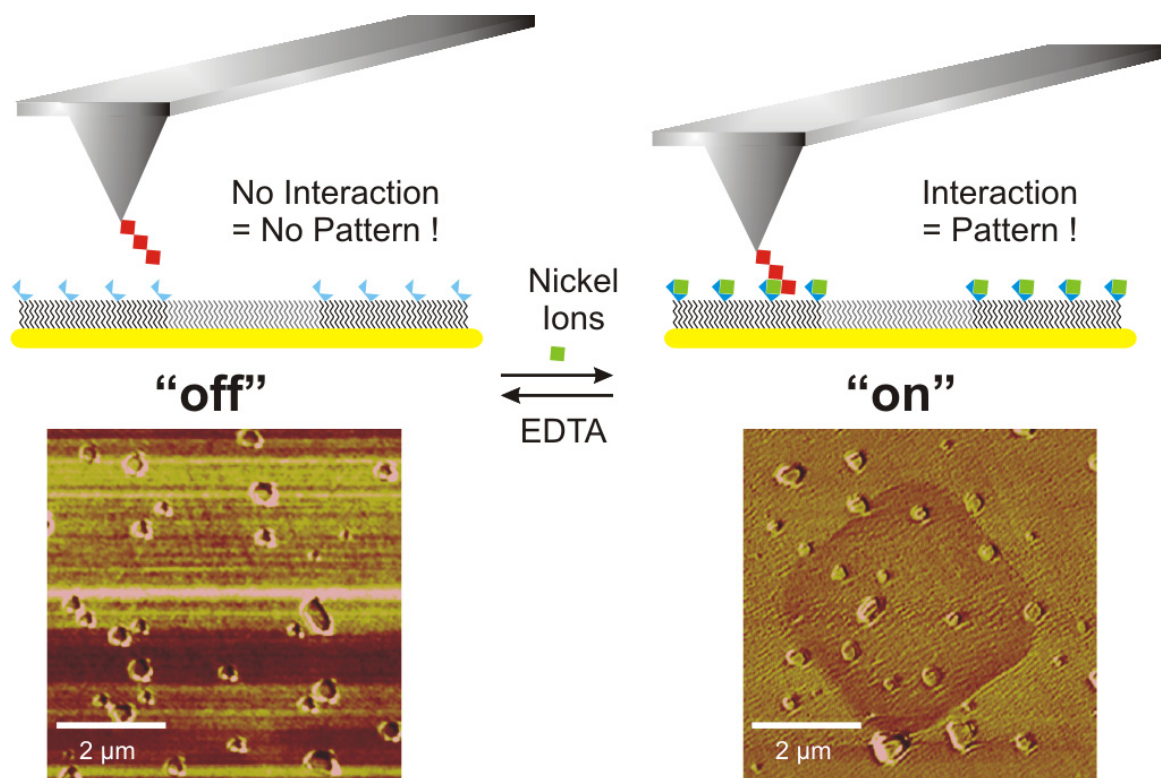


Figure 24: Chemical force microscopy enables affinity imaging of surfaces at nanoscale. In absence of nickel ions there is no specific interaction between the His-tag modified AFM tip and the chelating SAM (“off”). Addition of nickel ions enables the specific interaction between the chemically modified AFM tip with the surface. The AFM tip has different affinities to different surface areas. The contrast of the printed square becomes clearly visible (“on”). By addition of complexation agents like EDTA, nickel ions are captured and the original state becomes re-established (“off”). The scattered spots are surface defects.

5.1.4 Protein Immobilization Proofing Specificity, Activity, and Reversibility

As a model system to evaluate the developed sensor surface biochemically, the His₆-tagged extracellular domain of the human interferon receptor ifnar2 (His₆ ifnar2) and its ligand IFNα2 were chosen. This protein was shown to be highly sensitive to immobilization procedures¹⁹³, and thus is well suited for studying functional immobilization. Here, receptor immobilization and subsequent ligand binding was monitored in real-time by surface plasmon resonance.

First, protein immobilization on a bis-NTA chip surface (SAM **12b**) was monitored by injection of His₆ ifnar2 (300 nM). After following receptor association and dissociation, the chip surface was regenerated by imidazole (1 M) and EDTA (200 mM) and used again. Figure 25a shows three overlaid sensorgrams of repeated His₆ ifnar2 immobilization on an individual chip. The signal response, which is proportional to the amount of immobilized protein, remains almost constant at approximately 850 resonant units (RU), demonstrating efficient regeneration and high reproducibility of protein immobilization on the chip surface. For the sake of simplicity the regeneration steps are omitted in the sensorgrams. Hence, the same chip can be re-used for protein immobilization many times with the same binding capacity.

Next, ligand-receptor interaction assays with His₆ ifnar2 and its ligand IFN α 2 were performed on multivalent chelator SAMs. In Figure 25b, the sensorgram of receptor immobilization on a bis-NTA SAM is shown. After activation of the bis-NTA chips with nickel ions followed by washing with buffer, the injection of His₆ ifnar2 (300 nM) yielded a stable signal of approximately 750 RU (step 1). Subsequent binding of IFN α 2 demonstrates that approximately 90% of immobilized His₆ ifnar2 remain functional (step 2). IFN α 2 dissociates from His₆ ifnar2 with its typical dissociation rate constant of around 0.01 s^{-1} ¹⁹³ and thus confirms the specificity of the interaction to the immobilized His₆-tagged receptor. After injection of imidazole (1 M) and EDTA (200 mM) (step 3 and 4) immobilized His₆ ifnar2 is almost completely removed and the metal-chelating surface is recovered. In contrast to this specific binding assay, non-specific binding of the receptor to the functionalized surface was negligible low in absence of nickel ions (approx. 40 RU, dashed line). In the absence of immobilized receptor under identical conditions, only 1% non-specific binding of IFN α 2 was observed (data not shown).

Both types of chelating SAMs, with mono-NTA thiols as well as with bis-NTA thiols, show a protein binding behavior similar in respect to specificity and functionality of the immobilized protein. The key difference between mono- and multivalent chelator SAMs becomes evident in imidazole competition assays. The effect of dissociation of His₆ ifnar2 from mono-NTA and bis-NTA SAMs was systematically compared at increasing imidazole concentrations (0-20 mM) (Figure 26a and 26b). The strongly decreased dissociation rate of the His₆-tagged protein from the bis-NTA group in comparison to the conventional mono-NTA group is evident. Unlike the conventional mono-NTA, multivalent chelator chips exhibit a decreased dissociation rate of His₆ ifnar2 (Figure 26c). The desorption kinetics of His₆ ifnar2 from the mono- and multivalent chelator surface in dependence of the imidazole concentration is compared in Figure 26d. A clear shift of the imidazole-induced complex dissociation to higher imidazole-concentrations from mono-

NTA to bis-NTA complexes was observed. In comparison to the mono-NTA/His₆-tag complex the half-life of protein binding was prolonged in the bis-NTA/His₆-tag complex due to multivalent interactions. These different dissociation properties enable orthogonal protein immobilization using the same tag but various (mono- or multivalent) chelators. Furthermore, chip-to-chip variations are negligible as demonstrated by the remarkable high reproducibility of the SPR experiments. The introduction of the bis-NTA unit enables quasi-irreversible, highly specific, and switchable immobilization of functional His₆-tagged proteins.

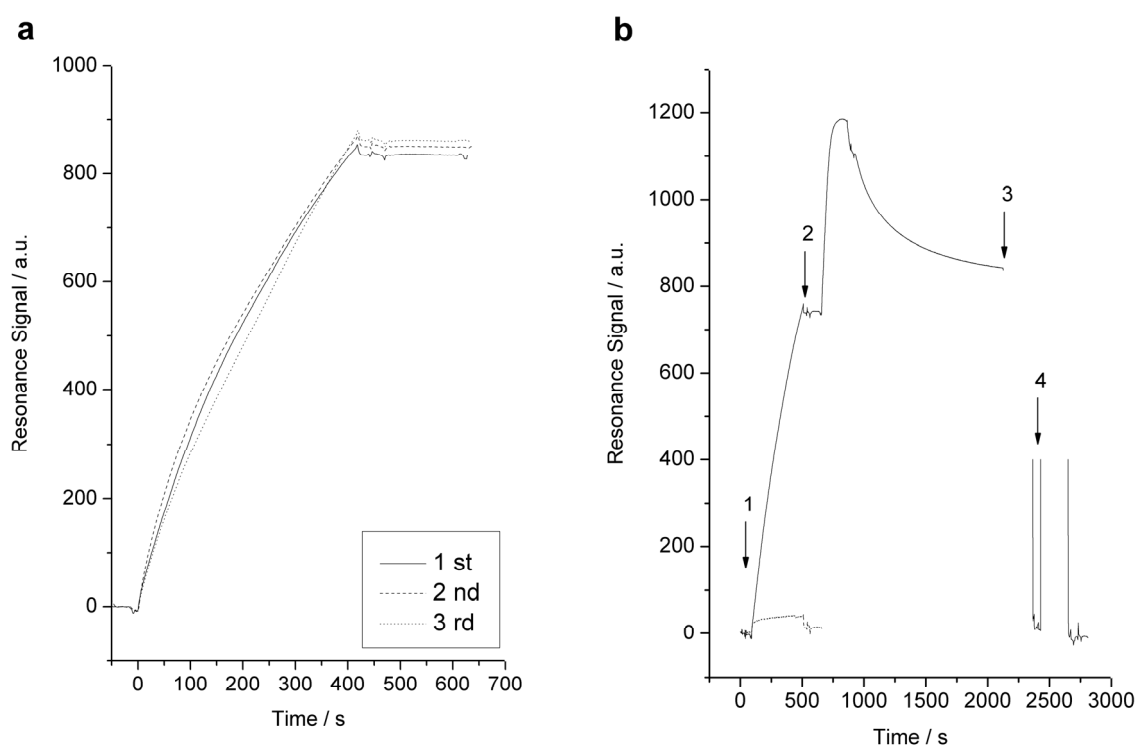


Figure 25: Specific receptor binding and ligand interaction followed by surface plasmon resonance. (a) A bis-NTA chip was used for immobilization of His₆-tagged receptor His₆ ifnar2 and regenerated completely three times demonstrating the high reproducibility of the protein immobilization. Regeneration of the chip surface is achieved by injection of imidazole and EDTA. The sensorgrams of the first, second and third cycle of immobilization are overlaid. The regeneration steps are not shown. Resonance units (RU) are plotted in arbitrary units (a.u.). (b) Typical sensorgrams of immobilized His₆ ifnar2 and subsequent binding of its ligand IFN α 2 on a functionalized multivalent bis-NTA surface with (solid) and without (dashed) loaded nickel ions. Injection of His₆ ifnar2 (1), followed by IFN α 2 (2). After the binding experiment, the chip surface was regenerated with imidazole (3), and EDTA (4).

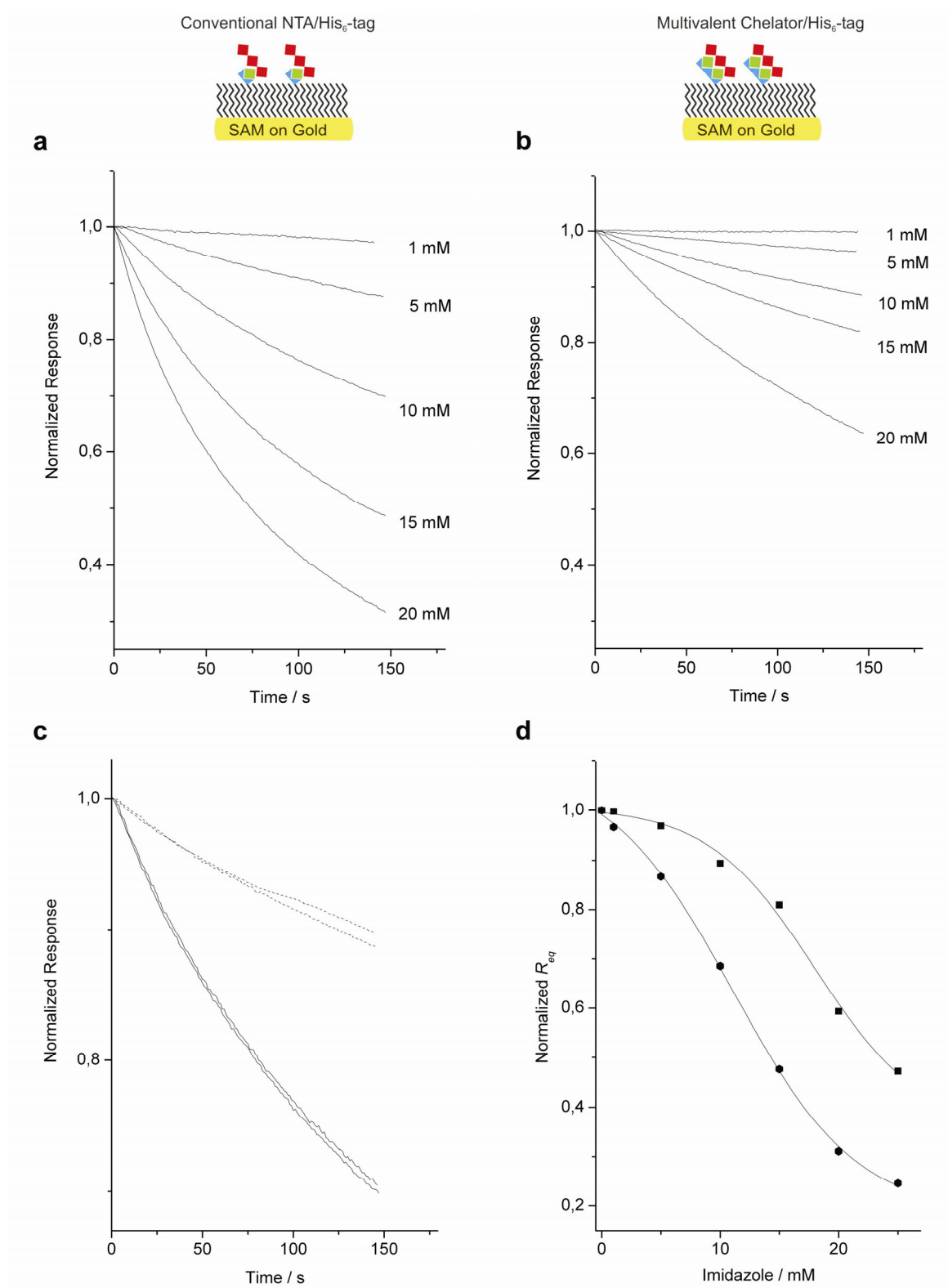


Figure 26: Different stability of protein binding to the mono-NTA and bis-NTA chips. (a) Increasing concentrations of imidazole induce dissociation of immobilized His₆ ifnar2 on the mono-NTA and (b) on the bis-NTA surface with different rates. (c) 10 mM imidazole affects dissociation of immobilized His₆ ifnar2 on two individual bis-NTA chip surfaces (dashed) and two individual mono-NTA surfaces (solid) with different efficiency. (d) Bis-NTA/His₆-tag complexes dissociate only at higher imidazole concentrations. Bis-NTA SAMs (circle) exhibit an increased stability of the complex in comparison to mono-NTA SAMs (square). Imidazole-induced complex dissociation is shifted to higher concentrations.

5.1.5 Patterned Protein Arrays on Multivalent Chelator SAMs

Since the multivalent chelator chip proved to be superior in terms of specificity, stability, and reversibility in the non-label detection (SPR) set-up, it would be also interesting to explore its compatibility with fluorescence techniques. In addition, the multivalent chelating surfaces arranged in the micro array format would be useful for the protein chip applications. Therefore, a surface with 100 μm -sized functional areas of bis-NTA SAMs with passivated separations of 45 μm was fabricated. First, micro-contact printing was employed to generate a hydrophobic eicosane thiol SAM on gold that formed a grid, separating the square-shaped areas, which were left available for the subsequent filling with multivalent bis-NTA SAM **12b**. Such chips were activated with nickel ions, and then sequentially exposed to fluorescence-labelled or non-labelled proteins. In general, the visualization of the fluorescent species on gold surface is complicated because of strong fluorescence quenching¹⁰². However, the separation between the fluorescent probes and the gold surface by the layer of bis-NTA SAM and along with a high laser power enabled us to record fluorescence images by laser scanning microscopy (Figure 27).

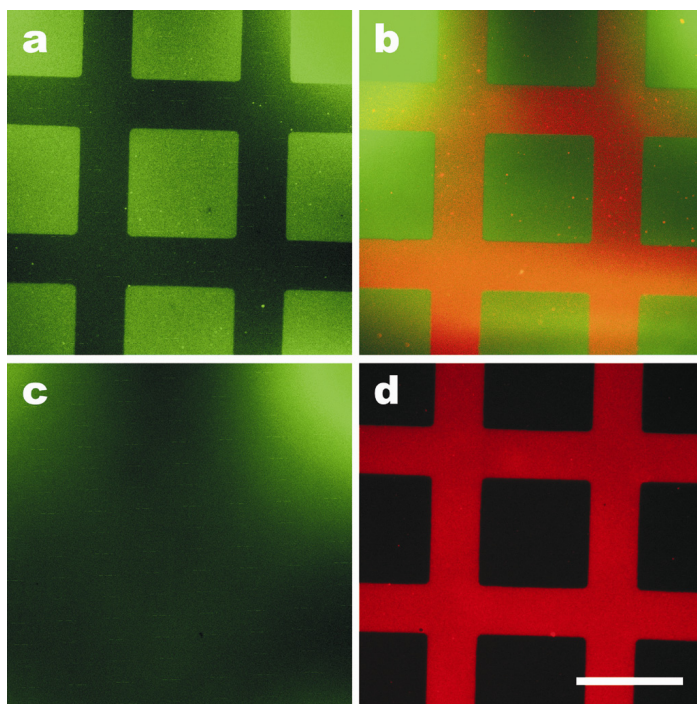


Figure 27: Laser scanning microscopy images of two patterned bis-NTA chips exposed to different fluorescent-labelled and non-labelled proteins. (a) Green fluorescence image of a chip, which was first loaded with BSA and then with Oregon Green-labelled (OG) His₆ MBP. (b) An overlay image of red and green fluorescence channels of another chip that was first loaded with Texas Red-labelled BSA and then with OG His₆ MBP. (c) The same chip as in b, but recorded with green fluorescence channel after injection of imidazole. (d) The same experiment as in c, red fluorescence channel. The scale bar is 100 μm .

It can be observed that BSA efficiently blocks the imprinted hydrophobic grid (dark areas, Figure 27a). The Oregon Green-labelled, His₆-tagged maltose-binding protein (OG His₆ MBP) binds specifically only to the micro arrays functionalized by multivalent chelator SAMs (green squares). An additional test on the selectivity of the patterned multivalent sensor surface can be performed by adsorbing Texas Red-labelled bovine serum albumin (TR BSA) to the chip structured in the same way as before (Figure 27b). Two-color imaging confirms that the unspecific binding of TR BSA to the pattern of bis-NTA SAM is extremely low and does not interfere with the binding of OG His₆ MBP. Such protein microstructures remained on the chip surface for at least 24 hours under buffer flow at room temperature (not shown). Moreover, as can be seen in Figure 27c and 27d, the chip could be easily regenerated by addition of imidazole. It is worth to mention, that the slight variation in fluorescence intensities is due to inhomogeneous laser illumination and due to a certain spectral cross-talk between the employed fluorescent probes. The later instrumental factor can be easily minimized when only one labelled protein is used (see Figure 27a). In summary, the high selectivity, stability, and reversibility of these multivalent NTA SAMs open the possibility to construct novel protein chip architectures for high throughput screening of ligand receptor and protein-protein interactions.

5.1.6 Purification on a Chip – One-step Enrichment and Analysis

Beside functional immobilization and lateral organization of proteins, this chip architecture can be also employed for purification and subsequent analysis of proteins on surfaces. A system for purification and enrichment of proteins on gold chips with multivalent chelator SAMs was developed and studied by mass spectrometry. The idea is to obtain a one-step method for purification of proteins from a complex protein mixture (e.g. cell lysate) and direct MALDI analysis on the same platform. As shown previously, the surface is activated with metal ions and proteins are immobilized specifically (Figure 28a). After addition of the matrix – an organic acid – captured proteins and also their interaction partners can be analyzed by mass spectrometry.

An *E. coli* cell lysate was spiked with His₆-tagged ubiquitin to a final concentration of 50 nM and applied either onto a conventional stainless steel or an activated and functionalized home-made gold MALDI target (Figure 28b). The resulting mass spectra of the two different targets demonstrate that the application of the conventional target does not allow detection of His-tagged proteins (“without purification”, blue line); whereas the one-step purification on the home-made target has such efficiency (“with purification”, red line), that the background is strongly reduced and the His₆ ubiquitin produces a strong peak (Figure 28c). Hence, by using this protein chip platform His-tagged proteins can be purified in a single step and immediately analyzed by mass

spectrometry. This methodology allows for screens of new interaction partners or post-translational modification of His-tagged proteins in complex mixtures with more than 1000 different proteins.

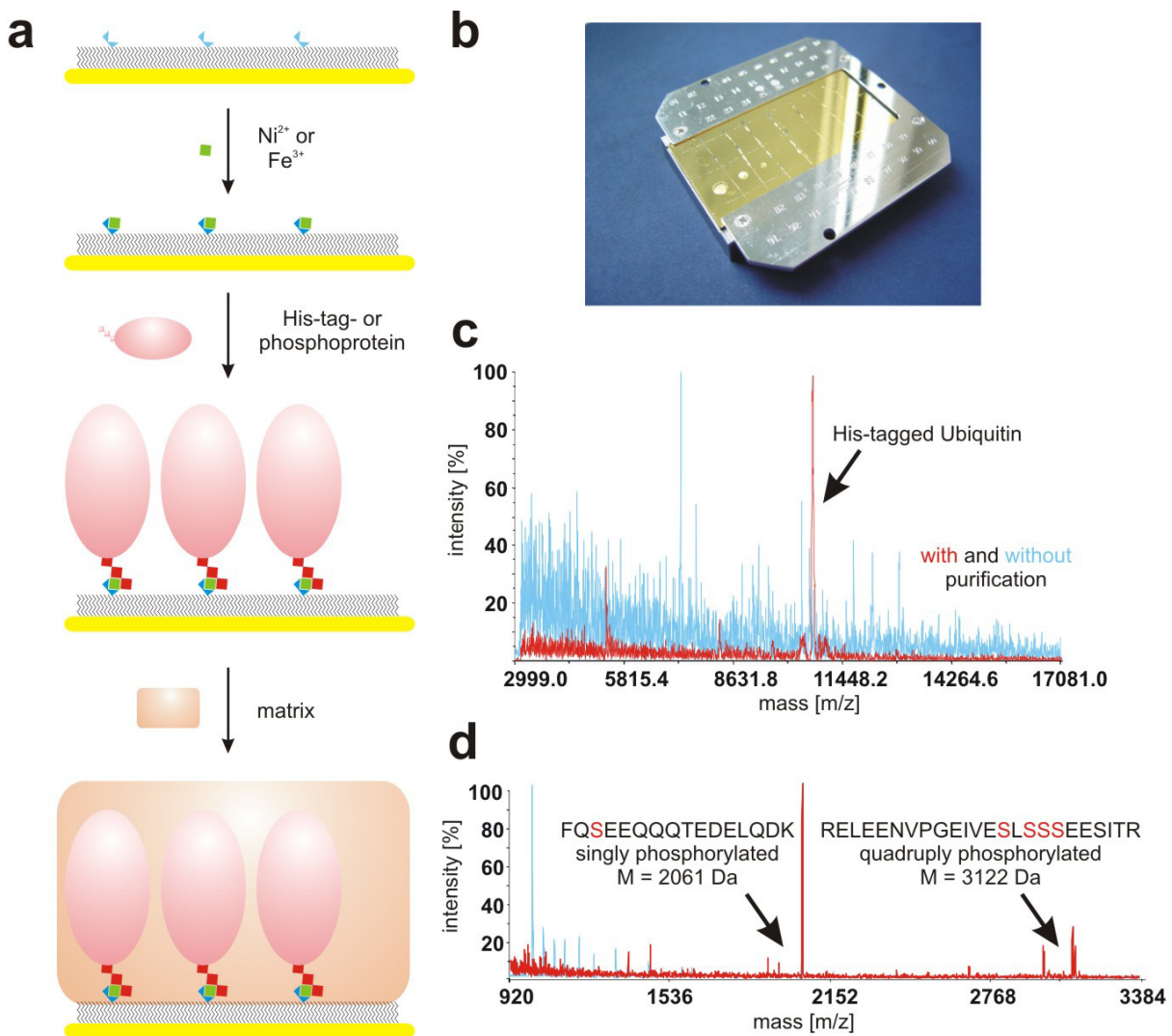


Figure 28: One-step Purification of proteins for mass spectrometric analysis. (a) Technical principle and (b) Photograph of a home-made and surface functionalized gold MALDI target. (c) Mass spectra of His₆-ubiquitin-spiked (50 nM) E. coli cell lysates without (→ conventional stainless steel target, blue) and with (→ functionalized gold target, red) purification on a MALDI target. (d) Phosphopeptides obtained by tryptic digest of β-casein are almost undetectable (blue line) with conventional mass spectrometric approaches. Enrichment of phosphopeptides by Fe³/NTA complexes enables detection with clear peaks (red line). See text for details.

One of the most important post-translational modifications and of key interest for functional proteomics is protein phosphorylation. Interestingly, if NTA groups form complexes with trivalent metal ions (e.g. Fe³⁺), they are able to recognize and capture specifically phosphopeptides or phosphorylated proteins^{194, 195}. Based on the previously presented single-step approach of protein

purification and analysis, a second screening technology, which targets phosphorylated proteins, was established. β -casein, a 23 kDa protein with 5 phosphorylation sites, was employed as test system. Tryptic digestion yields two phosphopeptides with either 1 or 4 phosphorylation sites. These peptides are almost not detectable at all on a conventional stainless steel MALDI target (Figure 28d, “without purification”, blue line). Whereas, enrichment of these peptides is enabled on Fe^{3+} -activated chelating SAMs and allow clear detection by mass spectrometry (Figure 28, “with purification”, red line). This technology expands the proteomics tool box with a phosphoproteome analysis platform. Especially of high interest are – beside proteome-wide profiling of phosphoproteins – monitoring of *in vitro* kinase assays, detection of phosphorylation sites, and protein-protein interaction analysis with mass spectrometric methods.

5.1.7 Uniform Orientation of Protein Complexes Monitored at Single-Molecule Level

Observation of the chip surface at the molecular scale gives insights into the orientation and structure of immobilized proteins. AFM is the method of choice to investigate surface topography and properties at molecular scale. SAMs of multivalent chelator thiols were prepared on ultra-flat, template-stripped gold (TSG) and studied during the process of protein immobilization. The model system for these AFM-based studies was the 20S proteasome from *Thermoplasma acidophilum*¹⁹⁶. This barrel-shaped multicatalytic protease complex (700 kDa) is fundamental in protein degradation in the cytosol and therefore essential for many cellular processes¹⁹⁷⁻¹⁹⁹. Because of its molecular dimensions of 11 x 15 nm²⁰⁰, the proteasome is ideal for single molecule studies by AFM. For specific binding to chelator SAMs, His₆-tagged proteasomes (βC -His₆ proteasome) enabling a well-defined and uniform immobilization in the “side-on” orientation were used. Previous studies using metal-chelating lipid layers demonstrated the absolute control of the orientation of immobilized proteasomes^{39, 40}. Figure 29a shows a representative topographic AFM image of a bis-NTA SAM formed on TSG before addition of protein. The image was obtained in TappingMode™ under buffer and is largely featureless (RMS value $\sim 5 \text{ \AA}$), which is due to the high quality of the ultra flat gold surface (RMS value $\sim 2 \text{ \AA}$). After activation with nickel ions and immobilization of His₆-tagged proteasome, a homogenous distribution of proteasome molecules becomes visible (Figure 29b). After subsequent washing with imidazole and EDTA, the surface was largely recovered and only few isolated traces of unspecific adsorbed proteins are visible (Figure 29c).

The AFM experiments demonstrate that immobilization is uniform even on single molecule level. The height of the immobilized molecules determined by image analyses amounts to 10-11 nm, which is in accordance to the diameter of the 20S proteasome (11 nm)²⁰⁰. (A very straightforward method to determine the height of the immobilized protein monolayer, and hence

the molecular orientation, is local detachment of the proteins, which yields a value of 10 nm.) The lateral dimensions however are 15-20 nm. This value, slightly larger than the proteasome dimension (15 nm), can be explained by the tip-broadening effect in AFM²⁰¹. Due to the location of the His₆-tag, immobilized proteasome molecules are entirely oriented in this “side-on” orientation as can be seen in Figure 29d/e. Barrel-shaped or oval molecules are visible at scans of 415 x 415 nm (Figure 29d). The homogenous orientation and distribution of immobilized protein complexes on this chelating surface allows an almost absolute control on the state of the protein and thus represents an optimal platform for single molecule studies, force spectroscopy experiments and quantitative protein-protein interaction studies where control of ligand-binding site is desirable. High-density packing of immobilized proteins allows tailoring of protein chip architectures in nano-dimensions.

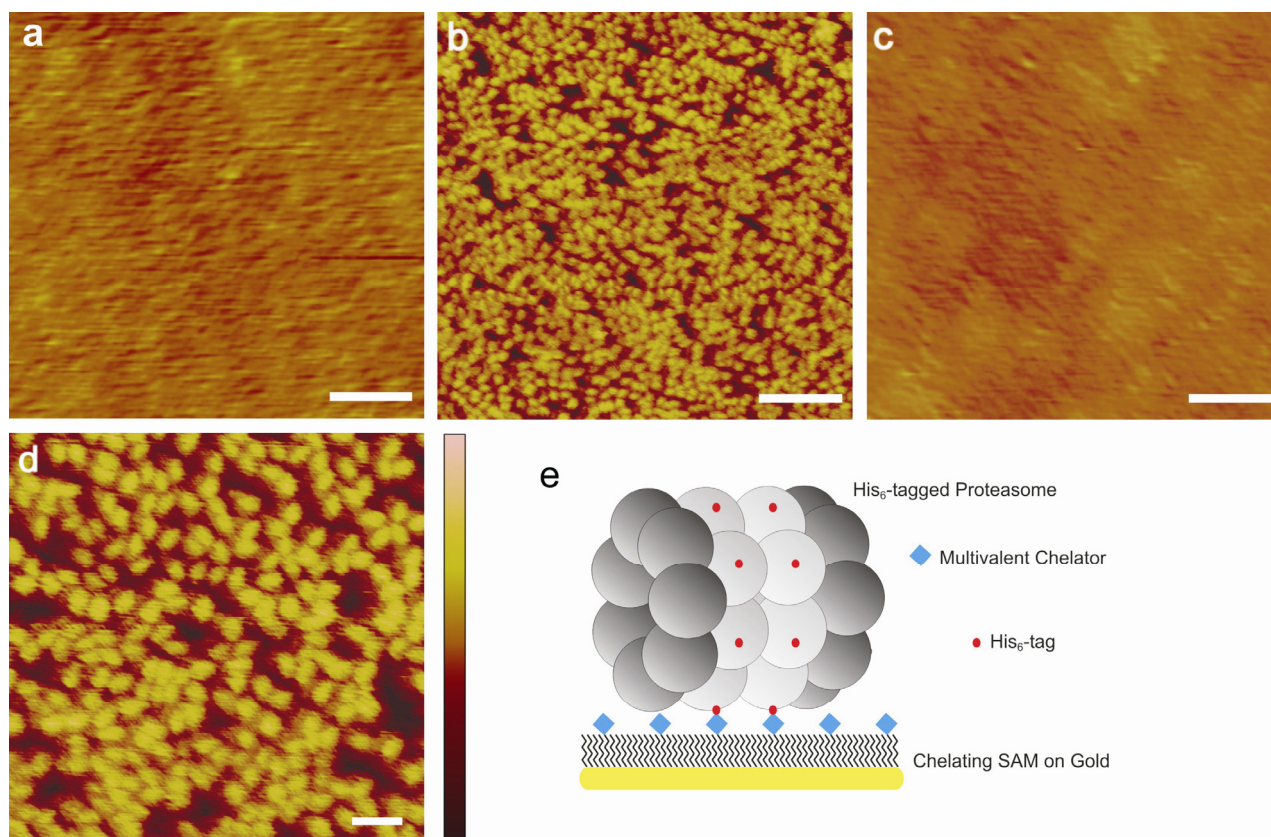


Figure 29: AFM study of protein immobilization on chelating SAMs. (a) SAM of bis-NTA thiol on template-stripped gold before and (b) after immobilization of β C-His₆ proteasomes, and (c) after regeneration with imidazole and EDTA. The scan size was always 1 μ m and the scale bar is 0.2 μ m. (d) In this 415 nm AFM scan the so-called “side-on” orientation of the proteasome is obvious. The scale bar is 50 nm. (e) The cartoon illustrates the sites of the His₆-tags on this proteasome variant and the orientation of the proteasome in the immobilized state on the multivalent chelating SAM. The z-data scale in all AFM images represents the height from 0 to 15 nm.

5.1.8 Conclusions

The conventional NTA/His₆-tag technique was successfully extended to self-assembling, multivalent chelator thiols for high-affinity recognition as well as stable and uniform immobilization of His₆-tagged proteins on chip surfaces. Bis-NTA was linked via an oligoethylene glycol to alkyl thiols by an efficient modular synthesis strategy yielding a novel, multivalent compound for formation of mixed SAMs on gold. His-tag recognition and capturing, as well as its metal ion-dependent nature was studied and visualized by CFM. SPR experiments with receptors successfully demonstrated the suitability of this format for delicate biophysical assays with high reproducibility. Multivalent chelator chips allow a specific, high-affinity, reversible, long-term immobilization of His₆-tagged proteins. Micro-structured chip surfaces allow the generation of protein micro arrays for high-throughput screening by fluorescence techniques. Furthermore, this chip platform was successfully applied for one-step purification and mass spectrometric analysis of His-tagged and phosphorylated proteins from complex mixtures as complete cell lysates. In AFM studies reversibility of the specific protein immobilization process was visualized at single molecule level. The entire control over the orientation of the immobilized protein promotes this chip surface to an optimal platform for studies focusing on research targets at single molecule level and nanobiotechnology. Homogenous orientation and distribution of immobilized proteins demonstrate the high quality of the designed surface, and qualify its application in nano-scaled protein chip architectures.

5.2 Write, Read and Erase – Native Protein Nanolithography

5.2.1 Concept of Native Protein Nanolithography

Controlled self-assembly of proteins into bioactive nanostructures is a key challenge in nanobiotechnology, including the potential towards protein chips with single molecule resolution. High multiplexing capacity, short diffusion times, and extremely low amount of samples required are ultimate advantages of nanoarrays^{13, 202, 203}. A novel easy-to-use technology for generation of protein nanoarrays under physiological, non-denaturing condition, based on a metal-chelating self-assembled monolayer on gold (see 5.1) combined with scanning probe-based nanolithography was developed during this Ph.D. thesis. His-tagged proteins form a dense and uniformly oriented monolayer on metal-chelating SAMs during immobilization¹⁸³. As proteins are subtle entities, AFM imaging has to be conducted gently with soft cantilevers in a physiological liquid environment using TappingMode™, where the AFM tip periodically contacts the sample, thus reducing lateral forces. The presented method allows switching from this gentle “imaging mode” with low forces to a “patterning mode” with enhanced loading force. In the latter mode it is possible to displace immobilized proteins mechanically while imaging of the chip surface is still possible and the functionalized SAM remains intact. For lateral structuring and organization of multiplexed protein assemblies, immobilized proteins can be detached and replaced simultaneously or sequentially by other His-tagged proteins using this novel AFM-based approach (Figure 30).

5.2.2 Reversible Patterning of Protein Monolayers by Contact Oscillation Mode

Imaging with amplitude feedback control of the AFM works properly as long as the amplitude signal decreases with decreasing distance between sample and cantilever holder. In the amplitude signal (Figure 31a) two such regimes can be seen: region I-II-III for gentle imaging with forces applied in the range up to 1.5 nN and region IV-V-VI for brushing proteins away with forces from 15 nN up to 50 nN. While approaching the surface the cantilever is oscillating in the first oscillation mode (Figure 31a, bottom right), and the amplitude is expected to decrease continuously to zero (Figure 31a, black dashed line). However, beyond point III, the amplitude signal rises again, which can be explained as the onset of a cantilever oscillation in a second vibrational mode (Figure 31a, bottom left) with the tip in constant contact with the sample. The two modes are reflected by two resonance frequencies: 4 kHz in region I-II-III, and 14 kHz beyond region III. The excitation frequency at 8.9 kHz in between the two peaks enables the excitation of each EIGEN mode in dependence on the boundary conditions. This new AFM mode was termed “contact oscillation mode” (COM). Decisive advantage of this AFM setup is the ease of switching between

gentle imaging mode (Tapping ModeTM, region I-II-III) and a detach/imaging mode (COM, region IV-V-VI) just by changing the amplitude set point (arrows in Figure 31a).

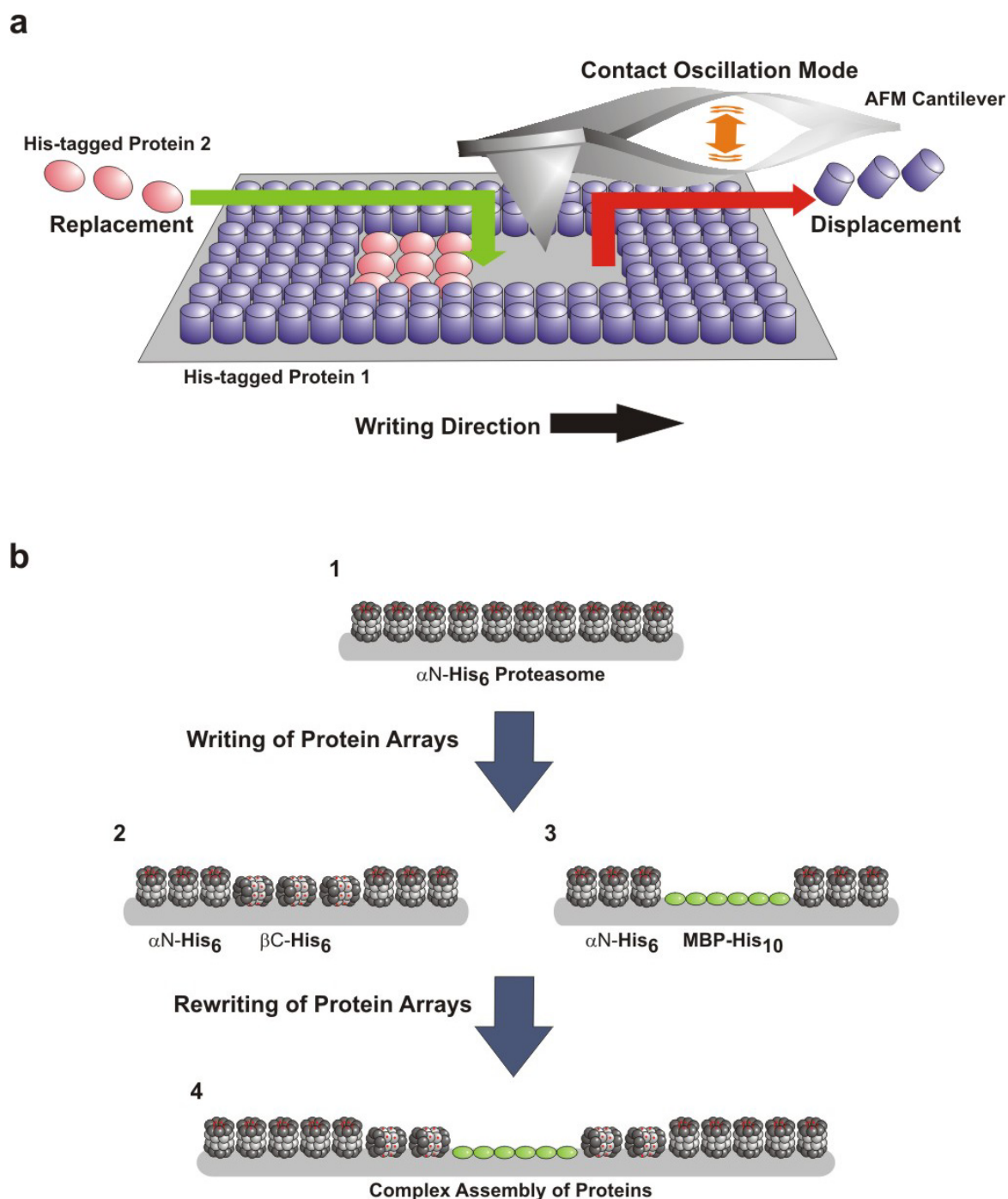


Figure 30: Nanofabrication of rewritable protein nanoarrays on metal-chelating interfaces. (a) Uniformly oriented His-tagged proteins are removed (“displacement”) with an AFM tip in contact oscillation mode (COM) and substituted either simultaneously or sequentially with other His-tagged proteins (“replacement”). (b) In subsequent write-and-erase processes, patterns of different proteins are generated. Proteins and molecular machineries in different orientations (maltose-binding protein and proteasome complexes) are organized in nanostructured protein arrays and assemblies (1–4).

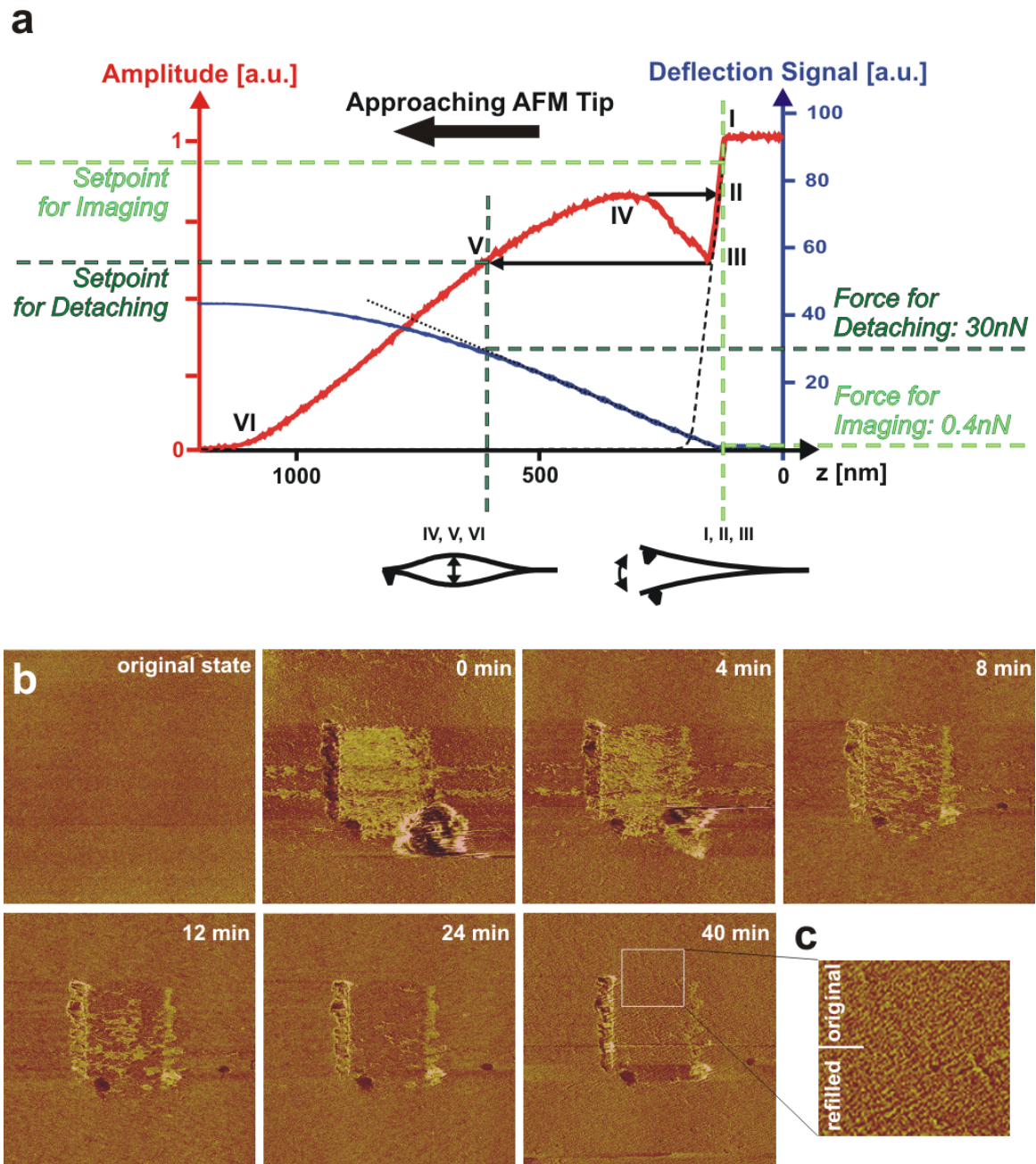


Figure 31: Reversible patterning of self-assembled protein monolayers by contact oscillation mode (COM). (a) Amplitude and mean deflection (related to a mean force) while a cantilever approaches the surface (displayed from right to left, origin of z is arbitrary). Parameters for gentle imaging (*TappingMode*TM) and detachment (COM) are indicated. By adjusting the amplitude set point the oscillating system switches between two modes sketched at the bottom. The switching is indicated by the arrows III \rightarrow V and IV \rightarrow II. The dotted line in the deflection curve describes the correction of the detector non-linearity and allows the calculation of forces. The scale numbers correspond to nN for the corrected deflection. See text for details. (b) Series of AFM phase images showing detachment of immobilized proteasomes and refilling of the structured area. Uniformly immobilized proteasome complexes are detached with the AFM tip in COM by scanning a 1- μ m square. At the turning points of the fast scan lines detached proteins cumulate, which disappear partially after several scans. This accumulation does not impair specific binding of His-tagged proteins to the metal-chelating area. The pattern disappears due to immobilization of subsequently added protein on the accessible metal-chelating area. The protein monolayer is closed again by self-assembly after 40 min. These AFM scans are recorded in Phase ImagingTM, which responds sensitively to changes on surface properties. The data scale in the AFM images represents a phase range of 5°. (c) The surface shows no memory effect because of complete self-healing properties. The original and refilled protein monolayers cannot be distinguished.

This novel AFM technique can be applied for selective, local displacement of specifically immobilized proteins and fabrication of multiplexed protein nanoarrays under native conditions – i.e. aqueous buffer at physiological pH and ionic strength. One of the protein entities used in this study was the barrel-shaped multicatalytic 20S proteasome complex (700 kDa) from *Thermoplasma acidophilum*¹⁹⁶ as already introduced in Chapter 5.1. We employed His-tagged 20S proteasomes for functional immobilization and array fabrication (Figure 31b). It was striking that the SAM beneath the proteasome monolayer was not functionally impaired during the nanostructuring process and was able to be used for repeated specific metal ion-mediated immobilization of His-tagged proteins. Subsequent addition of the same protein refilled and cured the generated square pattern quickly by dynamic self-organization (Figure 31b). Hence, this nanolithography technique enables erasing and rewriting of structures with proteins on a solid interface. Notably, the original and the refilled area cannot be distinguished and the chip (Figure 31c).

5.2.3 Control of the Orientation of Protein Complexes on Rewritable Protein Chips

COM enables nanofabrication of complex arrays under native conditions by refilling the emptied areas again with different proteins. In order to obtain differential nanofabricated structures with highly organized proteins, first, patterns with the same protein complex but in different orientations are produced by refilling the structured areas with differently His-tagged proteins (Figure 30b-2). Depending on the engineered position of the His-tags, the proteasome complex can be forced into two different orientations on the metal-chelating surface. Affinity-captured α N-His₆ proteasomes lead to protein monolayers with a height of 15 nm (end-on orientation, Figure 32a, b), whereas β C-His₆ proteasome complexes are uniformly organized in side-on orientation with a height of 11 nm^{197, 200}. Setting the end-on oriented proteasome as a “matrix protein” and refilling the structured areas with the side-on oriented proteasome yields a height difference of about 4 nm between the pattern and the original self-assembled protein layer (Figure 32c). This high degree of organisation demonstrates the specificity of the patterning technique. Arrays of the same molecule but in different orientations can be generated, providing absolute control of orientation, symmetry, and function of proteins²⁰⁴ on the same protein chip.

This erase-and-write (“displacement” and “replacement”) technique allows also more complex lateral organisation of proteins in a multiplexed manner. In order to achieve such nanofabrication of protein assemblies, rewritability of the generated protein patterns was demonstrated. Affinity-captured matrix protein (α N-His₆ proteasome) was locally replaced by maltose-binding protein with a C-terminal His₁₀-tag (MBP-His₁₀) (Figure 30b-3). The difference in

height between both proteins amounts to 9 nm (c.f. Figure 33c), in good agreement with the molecular dimension of MBP (3 nm x 6.5 nm) in the crystal structure.²⁰⁵

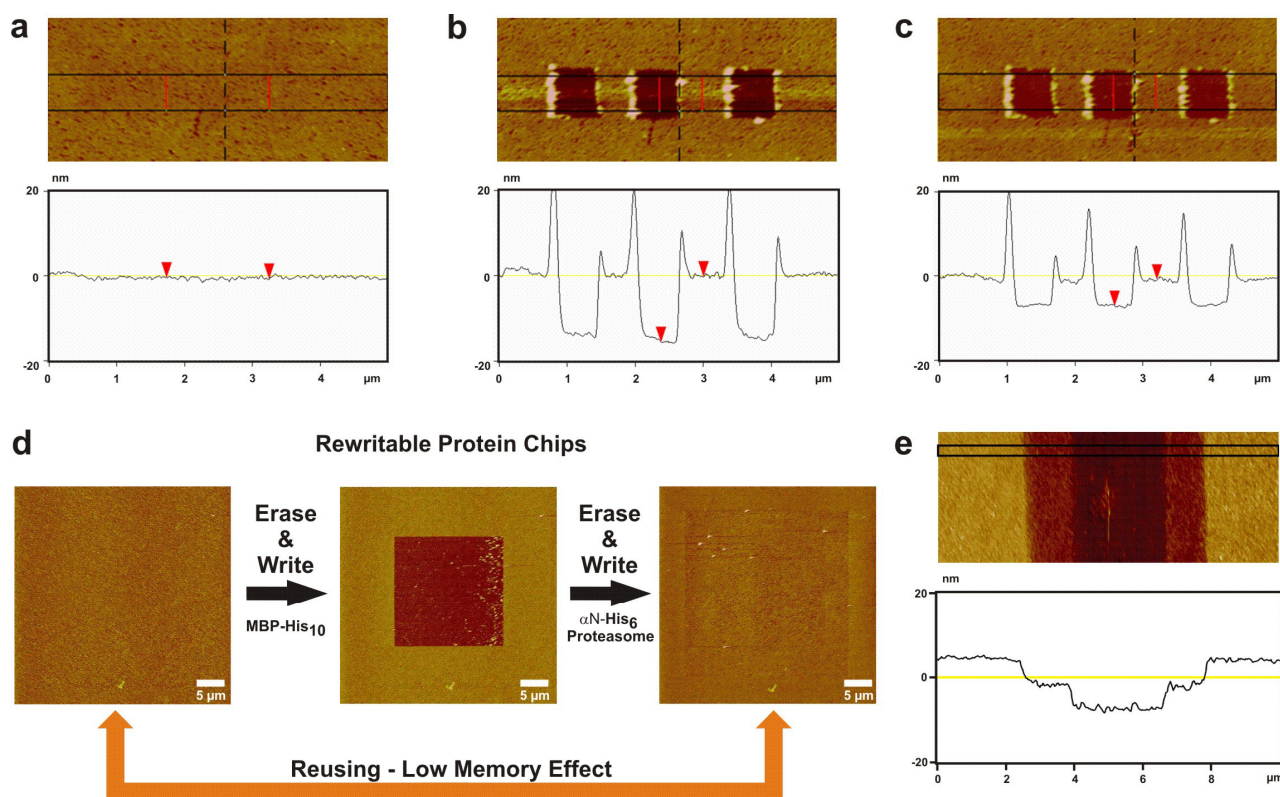


Figure 32: Orientation control of protein complexes on rewritable protein chips. (a) Monolayer of affinity-captured αN -His₆ proteasome complexes. (b) Using COM as a nanolithography tool, patterns of 500-nm squares are generated. These squares have a depth of 15 nm. This value corresponds to the thickness of a monolayer of end-on oriented proteasome complexes. (c) Freshly added βC -His₆ proteasomes are affinity-captured at the free metal-chelating areas in the side-on orientation. The resulting height difference of 4 nm between both monolayers is due to the two orientations of the proteasome complexes (11 x 15 nm). (d) In erase (“displacement”)-and-write (“replacement”) processes, 20 × 20 μm arrays of MBP-His₁₀ are generated. Then this pattern is deleted by detachment within a 25 μm × 25 μm array and refilled with αN -His₆ proteasome. This chip platform can be reused for structuring due to the low memory effect. (e) Multiplexed protein assemblies of αN -His₆, βC -His₆ proteasomes, and MBP-His₁₀ are organized within subsequent erase-and-write processes (see also Scheme 30b-4). The section analysis shows the characteristic height differences between the protein species applied. All AFM images are topographic and the z-scale represents 40 nm.

After writing and reading, the MBP pattern was erased and replaced by the matrix protein (Figure 32d). Thus, the original state of the chip can be re-established with a negligible memory effect. Based on this capability, this nanofabrication tool can also be used to generate complex protein assemblies consisting of a series of different proteins and protein complexes in unique orientation (Scheme 30b-4). The assembly of αN - and βC -His-tagged proteasomes with MBP-His₁₀ and the characteristic height profile of the resulting protein array are shown in Figure 32e. These

experiments demonstrate rewritability enabling the assembly of multiplexed protein arrays under native conditions.

5.2.4 Bioactive Protein Nanoarrays down to 50 nm

Fast and parallel read-out of nanostructured arrays can be achieved by fluorescence microscopy. Due to strong quenching of fluorescent species on conducting surfaces¹⁰², glass instead of gold surfaces were used. These glass-type chips are modified with an ultra-thin polymer brush carrying bis-NTA head groups, which bind His-tagged proteins with high stability and selectivity as confirmed by solid phase detection¹¹³. Starting with densely packed self-assembled α N-His₆ proteasome monolayers as a matrix, micro- and nanoarrays of Oregon Green-labelled MBP-His₁₀ (OG His₁₀ MBP) were fabricated on the glass-type chips (Figure 33a, b). This nanolithography technique enables generation of patterns with high precision demonstrated by the sharp edges in Figure 33a. The smallest size of these structures amounts to 50 nm as detected by parallel AFM imaging (Figure 33c). The minimal size of the structures is limited only by the width of the AFM tip, which can be further reduced. The depth of the arrays is 9 nm, which corresponds to the height difference between the MBP and proteasome monolayer verifying the authenticity of the patterns.

Key advantage of this nanolithography technique is the fabrication of protein nanoarrays under native conditions (i.e. aqueous buffer, physiological pH, and ionic strength). Such conditions, which preserve functionality of proteins, are highly desirable in biochip applications. As a representative example for demonstrating the biological activity of nanofabricated protein arrays specific protein-protein interaction of ligand-receptor pairs was monitored. For this purpose, the extracellular domain of the human type I interferon receptor (His₁₀ ifnar2) was nano-arrayed and binding of interferon- α 2 (IFN α 2) labelled with Quantum Dots was monitored by fluorescence microscopy (Figure 33d). This clinical relevant system has been shown to be highly sensitive to immobilization procedures¹⁹³, and thus is well suited for proving functional immobilization. IFN α 2 bound exclusively to the nano-arrayed ifnar2, but not to the surrounding protein matrix. These results corroborate functional protein immobilization suitable for probing protein-protein interactions in nanoscale dimensions.

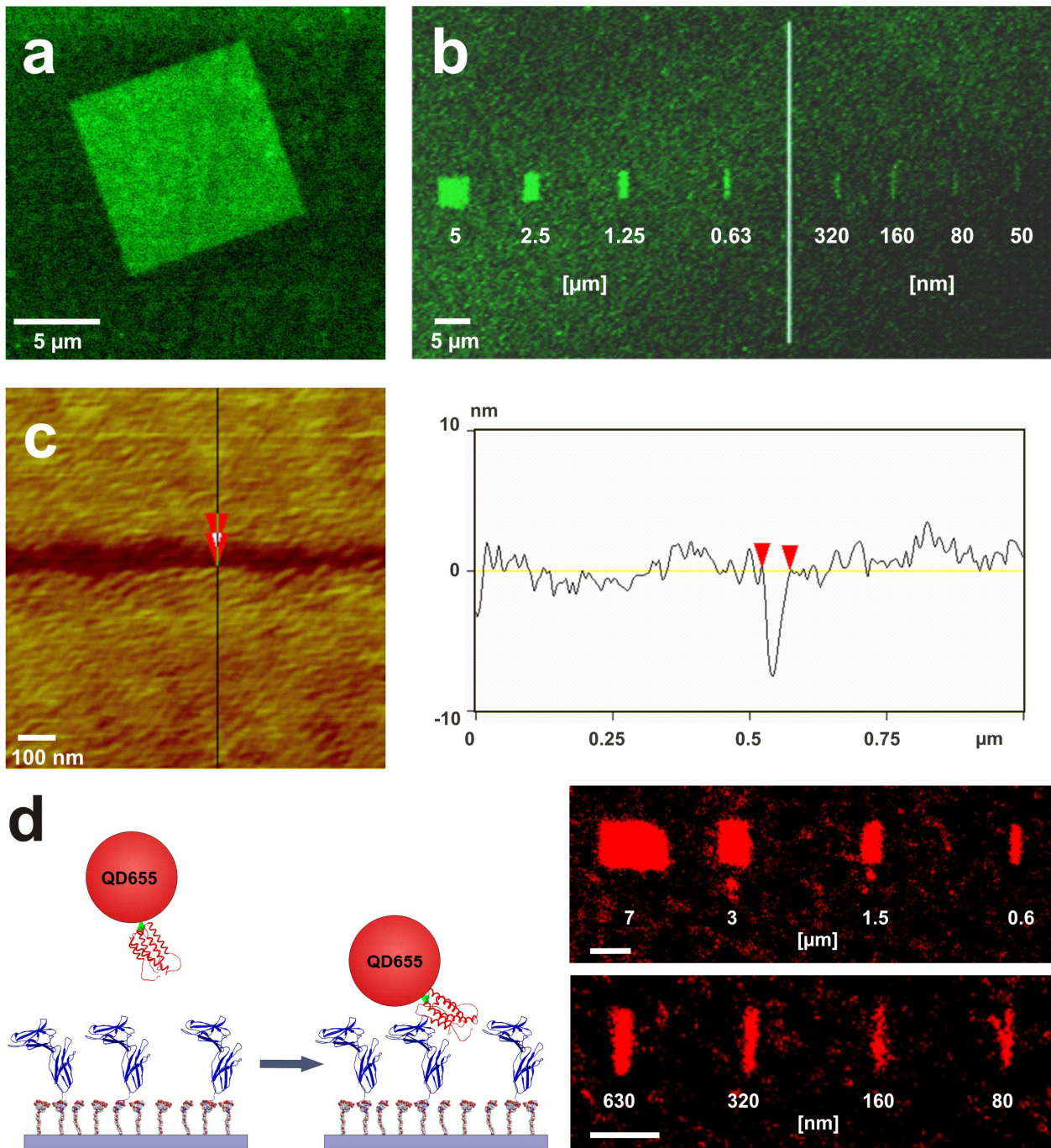


Figure 33: Bioactive protein nanoarrays fabricated down to 50 nm. (a, b) Micro- and nanoarrays were generated by controlled, local exchange of affinity-captured proteasome complexes (α N-His₆) with OG His₁₀ MBP (Scheme 30b-3) and imaged by confocal laser scanning fluorescence microscopy. (c) In parallel the smallest nanostructure was analyzed by AFM demonstrating patterns at 50-nm resolution. An approximately 9 nm deep trench (cross section) corresponds to the height difference between MBP and the proteasome complex. The AFM image is topographic and the z-scale represents 40 nm. (d) Protein-protein interactions in micro- and nano-structured arrays: specific binding of Quantum Dot 655-labelled IFNa2 (red) to immobilized His₁₀ ifnar2 (blue) was probed by confocal laser scanning fluorescence microscopy. Strong fluorescence emission at 655 nm was detected only in the arrays. The few non-specifically adsorbed Quantum Dot aggregates can easily be distinguished from the prominent micro- and nanostructures. The white bar corresponds to 5 μm.

5.2.5 Conclusions

For the first time rewritable protein nanolithography under physiological conditions enabling versatile fabrication of functional biomolecular patterns on self-assembled monolayers and polymer-brush architectures was established. Native protein nanolithography serves requirements in nanobiotechnology, where physiological ambient conditions are highly desirable for ensuring maintenance of biological functionality during and after array fabrication. This AFM technique permits instant switching between imaging and replacement of immobilised proteins at native state without any change of the setup or the tip. The first self-assembled protein layer acts hereby as a biocompatible and ductile patterning material. Affinity-captured proteins can be replaced by the AFM tip applying COM; the generated structures can be erased and refilled specifically with different proteins in uniform and functional manner. This COM-mediated nanostructuring proved powerful for multiplexed patterning of protein assemblies in situ. In future work, extended multi-protein arrays and molecular assembly lines will be systematically fabricated by iterative erase-and-write processes and applied for protein interaction analysis and as nanocatalytic centres. Furthermore, transient, reversible patterns of proteins will be useful for biological experiments, in which different proteins can be written and replaced at different states, e.g. after ligand binding, formation of ternary complexes or photo bleaching.

5.3 High-Affinity Protein Chip Fabrication by Chemical E-Beam Nanolithography

5.3.1 Coupling of Multivalent Chelators to Biphenyl SAMs

Chemical e-beam nanolithography enables functionalization of surfaces with focussed electron beams. This technology allows the reduction of nitro groups to amines and further modification with amide coupling chemistry as described in Chapter 1.5.2. Using multivalency as a design principle, a chemical recognition unit with exceptionally high affinity for oligohistidine-tagged proteins was designed.²⁰⁶ Three *N*-nitriilotriacetic acid (NTA) moieties were grafted on a cyclic scaffold to form tris-NTA, which contained an additional functional group for further modifications. Tris-NTA potentially coordinates six imidazole moieties and thus perfectly matches the coordination demands of a His₆-tag. The nanomolar binding affinities and the stable binding of these multivalent chelators with histidine-tags is achieved by complex formation of nickel ions²⁰⁶. Chips with laterally organized multivalent chelators for specific high-affinity immobilization of His-tagged proteins were fabricated within four steps (see Figure 34a):

- i. Formation of nitrobiphenyl thiol SAM: First, a densely packed monolayer of 4'-nitro-1,1'-biphenyl-4-thiol (NBT) was self-assembled on a gold surface.
- ii. Chemical nanolithography: E-beam writing was used to locally reduce the terminal nitro groups to amino groups, while the aromatic layer is dehydrogenated and cross-linked. The generated well-ordered templates of amino groups can be used for specific covalent coupling of biological recognition units like tris-NTA.
- iii. Exchange of non-cross-linked thiols by protein-repellent matrix thiols: This exchange reaction was aimed to improve the protein-repellent properties of the structured SAM. Non-cross-linked NBTs were thermally desorbed and replaced by protein-repellent EG3 matrix thiol **6** (Figure 34b).
- iv. Chemical coupling of tris-NTA modules to reduced amino-terminated SAMs: After exchange of the thiols, the amino groups of the remaining and cross-linked biphenyl thiols are modified by coupling of *tert*-butyl protected carboxy-tris-NTA modules (Figure 34c). After deprotection with TFA, the surfaces were applied for specific, high-affinity immobilization of His-tagged proteins.

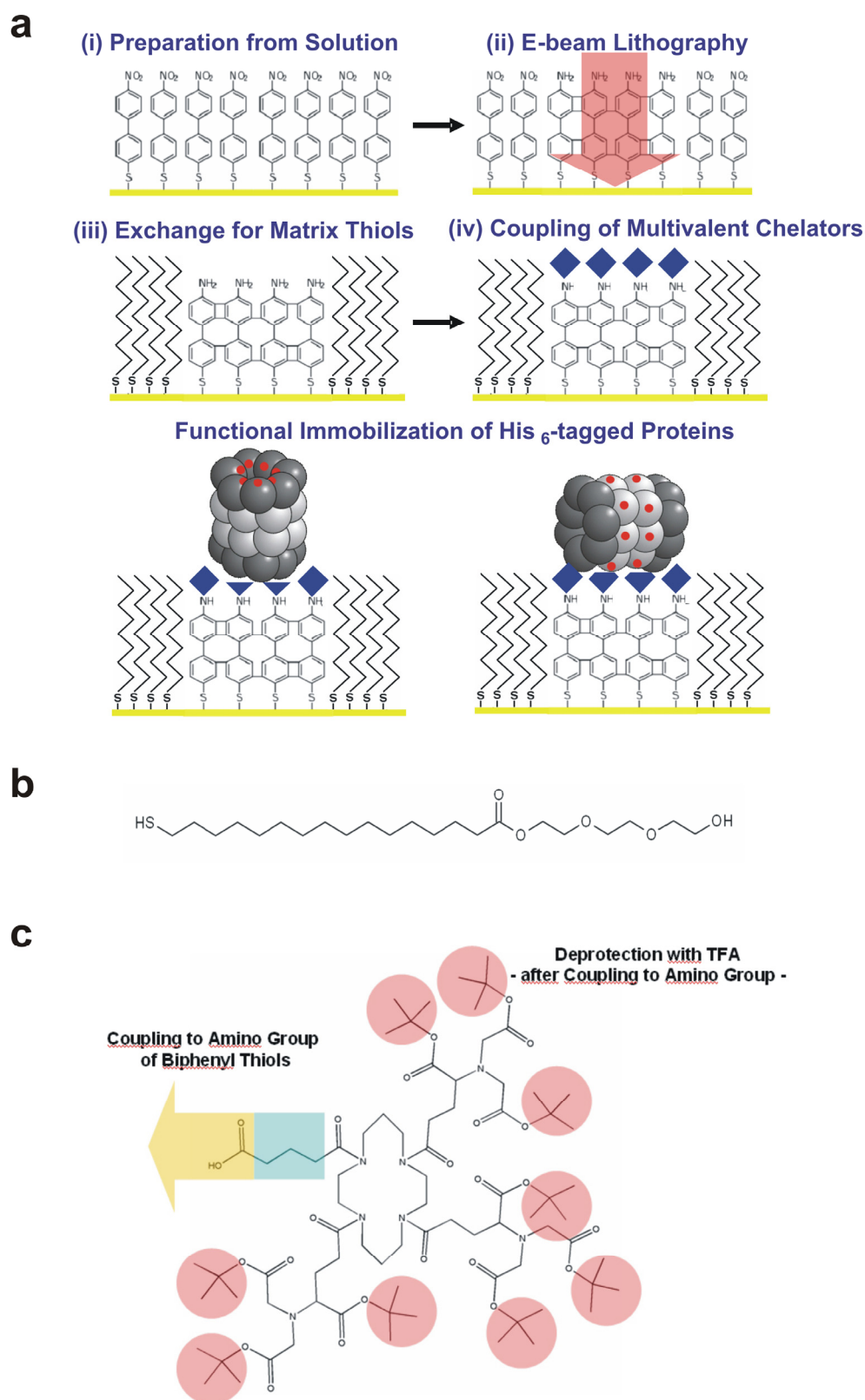


Figure 34: Fabrication of cross-linked biphenyl SAMs and subsequent chemical modification of the gold surface with multivalent chelators for high-affinity capturing of His-tagged proteins. (a) Schematic view of chemical e-beam nanolithography and further chemical modification steps with (b) matrix thiol **6** and (c) the multivalent chelator tris-NTA. For the sake of clarity matrix thiol **6** is depicted simplified in (a). See text for details.

5.3.2 Surface Physical Monitoring and Characterization of Multivalent Chelator Biphenyl SAMs

In order to verify this multi-step modification process (i-iv, see previous section), substrates were analyzed with surface-sensitive techniques as AFM (c.f.), IRAS (data not shown), and XPS. As x-ray photoelectron spectroscopy yields direct chemical information, these analyses will be presented here. Characteristic changes in the signals of nitrogen (N1s), oxygen (O1s), and carbon (C1s) are shown in Figure 35. The exchange of non-cross-linked areas through protein-repellent matrix thiols was obvious in the XPS analysis (compare i and iii). Different chemical states were observed in the carbon signal after exchange of nitro-biphenyl thiols for EG3 matrix thiols shows the existence of different carbon species, due to the different chemical environment. The nitrogen signal disappears after this exchange. The reason is the disappearance of nitrobiphenyl thiols, hence N-containing nitro groups are diminishing. Oxygen signals are increasing during the exchange process. This increase is due to the ethylene glycol groups in the matrix thiol. Coupling of the tris-NTA modules to the amino-terminated, cross-linked SAM were recognized from the increase of carbon intensity and the broadening of the peak (iv). The increase of the carbon, nitrogen, and oxygen signals correlated well with the stoichiometries of these elements in the tris-NTA module. AFM images showed slight changes in the height which correspond to changes in the surface architecture, as well (data not shown).

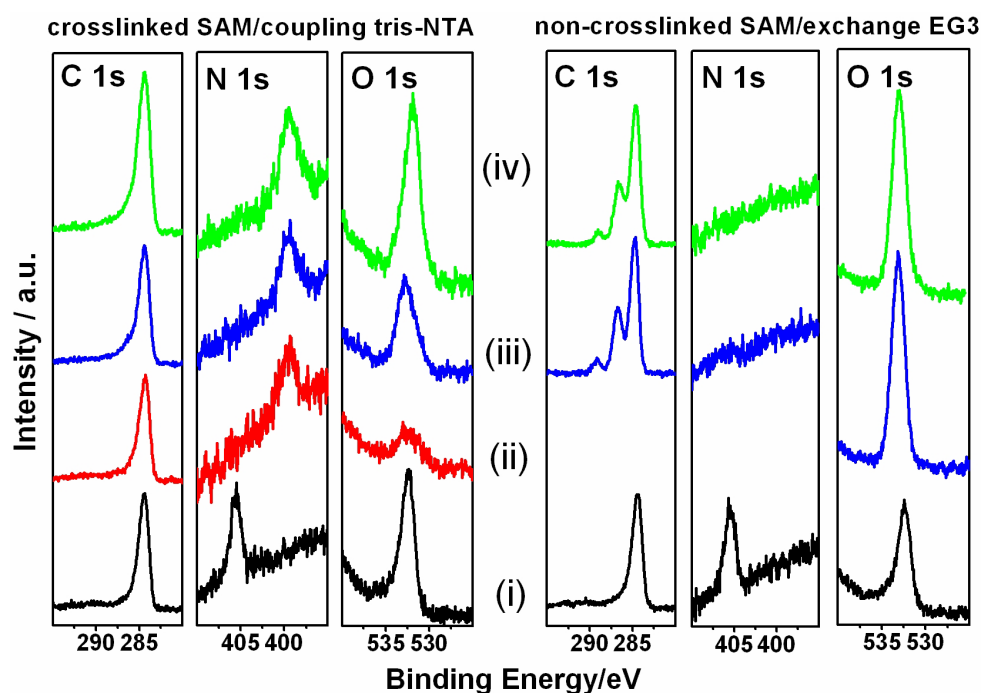


Figure 35: XPS spectra of cross-linked and non-cross-linked biphenyl SAMs for monitoring exchange of thiols and coupling of multivalent chelator modules. See text for details.

5.3.3 Protein Capturing on E-Beam-modified Biochips followed *in situ*

Due to its well-known immobilization characteristics from previous studies, His-tagged 20S proteasome complexes were employed as a model system in protein capturing experiments. The beauty of this system became obvious in these immobilization procedures. N-terminal His-tagged proteasomes organize into the end-on orientation, as soon, as they are captured by the multivalent chelators on the chip surface. This information, encoded as height data in AFM imaging, allows to judge about the specificity and functionality of affinity capturing. Topographic AFM data (Figure 36a, b) show, that proteasomes were captured only at the tris-NTA-modified islands, but not at the surrounding areas. The same protein chips were regenerated (imidazole, EDTA) and used in another protein immobilization experiment, with fluorescence-labelled MBP. Specificity and homogeneity of the e-beam lithographically produced micropatterns were confirmed by confocal laser scanning microscopy (Figure 36c).

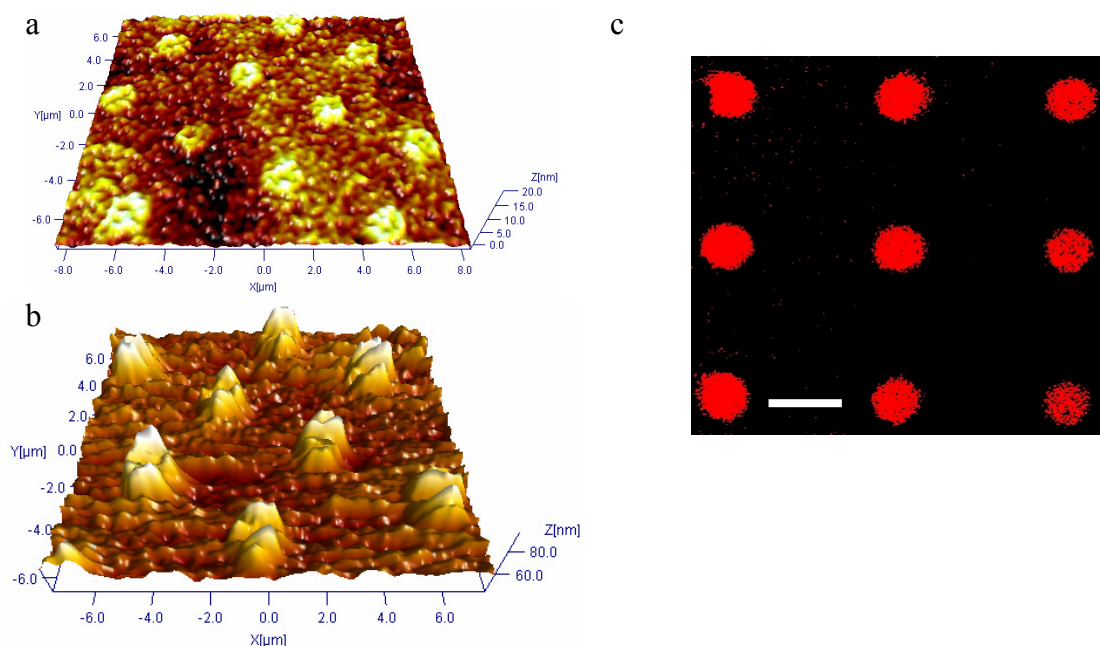


Figure 36: Immobilization of His-tagged proteins on e-beam lithographically produced microstructures. (a) AFM images before and after (b) affinity capturing of proteasome complexes. (c) Confocal laser scanning microscopy was used for detection of immobilized fluorescence-labelled MBP. Fabricated patterns had lateral dimensions of 1 μm .

5.3.4 Conclusions

This combined application of methodologies from surface chemistry, semiconductor technology, and chemical biology demonstrates successfully how pre-patterned templates for micro- and nanoarrays for protein chips are fabricated. The surface physical, as well the biophysical experiments, proved the functionality of this technology. Future goals are the establishment of such pre-patterned templates down to a few nanometers, in order to achieve single molecular arrays of biological entities. Further target is the transfer of the complete fabrication process into gas phase deposition. As many parameters for gas phase fabrication of processes as chemical coupling are not known, this approach is challenging. The promises of such process technology are fast and economic fabrication of ready-to-use nanostructured biochips at industrial scale.

5.4 Nanostructured Silicon Chips for Analysis of Membrane Protein Function at Single Molecule Level

5.4.1 The Microcavity Concept

At present, no protein chip format suitable for the study and analysis of membrane proteins is available. Key prerequisites are maintenance of protein functionality and bilateral accessibility to the membrane protein for controlling the biochemical environment during application. Another important issue is the implementation of proper read-out techniques. Standard techniques as CLSM and electrical read-out should be compatible with any chip format dedicated to the study of membrane proteins. A protein chip technology solution based on Silicon-on-Insulator (SOI) architectures²⁰⁷ for lateral organization of membrane proteins was targeted (Figure 37). Due to high level advancements in semiconductor technologies, SOI architectures are highly favored in Micro-Total-Analysis-Systems (μ TAS) or Lab-on-Chip applications and allow the implementation of microfluidics for sample delivery^{208, 209}. The SOI architecture employed in this project consists of a microcavity array with pore sizes from 45 nm to 10 μ m (Figure 38).

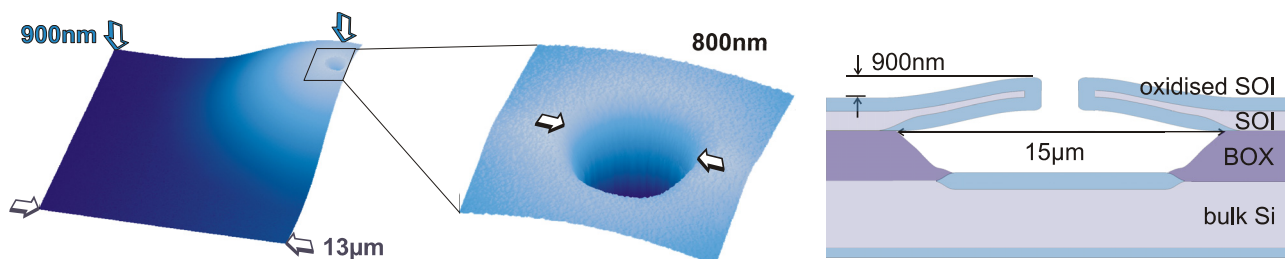


Figure 37: Architecture of a Silicon-on-Insulator (SOI) chip substrate with microcavities for lateral organization of membrane proteins. Pore size of microcavities varies in the range of 45 nm to 10 μ m. Surface bending results from the final oxidation process during manufacturing. The oxide thickness was calculated to be 170 nm, leaving 30 nm of residing SOI. Adapted from²¹⁰.

First objective was the sealing of the cavity pores with a membrane as illustrated in Figure 39. Transmembrane proteins can be trapped in the freely suspended membrane over the cavity opening (illustrated in the left cavity in Figure 39). Due to their extension beyond the membrane (extra- or intra-cellular domains) it is assumed that proteins cannot move out of their designated cavity, and are then trapped there. A degenerated transmembrane channel is drawn in between the two sketched cavities in Figure 39.

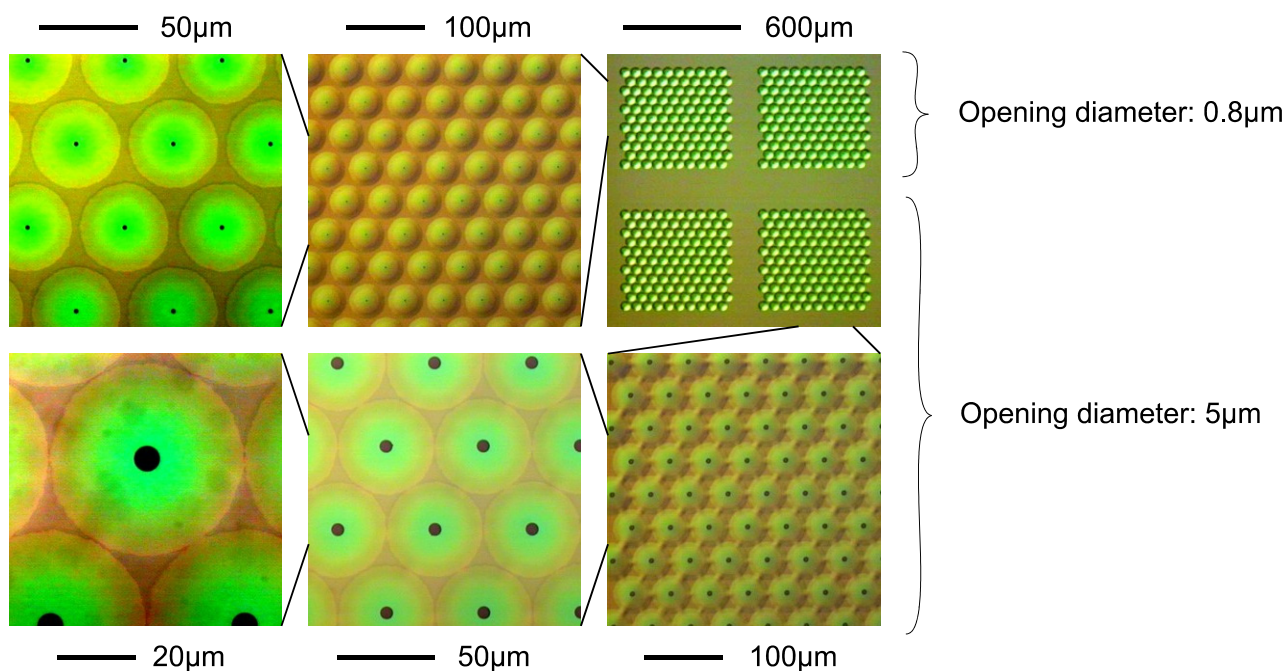


Figure 38: Light microscope images of microcavity arrays dry (top view). Adapted from ²¹⁰.

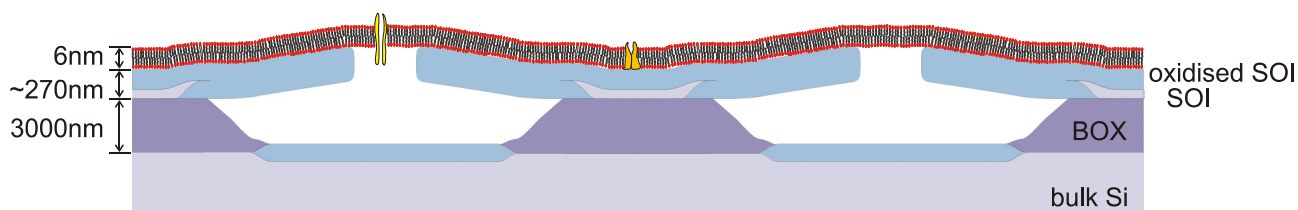


Figure 39: A membrane spanning over the cavity openings (not drawn to scale). Adapted from ²¹⁰.

The microcavity concept allows addressing a single, small aperture. If the percentage of membrane proteins in the membrane is chosen to be small enough, a single protein might be trapped in the opening of a cavity and anything passing through this channel or pore protein is collected in the cavity. Since the “lid” or the “sealing” of the cavity is the SOI layer, it is easily possible to integrate electronics such as ion-sensitive field-effect transistors (ISFETS) or planar field effect transistors into the top of each cavity. The liquid inside each cavity could then be investigated separately.

5.4.2 Membrane Formation on Silicon Substrates

The bilayers were formed on the silicon dioxide surface by vesicle fusion. In order to obtain a hydrophilic surface – which is critical for vesicle fusion – the silicon surface was oxidized chemically before membrane deposition. The vesicles were allowed to fuse on the surface for

30-45 minutes. Afterwards, the substrate was extensively rinsed in water to remove excess Liposomes.

For fluorescence microscopy studies, 1 mol% of Oregon green (OG)-labelled 1,2-dihexadecanoyl-glycero-3-phosphoethanolamine (DHPE) was mixed to SOPC in solution during vesicle preparation ($\lambda_{\text{abs/em}} = 492/515$ nm). Details of the membrane composition, vesicle fusion time, and the used substrates are listed in Table 3 (see section 4.2.2 for further information).

Table 3: Information about the lipid bilayers and the cavity geometries.

Experiment	Matrix Lipid	Functional Lipid	Vesicle Fusion Time	Oxide Thickness
Sample 1 (FRAP, Figure 40)	2 mM SOPC	1 mol% OG DHPE	30 min	~200 nm
Sample 2 (TAMRA on OG, Figure 42, 43)	2 mM SOPC	1 mol% OG DHPE	45 min	~110 nm
Sample 3 (TAMRA on unlabelled bilayer, Figure 44)	2 mM SOPC	-	45 min	~110 nm
Sample 4 (OG, Figure 46)	2 mM SOPC	1 mol% OG DHPE	45 min	~250 nm
Sample 5 (OG-His ₁₀ -MBP, Figure 46)	2 mM SOPC	5 mol% DODA-NTA	45 min	~250 nm

For protein immobilization on the membrane, 5 mol% of 1,2-dioleoyl-glycero-3[*N*-(5-amino-1-carboxypentyl)iminodiacetic acid)succinyl] (DODA-NTA or chelator lipids) were mixed to the SOPC before vesicle formation. DODA-NTA lipids were synthesized as described by SCHMITT et al.³⁶. These metal chelating lipids were used to immobilize His-tagged proteins. Here His-tagged maltose binding protein (His₁₀ MBP) was immobilized on the membrane via the chelator lipids.

5.4.3 FRAP-based Verification of Lipid Bilayer Formation

The highly ordered lipid bilayer can be considered to be a two dimensional liquid crystal. In its natural environment membrane proteins can move within the cell surface. The diffusion time constant can be measured by fluorescence recovery after photobleaching (FRAP)²¹¹. The fluorescent dyes of the membrane in a defined area were bleached by exposure to laser light with

high intensity. The fluorescence of the bleached region recovers due to diffusion processes of bleached and intact dyes. The speed of the fluorescence recovery depends on the diffusion rate of the lipids in the bilayer.

The fluidity of the lipids in the membrane is preserved only on ultra flat surfaces. If the surface has a high roughness, the diffusion is slow or not measurable, or the membrane might be even ruptured. Unoxidized cavity samples had a roughness of only 0.16 nm with a maximum elevation of 1.5 nm. Fluorescence could not be observed due to quenching effects^{212, 213}. For enabling optical analysis the chips were oxidized. The RMS surface roughness of the oxidized cavity samples amounted to 0.25 nm, and the highest elevation was 2.7 nm, which is approximately half of the membrane thickness (data not shown).

If the chip surface is covered homogeneously with a lipid bilayer membrane, fluorescence recovery should be possible. The observed fluorescence on oxidized samples was distributed homogeneously over the complete surface – photobleaching and recovery was possible for all the measurements shown on cavity substrates. On a sample with an oxide thickness of roughly 120 nm the fluorescence of a bleached spot recovered almost completely after 300 s (Figure 40).

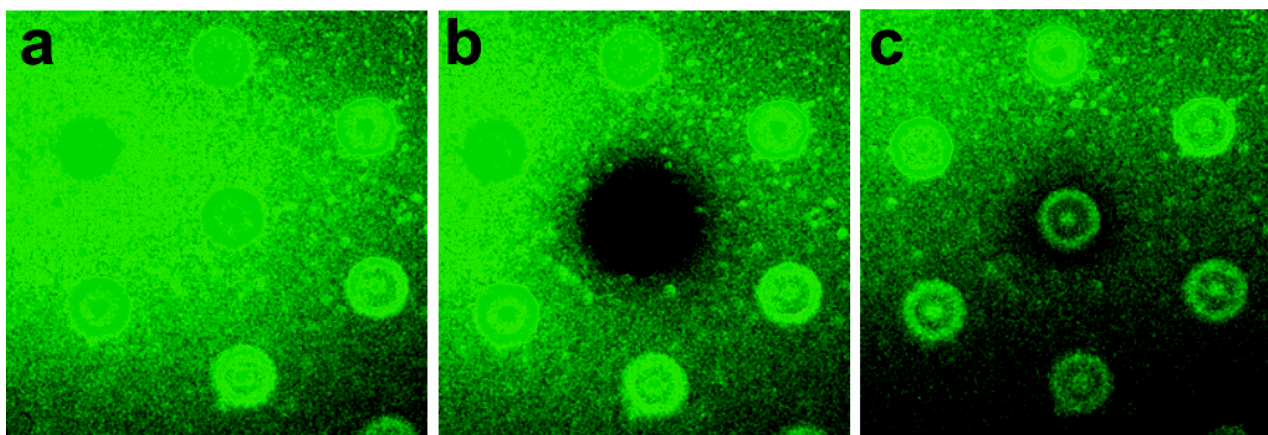


Figure 40: Fluorescence recovery after photobleaching (FRAP) on cavities with a pore size of 5 μm (sample 1): (a) before bleaching, (b) after bleaching, and (c) recovery after 300 s.

The translational diffusion coefficient D of the membrane can be calculated by

$$D = \frac{r^2}{4t}$$

where r is radius of the bleached spot, and t is the recovery time. The calculated diffusion coefficient was in the range of $0.1 \mu\text{m}^2/\text{s}$ to $1 \mu\text{m}^2/\text{s}$ for all measurements shown in this chapter. This corresponds well to values given in literature: The diffusion coefficient of lipids of erythrocytes has been determined to be $3.4 \mu\text{m}^2/\text{s}$ ⁴⁴. From these experiments it was evident that the sample surface was covered with a membrane, but it was not clear if the membrane spans the cavity opening. It is also possible, that the membrane covered the inside of the cavity as illustrated in Figure 41. Further experiments using fluorophores of two colours were conducted to clarify the situation.

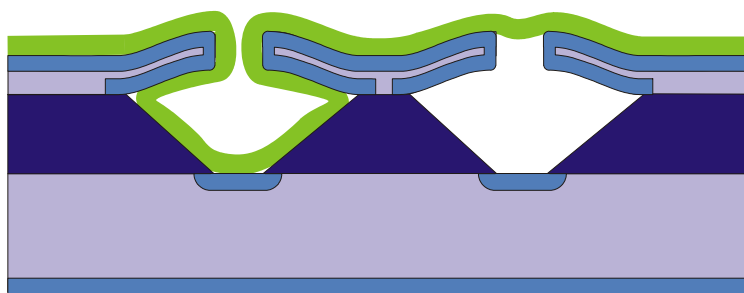


Figure 41: Different scenarios of membrane distribution after vesicle fusion on SOI chips. Adapted from ²¹⁰.

5.4.4 Dual-Color Studies on Membrane Formation at Microcavities

Similar to the measurement shown in the section above, an Oregon Green-labelled bilayer was fused from SUVs. A close-up image is shown in Figure 42a. The rings of brighter and darker fluorescence were assigned to constructive and destructive interference as illustrated in Figure 42b. The variation in phase shift of the light reflected from the interfaces was caused by the wedge-shaped walls inside the cavity. An increased underetch will reduce the presence of interference rings to regions far away from the pore and change the optical properties in this region.

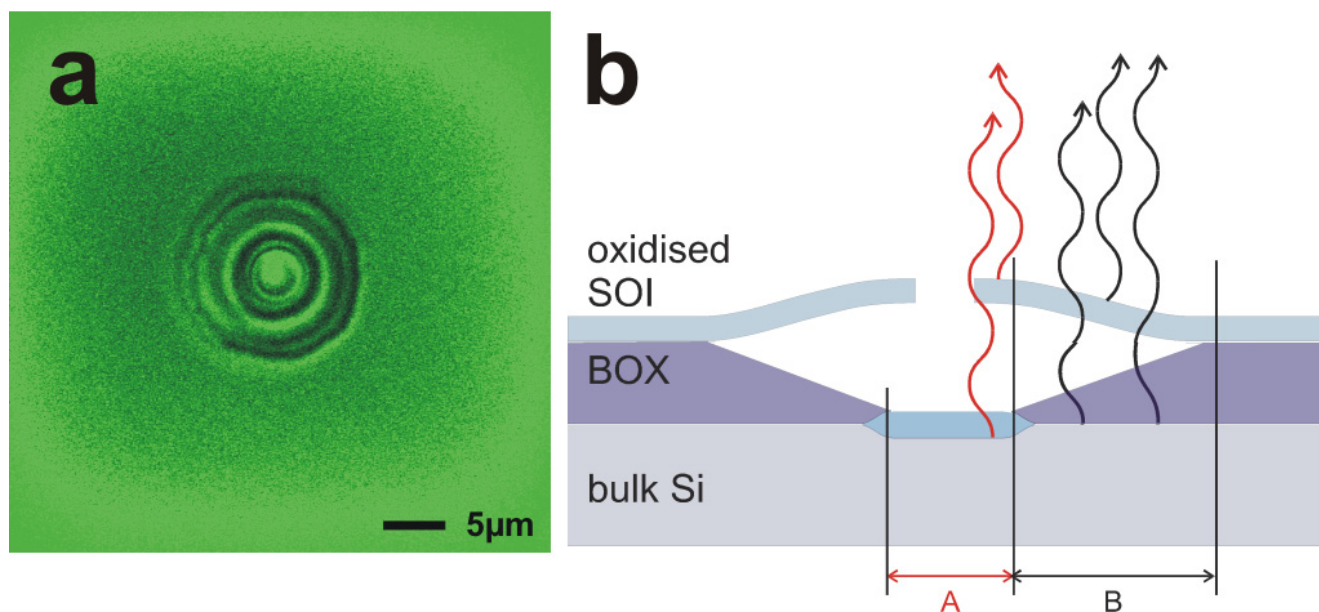


Figure 42: OG labelled lipid bilayer on a 2 μm pore with an underetched cavity of roughly 15 μm diameter. (a) Top view, the fluorescence is continuous, even at the pore position. (b) Illustration of constructive and destructive interference in the regions of the wedge-shaped cavity walls (region B) underneath the thin SOI layer. The light emitted from the labelled membrane interferes with the fluorescence reflected from the cavity bottom. No or constructive interference in the regions of the flat, evenly oxidized cavity bottom (region A). Part b adapted from ²¹⁰.

In a next step, red TAMRA dye was injected into the flow chamber and covered the OG-labelled lipid bilayer. The fluorescence of the red and the green dye was recorded simultaneously. Three-dimensional reconstructions of these measurements are shown in Figure 43. The separation of the two layers aroused from the representation of the data. By setting a threshold value on the fluorescence intensity (using the Imaris software, BitPlane AG, Zurich, Switzerland), the regions of low intensity, due to cross-talk or noise, were masked out. Red-fluorescence due to TAMRA is only measured in the bulk solution above the membrane, which is presented in green. No dye can penetrate an intact lipid bilayer; hence the lack of red fluorescence in the cavities was an indication for a defect-free, pore spanning membrane. A similar measurement was conducted by adding TAMRA in solution onto an unlabelled SOPC bilayer. No fluorescence was observed in the microcavities. Hence, the dye molecules did not pass the membrane. The obtained results were similar to Figure 43 and shown in Figure 44.

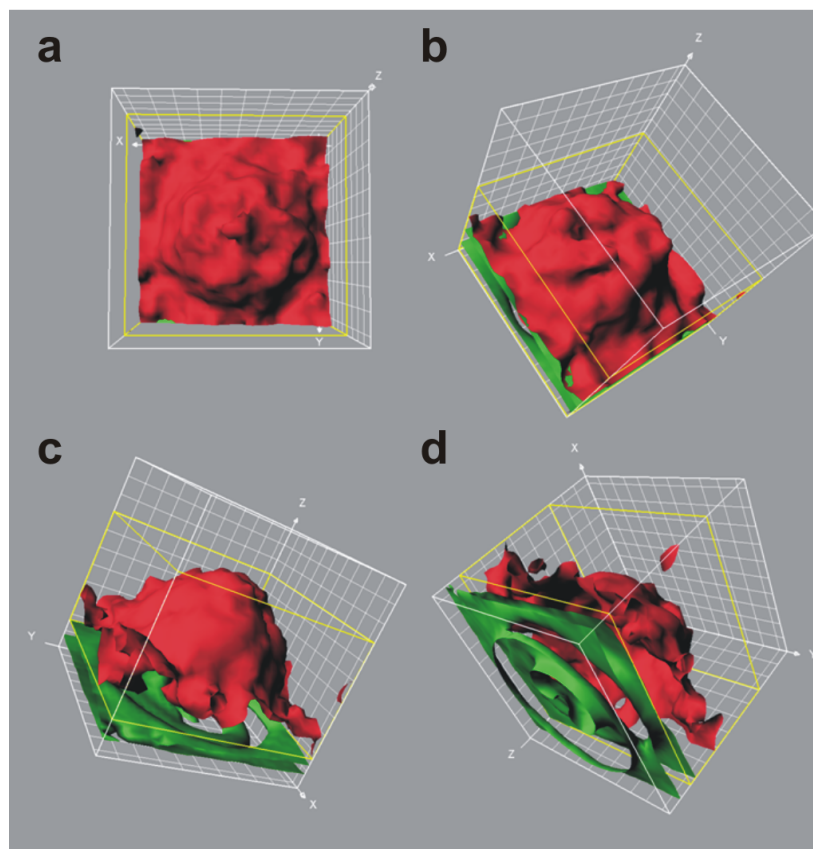


Figure 43: Red TAMRA dye was added on an Oregon Green labelled lipid bilayer (sample 2). (a) Top view, (b) and (c) rotations to the (d) bottom view. The scale is $2.3 \mu\text{m}/\text{div}$ in all three dimensions. The experiment was performed on a pore of $2 \mu\text{m}$ diameter.

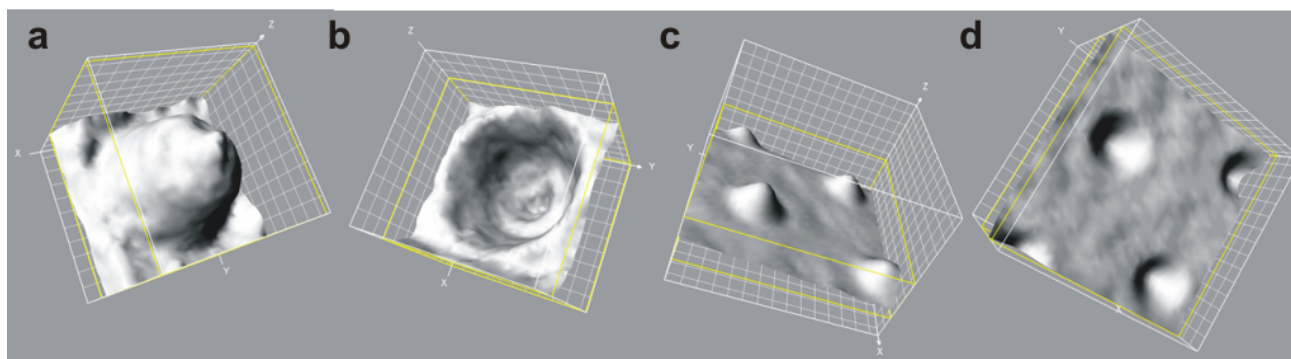


Figure 44: Red TAMRA dye was added on an unlabelled lipid bilayer (sample 3). (a, c) Top view, (b, d) bottom views. The scale is $23 \mu\text{m}/\text{div}$ in all three dimensions for (a) and (b); $7 \mu\text{m}/\text{div}$ for (c) and (d). The experiment was performed on a pore of $2 \mu\text{m}$ diameter.

5.4.5 Membranes Formation at Microcavities of Optimized SOI Chips

For all measurements below the samples were improved in two ways: the cavity diameter was doubled by increasing the underetch time and a 250 nm thick oxide layer was grown on the SOI layer. The complete oxidation in the underetched regions causes the top layer to be transparent.

SOPC/OG DHPE vesicles were fused under the same conditions as above on the surface of the fully oxidized top layer. The surface fluorescence topology is plotted in Figure 45. The interference rings were visible in the regions of wedge-shaped cavity walls. One more interference ring appeared at the edge of the pore, where the top oxide thickness decreased due to the rounding of the edges.

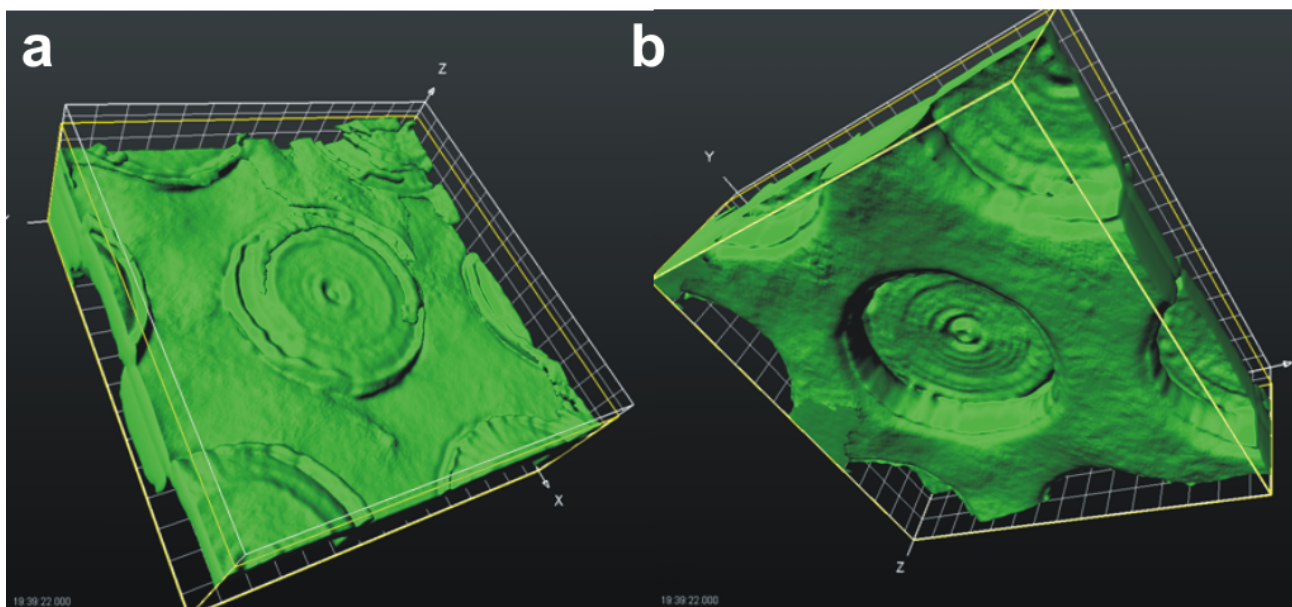


Figure 45: Fluorescence topology of an OG labelled membrane on the improved substrate (sample 4). (a) Top view and (b) bottom view: Interference rings are restricted to the outer region of the cavities, the region around the pore shows evenly distributed fluorescence. The scale is 2.5 $\mu\text{m}/\text{div}$.

The fluorescence was evenly distributed over the complete cavity and the planes in between cavities. This demonstrates that the lipid bilayer is spanned across the pore. The pore geometry appears more regular and flatter than in the earlier SOI chip generations.

Altogether the oxidation enabled visualization of the membranes on the SOI surface. Reduction of artificial optical effects in the inner region was improved by increasing the cavity size by prolonged underetching. Nevertheless, the optics of the cavity was still complicated. Further improvements could be obtained by complete oxidation of the SOI layer in the non-underetched regions to simplify the interpretation of the optical investigations. First functionality of the lipid bilayer on the cavity substrates will be presented in the next section.

5.4.6 Immobilization of His-tagged Proteins on Chelator Lipid Membranes

Small unilamellar vesicles containing DODA-NTA were formed in a solution containing 50 μM TAMRA. TAMRA was present inside and outside of the vesicles before and during vesicle

fusion. After membrane formation the TAMRA was washed thoroughly from the surface and the red dye was present only underneath the membrane, as illustrated in Figure 46.

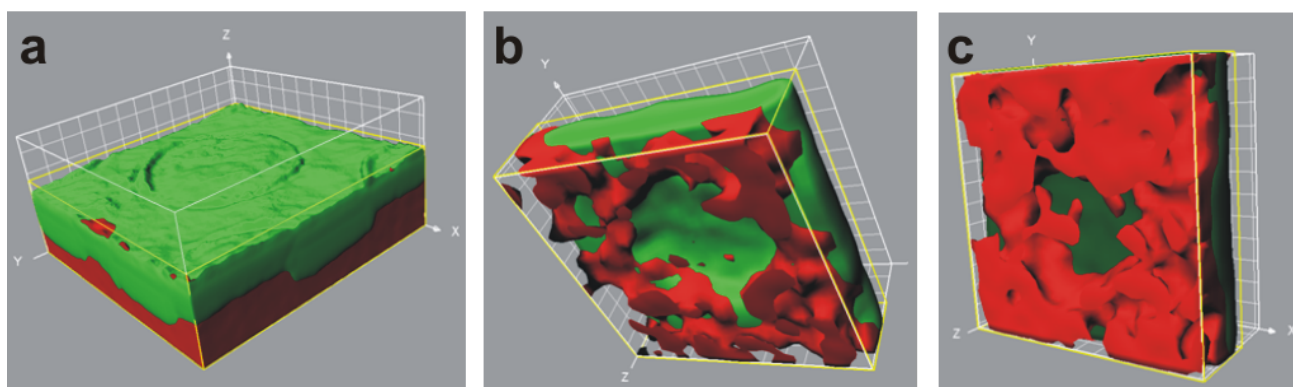


Figure 46: TAMRA is captured below a closed membrane of SOPC/DODA-NTA (sample 5) with immobilized OG-labelled His₁₀ MBP. (a) Top rotated to a (b) low side and (c) bottom view. The scale is 2.5 $\mu\text{m}/\text{div}$.

Subsequently His-tagged maltose binding protein (OG His₁₀ MBP) was immobilized onto the DODA-NTA lipids on the membrane. The green labelled protein was dispersed homogenously on the surface – even in the pore region. Hence, this result suggests that the membrane spanned and covered the pores as well. Otherwise the pores would have been visible as dark spots in the microscopic images. Red fluorescence (due to the added TAMRA dye) was only detected beyond the pore regions and demonstrated that the dye was trapped between the membrane and the chip surface. Dye molecules in the pore region were not detectable with CLSM probably due to diffusion processes at different focal planes.

5.4.7 Conclusions

Membrane proteins are complicated in handling and hence require sophisticated solutions for chip technological application. A silicon-on-insulator (SOI) chip substrate with microcavities and nanopores was employed for first technological investigation to construct a protein chip suitable for membrane proteins. The formation of an artificial lipid bilayer using vesicle fusion on oxidized SOI cavity substrates was verified by CLSM. The fluidity of the membrane was proven by FRAP experiments and the functionality of the membrane was shown by immobilization of OG His₁₀ MBP to chelator lipids. AFM experiments, in analogy to previous work²¹⁴, will give further insights into the chip architecture and topography. This will provide last evidence of the sealing of the cavity by the lipid bilayer. Regeneration of the membrane-covered chip surface will be achieved by addition of imidazole and EDTA. Transmembrane proteins, as for example α -hemolysin^{215, 216} or

the transport machinery TAP²¹⁷, will be employed for reconstitution experiments on this membrane protein chip platform.

For future applications sensors can be integrated into the top silicon layer. The cavities can then be separated from each other by an additional etching step as it has been shown for sensors integrated into microfluidic devices²¹⁰. After the integration of local sensors to the cavities, the content of each cavity can be measured separately, as illustrated in Figure 47. The sensing area is equivalent to the size of the cavity sealing, and a four point measurement would be possible, as well. Large arrays of sensors could then be measured simultaneously and employed in nanobiotechnological applications.

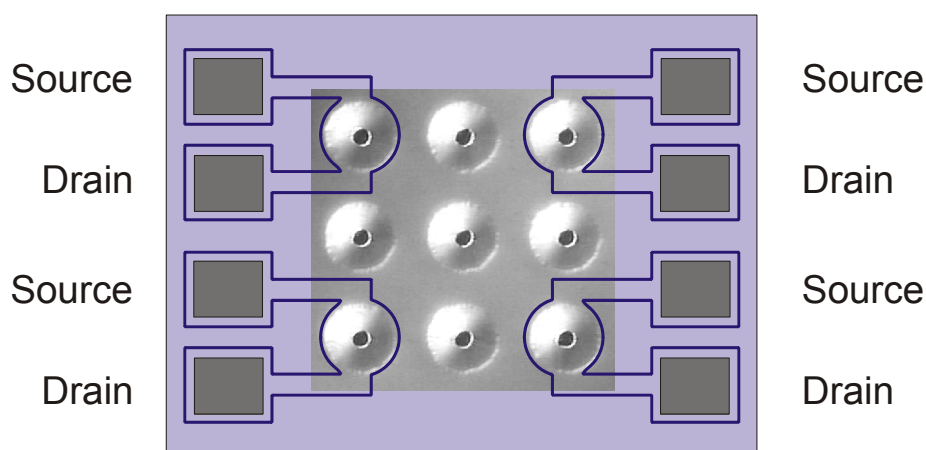


Figure 47: Each cavity can be separately addressed by a planar field effect sensor.

By means of nanospotting or membrane patterning technologies various transmembrane proteins could be trapped in each cavity pore. Lateral organization and guiding of cells on surfaces is another future vision within the scope of this project. Via microfluidic channels it will be possible to address each microcavity differentially and hence, control cellular locomotion and signal transduction in complete artificial environments. This technology will provide a platform at the interface between nanotechnology and systems biology.

The growing emphasis on single-cell analysis derives from increasing appreciation of phenotypic heterogeneity among cells in a population and of the scientific insight that derives from accurately assaying this heterogeneity. Physicochemical modelling of biological processes also demands single-cell data, or at least information about the distributions of key parameters. However, notable challenges remain in the detection of low-abundance proteins, which tend to adhere non-specifically to surfaces (which are larger per unit volume in many microsystems than in

laboratory-scale devices). Trade-offs are likely to exist between measuring more variables and using fewer cells. Excessive emphasis on single-cell analysis, rather than on the use of microtechnology to link complex heterogeneous cultures, controlled perturbations and cell fractionation, is unwarranted. Although significant challenges face routine applications of “cells on chips”, tremendous advances have been realized over the past decade, and a future in which chips effectively compete with laboratory-scale technologies in the analysis of complex biological phenomena is clearly in sight. Highly integrated microdevices will find application in basic biomedical and pharmaceutical research, whereas robust and portable point-of-care devices will be used in clinical settings²¹⁸.

6 Summary, Conclusions & Perspectives

Iucundi acti labores.

Arbeiten sind angenehm, wenn sie getan sind.

CICERO

6.1 English Version

First milestone of this Ph.D. thesis was the successful extension of conventional NTA/His₆-tag technique to self-assembling, multivalent chelator thiols for high-affinity recognition as well as stable and uniform immobilization of His₆-tagged proteins on chip surfaces. Bis-NTA was linked via an oligoethylene glycol to alkyl thiols by an efficient modular synthesis strategy yielding a novel, multivalent compound for formation of mixed SAMs with anti-adsorptive matrix thiols on gold. His-tag recognition and capturing, as well as its metal ion-dependent nature was studied and visualized by CFM. SPR experiments with receptors successfully demonstrated the suitability of this format for delicate biophysical assays with high reproducibility. Multivalent chelator chips allow a specific, high-affinity, reversible, long-term immobilization of His₆-tagged proteins. Micro-structured chip surfaces allow the generation of protein micro arrays for high-throughput screening by fluorescence techniques. Furthermore, this chip platform was successfully applied for one-step purification and mass spectrometric analysis of His-tagged and phosphorylated proteins from complex mixtures as complete cell lysates. In AFM studies reversibility of the specific protein immobilization process was visualized at single molecule level. The entire control over the orientation of the immobilized protein promotes this chip surface to an optimal platform for studies focusing on research targets at single molecule level and nanobiotechnology.

Based on the constructed protein chip platform above and a novel AFM mode (contact oscillation mode, COM) – developed during the current Ph.D. work – protein nanolithography under physiological conditions enabling fabrication of active biomolecular patterns in countless variety has been established. Reversible COM-mediated nanostructuring is exceptionally suitable for multiplexed patterning of protein assemblies *in situ*. This AFM technique elegantly permits instant switching between imaging and replacement of immobilized proteins at native state with no need to change the setup or the tip. The first self-assembled protein layer acts as a biocompatible and ductile patterning material. Immobilized proteins can be replaced by the AFM tip applying COM, and the generated structures can be erased and refilled with different proteins, which are immobilized in a uniform and functional

manner. Multi-protein arrays can be systematically fabricated by iterative erase-and-write processes, and employed for protein-protein interaction analysis. Libraries of proteins, protein assemblies as well as virus particles or cellular domains can be organized at nanoscale. Fabrication of two-dimensionally arranged nanocatalytic centres with biological activity will establish a versatile tool for nanobiotechnology.

Different application sites require different protein chip technologies. As an alternative chip fabrication approach, the combined application of methodologies from surface chemistry, semiconductor technology, and chemical biology demonstrated successfully how pre-patterned templates for micro- and nanoarrays for protein chips are fabricated. The surface physical, as well the biophysical experiments, proved the functionality of this technology. Future goals are the establishment of such pre-patterned templates down to a few nanometers, in order to achieve single molecular arrays of biological entities. Further target is the transfer of the complete fabrication process into gas phase deposition. As many parameters for gas phase fabrication of processes as chemical coupling are not known, this approach is challenging. The promises of such process technology are fast and economic fabrication of ready-to-use nanostructured biochips at industrial scale.

Membrane proteins are complicated in handling and hence require sophisticated solutions for chip technological application. A silicon-on-insulator (SOI) chip substrate with microcavities and nanopores was employed for first technological investigation to construct a protein chip suitable for membrane proteins. The formation of an artificial lipid bilayer using vesicle fusion on oxidized SOI cavity substrates was verified by CLSM. The fluidity of the membrane was proven by FRAP experiments and the functionality of the membrane was shown by immobilization of His-tagged proteins to chelatorlipids. Future AFM experiments will give further insights into the chip architecture and topography. This will provide last evidence of the sealing of the cavity by the lipid bilayer. Transmembrane proteins, as for example α -hemolysin or TAP, will be employed for reconstitution experiments on this membrane protein chip platform. For future applications sensors can be integrated into the top silicon layer. The cavities can then be separated from each other by an additional etching step as it has been shown for sensors integrated into microfluidic devices. Highly integrated microdevices will find application in basic biomedical and pharmaceutical research, whereas robust and portable point-of-care devices will be used in clinical settings.

6.2 German Version – Ausführliche Zusammenfassung

Die Entschlüsselung des menschlichen Genoms zur Jahrtausendwende lieferte einerseits Zugang zu dieser riesengroßen „biologischen Datenbank“, andererseits wurde nun jedoch auch bewusst, dass die genetische Information alleine für ein umfassendes Verständnis biologischer Prozesse nicht hinreichend ist. Das Studium der zahllosen Produkte der etwa 20.000-25.000 menschlichen Gene wird die biologische Forschung der nächsten 20 Jahre bestimmen. In der jetzigen post-genomischen Ära, werden nun internationale Forschungsprojekte – ähnlich dem Human-Genom-Projekt in den 80er und 90er Jahren – zur Kartierung des menschlichen Proteoms initiiert. Die sogenannte Proteomik oder Proteomforschung hat das Ziel der systematischen Erforschung der Myriaden von Protein-Protein-Wechselwirkungsnetzwerken und ist die aktuelle Herausforderung der Biowissenschaften. Multiplexe und hochparallele Biosensoren und Proteinchip-Technologien liefern nützliche Werkzeuge für diese Herausforderung. Interaktionsstudien an einzelnen Biomolekülen versprechen neue mechanistische Erkenntnisse über die biologischen Prozesse der Signal- und Energiewandlung. Zur Realisierung solcher Studien besteht ein großes Interesse in der Organisation und Manipulation von funktionalen Biomolekülen an kontrollierten Positionen von Chipoberflächen im Nanometermaßstab. Solche Nanoarrays bieten zudem auch wirtschaftliche Vorteile, da nur noch Kleinstmengen an (zumeist in der Herstellung kostbaren) Proteinen benötigt werden. Verschiedenste ausgefeilte Technologien werden bereits erfolgreich zur Erzeugung von Mikro- und Nanoarrays mit Proteinen eingesetzt. Aktuelle Strategien zur Anbindung von Proteinen an Oberflächen, Oberflächenmodifikation von Chipsubstraten und nanolithographische Methoden werden in der Einleitung (Kapitel 1) beschrieben.

Idealerweise sollten Proteine ausschließlich unter physiologischen Bedingungen in einheitlicher molekularer Orientierung immobilisiert werden. Nur dann kann der Funktionserhalt der immobilisierten Proteine gewährleistet werden. Weiterhin ist die Spezifität der Immobilisierungsreaktion ein bedeutender Parameter – schließlich sollten ausschließlich die Proteine von Interesse an die Chipoberflächen angebunden werden. Basierend auf dem Konzept der NTA/His₆-tag-Interaktion und Multivalenzeffekten versprechen kumulierte NTA-Chelatorgruppen die hochaffine Bindung jeglicher His-getaggtter Proteine unter physiologischen Bedingungen. Multivalente Chelatormodule wurden in verschiedenen, parallelen Projekten entworfen und für Proteinchip-Technologien optimiert.

Das Vorhaben eines Entwurfs von Proteinchip-Technologien im Nanometermaßstab beinhaltet die Integration verschiedenster experimenteller Ansätze, Methoden und Schritte. Im folgenden Fließdiagramm sind die unterschiedlichen Strategien und Meilensteine der vorliegenden Arbeit illustriert (Abbildung 48).

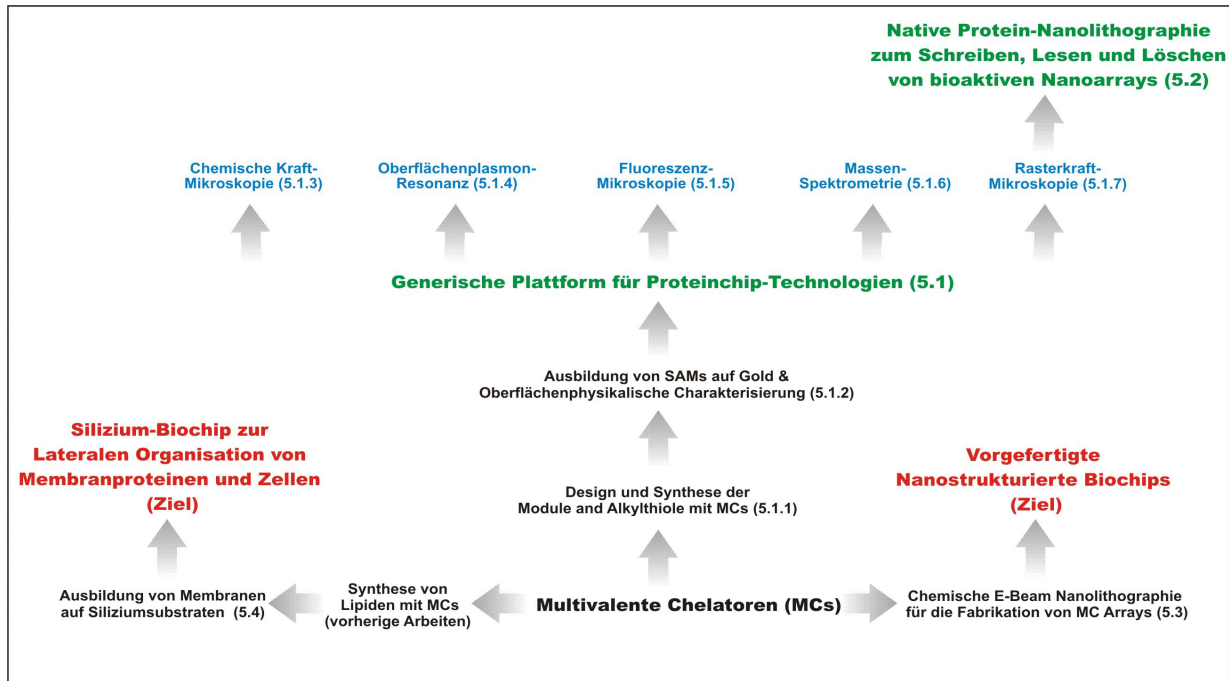


Abbildung 48: Strategie und Meilensteine für die Entwicklung einer generischen Proteinchip-Plattform und nanoskaliger Proteinarrays. Schwarz hervorgehobene Schritte sind wesentlich für die Realisierung des jeweiligen Ansatzes. Grün hervorgehobene Meilensteine sind gänzlich neuartige Konzepte. Neue Anwendungen für die Bioanalytik, die aus den Projekten resultierten, sind blau gekennzeichnet. Rotmarkierte Schritte sind angestrebte Technologien, die in zukünftigen Arbeiten anwendungsreife haben werden. Jeder aufgeführte Schritt wird in den entsprechenden Kapiteln der vorliegenden Dissertation präsentiert und erörtert.

Erster Meilenstein der vorliegenden Arbeit war die erfolgreiche Erweiterung des konventionellen NTA/His₆-tag-Konzepts auf selbst-assemblierende, multivalente Chelatorthiole für die hochaffine Erkennung und stabile, einheitliche Immobilisierung His₆-getaggtter Proteine auf Chipoberflächen (Kapitel 5.1). Mittels einer effizienten, modularen Synthesestrategie wurden Bis-NTA-Module über Oligoethylglykoleinheiten an Alkylthiole angebunden. Diese Chelatorthiole wurden zusammen mit antiadsorptiven Matrixthiolen zur Ausbildung gemischter selbst-assemblierender Monolagen (SAMs) auf Goldoberflächen eingesetzt. Die selektive Erkennung sowie Metallionen-abhängige Bindung der His-tags wurde mit der chemischen Kraftmikroskopie (CFM) untersucht. Oberflächenplasmonen-resonanz (SPR)-Experimente mit Rezeptorproteinen demonstrierten mit hoher Zuverlässigkeit die hervorragende Eignung dieses Immobilisierungskonzeptes für empfindliche

biophysikalische Versuchsaufbauten. Die multivalenten Chelatorchips erlauben eine spezifische, hochaffine, umkehrbare und langfristige Immobilisierung His₆-getaggtter Proteine. Mikrostrukturierte Chipoberflächen ermöglichen die Bildung von Proteinmikroarrays für Fluoreszenz-basierte Hochdurchsatz-Screening-Technologien. Eine weitere Anwendung dieser Chipplattform wurde für die Ein-Schritt-Aufreinigung und massenspektrometrische Untersuchung von His-getaggtten und phosphorylierten Proteinen aus komplexen Gemischen, wie z. B. Gesamtzell-Lysaten, entwickelt. Die Umkehrbarkeit der spezifischen Proteinimmobilisierung wurde in rasterkraftmikroskopischen (AFM) Studien bis zur Einzel-Molekül-Ebene visualisiert. Die vollständige Kontrolle über die Orientierung immobilisierter Proteine qualifiziert diese entwickelte Chipoberfläche zu einer optimalen Plattform für Anwendungsbereiche der Einzelmolekülbiochemie und Nanobiotechnologie.

Basierend auf dieser Plattform für Proteinchips und einem – im Rahmen dieser Arbeit – neuentwickelten AFM-Modus (Kontakoszillationsmodus, COM) wurde die „Protein-Nanolithographie“ etabliert, welche die Fabrikation von aktiven, biomolekularen Strukturen in unzähliger Vielfalt ermöglicht (Kapitel 5.2). In Abbildung 49 wird das zugrunde liegende Prinzip dieser Technologie dargestellt. Die umkehrbare COM-vermittelte Nanolithographie ist insbesondere für die multiplexe Anordnung von Proteinverbänden *in situ* geeignet. Diese AFM-Technik erlaubt ein sofortiges Umschalten zwischen Abbildung und Schreiben immobilisierter Proteine im nativen Zustand ohne, dass der experimentelle Aufbau geändert werden muss. Die erste Schicht immobilisierter Proteine fungiert als ein biokompatibles und verformbares Strukturierungsmaterial. Diese immobilisierten Proteine können nun im Kontaktozillationsmodus mit der AFM-Spitze lokal entfernt („Löschen“) und gegen andere Proteine – die an die freigelegte Chipoberfläche ebenfalls spezifisch und funktional immobilisieren – ausgetauscht werden („Schreiben“). Arrays, bestehend aus mehreren unterschiedlichen Proteinen können nun systematisch in iterativen Löschen-und-Schreib-Vorgängen fabriziert und für Proteininteraktionsanalysen eingesetzt werden. Ganze Bibliotheken von Proteinen, Proteinverbänden oder Viruspartikeln und Zelldomänen können nun im Nanometermaßstab organisiert werden. Die Fabrikation von zwei-dimensional arrangierten nanokatalytischen Zentren mit biologischer Aktivität wird von besonderem Nutzen in der Nanobiotechnologie sein.

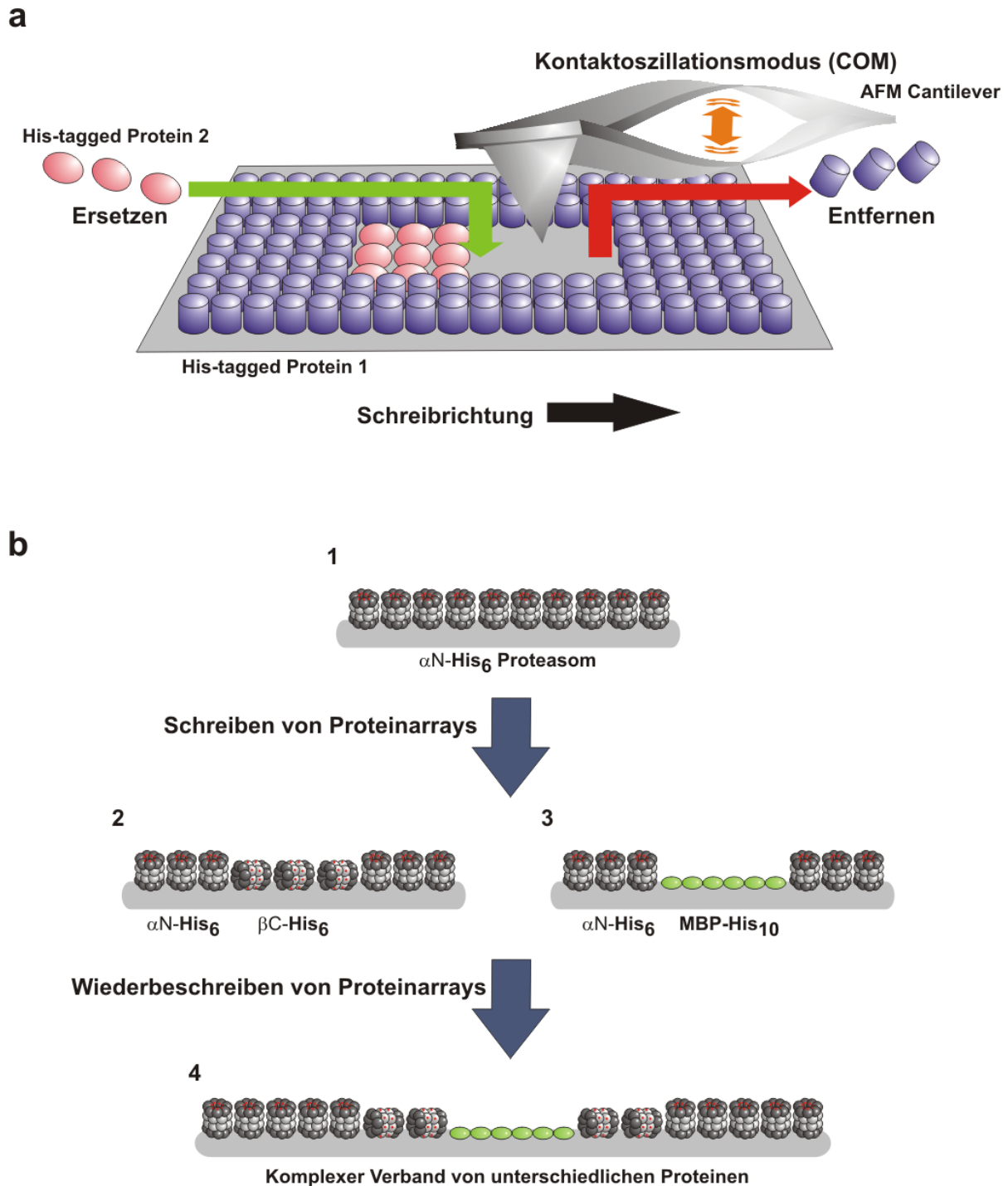


Abbildung 49: Nanofabrikation wiederbeschreibbarer Proteinnanoarrays auf Metallionen-chelatierenden Oberflächen. (a) Einheitlich orientierte His-tagged Proteine werden mit der AFM-Spitze im Kontaktoszillationsmodus (COM) entfernt und entweder gleichzeitig oder sukzessive gegen andere His-tag Proteine ersetzt. (b) In sequenziellen Schreib-und-Lösch-Vorgängen werden Strukturen aus verschiedenen Proteinen generiert. Proteine und makromolekulare Maschinerien (z. B. Maltosebindeprotein und Proteasomkomplexe) werden in unterschiedlicher Ausrichtung zu nanostrukturierten Arrays oder Verbänden organisiert (1–4).

Verschiedene Anwendungsbereiche erfordern verschiedene Technologien für Proteinchips. Eine alternative Herstellungsmethode aus einer Kombination von Oberflächenchemie, Halbleitertechnologie und chemischer Biologie wurde für die Fabrikation von vorstrukturierten Templaten für Mikro- und Nanoarrays entwickelt (Kapitel 5.3). Die Funktionalität dieser Chipplattform wurde anhand oberflächen- und biophysikalischer Experimente erfolgreich gezeigt. Zukünftiges Ziel ist die Anfertigung vorstrukturierter Template in der Dimension weniger Nanometer zur Ausbildung von Bio-Arrays mit einzelnen Molekülen. Ein weiteres Ziel besteht in der kompletten Verlagerung des Herstellungsprozesses in die Gasphase. Eine Produktion in der Gasphase verspricht eine schnelle und wirtschaftliche Erzeugung sofort einsatzbereiter nanostrukturierter Biochips im industriellen Maßstab.

Der Umgang mit Membranproteinen verlangt besondere Vorkehrungen im experimentellen Milieu, ebenso speziell sind die Bedürfnisse in den entsprechenden Chip-Anwendungen. Ein Chip mit Mikrokavitäten und Nanoporen, basierend auf der „Silicon-on-Insulator“ (SOI)-Technologie, wurde für erste technologische Studien zum Entwurf eines Proteinchips für Membranproteine eingesetzt (Kapitel 5.4). Künstliche Lipidmembranen wurden auf der SOI-Oberfläche mittels Vesikelfusion ausgebildet und mit konfokaler Laser-Scanning-Mikroskopie gezeigt. Die Fluidität der Membran wurde in Fluoreszenzerholungsexperimenten-nach-Lichtbleichung (FRAP) bestätigt. Die Funktionalität der Membran wurde durch die Immobilisierung His-getaggtter Proteine an Chelatorlipiden überprüft. Zukünftige AFM-Experimente werden weitere Einsichten in die Chiparchitektur und Topographie ermöglichen. Transmembranproteine, wie α -Hämolyisin oder TAP, werden in Rekonstitutionsexperimenten für funktionale Studien der Membranproteinchips eingesetzt. Für zukünftige Anwendungen können Sensoren in die obere Siliziumschicht integriert werden. Die Kavitäten können voneinander in zusätzlichen Ätzschritten getrennt und mit Mikrofluidiksystemen separat adressiert werden. Anwendungsbereiche solcher hochintegrierten Mikrosysteme sind sowohl in der biologischen Grundlagenforschung als auch in mobilen Diagnostikgeräten im klinischen Einsatz zu finden.

Das Hauptbestreben der gesamten Forschungsprojekte der vorliegenden Dissertation war die Entwicklung und Bereitstellung nanobiotechnologischer Werkzeuge für die Proteomforschung, Strukturbiologie und Biomedizin.

7 Synopsis of Collaborations

Coming together is a beginning; keeping together is progress; working together is success.

HENRY FORD

Due to the broad interdisciplinary nature of all research projects, the work was performed partially in frame of cooperations with institutions of different expertise. The project “*Formation of Self-Assembled Monolayers with Multivalent Chelator Thiols*” (Chapter 5.1.2) was performed in collaboration with Prof. Dr. Bo LIEDBERG and Dr. Ramūnas VALIOKAS at the Institute of Sensor Science and Molecular Physics Division, Dept. of Physics and Measurement Technology, Linköping University (Linköping, Sweden). Mass spectrometric experiments “*Purification on a Chip – One-step Enrichment and Analysis*” (Chapter 5.1.6) were conducted together with Prof. Dr. Michael KARAS at the Institute of Pharmaceutical Chemistry, BioCenter, Johann Wolfgang GOETHE University (Frankfurt am Main, Germany).

The physics behind “*Reversible Patterning of Protein Monolayers by Contact Oscillation Mode*” (Chapter 5.2.2) was investigated in kind collaboration with Dr. Reinhard GUCKENBERGER and Dipl.-Phys. Mirjam BEUTTLER at the Max Planck Institute of Biochemistry in Martinsried (Munich, Germany).

“*High-Affinity Protein Chip Fabrication by Chemical E-Beam Nanolithography*” (Chapter 5.3) was developed together with Prof. Dr. Armin GÖLZHÄUSER and Dr. Andrey TURCHANIN at the Faculty of Physics of the University Bielefeld (Bielefeld, Germany).

Prof. Dr. Marc TORNOW and Dr. Karin BUCHHOLZ from the Walter SCHOTTKY-Institute of Technical University Munich provided the silicon-on-insulator chips for the joint project “*Nanostructured Silicon Chips for Lateral Organization of Membrane Proteins*” (Chapter 5.4).

Furthermore, I was involved in different research projects addressing surface chemical and nanobiotechnological challenges, which are not described in the current thesis, but represented in my list of publications [e.g. with Prof. Dr. Peter HINTERDORFER, Prof. Dr. Hermann GRUBER, and Prof. Dr. Christoph ROMANIN at the Institute of Biophysics at the Johannes KEPLER University (Linz, Austria)].

8 References

Πάντες ἄνθρωποι τοῦ εἶδέναι ὀρέγονται φύσει

Alle Menschen streben von Natur nach Wissen.

ARISTOTELES

1. Venter, J. C. et al. The sequence of the human genome. *Science* 291, 1304-1351 (2001).
2. Lander, E. S. et al. Initial sequencing and analysis of the human genome. *Nature* 409, 860-921 (2001).
3. Peltonen, L. & McKusick, V. A. Genomics and medicine. Dissecting human disease in the postgenomic era. *Science* 291, 1224-1229 (2001).
4. Consortium, I. H. G. S. Finishing the euchromatic sequence of the human genome. *Nature* 431, 931-945 (2004).
5. McKusick, V. A. HUGO news. The Human Genome Organisation: history, purposes, and membership. *Genomics* 5, 385-387 (1989).
6. HUPO (Human Proteome Organization) 1st World Congress. 21-24 November 2002, Versailles, France. *Mol. Cell. Proteomics* 1, 651-752 (2002).
7. Goodsell, D. S. *Bionanotechnology - Lessons from Nature*. WILEY-LISS, Inc. Hoboken, New Jersey (2004).
8. Zhu, H. et al. Global analysis of protein activities using proteome chips. *Science* 293, 2101-2105 (2001).
9. Wilson, D. S. & Nock, S. Functional protein microarrays. *Curr. Opin. Chem. Biol.* 6, 81-85 (2002).
10. Washburn, M. P. Soft landing for protein chips. *Nature Biotechnol.* 21, 1156-1157 (2003).
11. Zhu, H. & Snyder, M. Protein chip technology. *Curr. Opin. Chem. Biol.* 7, 55-63 (2003).
12. Bertone, P. & Snyder, M. Advances in functional protein microarray technology. *FEBS Journal* 272, 5400-5411 (2005).
13. Lynch, M. et al. Functional protein nanoarrays for biomarker profiling. *Proteomics* 4, 1695-1702 (2004).
14. Lander, E. S. Array of hope. *Nature Genetics* 21, 3-4 (1999).
15. Southern, E., Mir, K. & Shchepinov, M. Molecular interactions on microarrays. *Nature Genetics* 21, 5-9 (1999).
16. Gershon, P. D. & Khilko, S. Stable chelating linkage for reversible immobilization of oligohistidine tagged proteins in the Biacore surface-plasmon resonance detector. *J. Immunol. Methods* 183, 65-76 (1995).
17. Martzen, M. R. et al. A biochemical genomics approach for identifying genes by the activity of their products. *Science* 286, 1153-1155 (1999).
18. Gokce, I. et al. The TolA-recognition site of colicin N. ITC, SPR and stopped-flow fluorescence define a crucial 27-residue segment. *J. Mol. Biol.* 304, 621-632 (2000).

19. Quetglas, S., Leveque, C., Miquelis, R., Sato, K. & Seagar, M. Ca^{2+} -dependent regulation of synaptic SNARE complex assembly via a calmodulin- and phospholipid-binding domain of synaptobrevin. *Proc. Natl. Acad. Sci. USA* 97, 9695-9700 (2000).
20. Riggs, P. Expression and purification of recombinant proteins by fusion to maltose-binding protein. *Mol. Biotechnol.* 15, 51-63 (2000).
21. Bach, H. et al. *Escherichia coli* maltose-binding protein as a molecular chaperone for recombinant intracellular cytoplasmic single-chain antibodies. *J. Mol. Biol.* 312, 79-93 (2001).
22. Bouchard, B. A., Furie, B. & Furie, B. C. Glutamyl substrate-induced exposure of a free cysteine residue in the vitamin K-dependent gamma-glutamyl carboxylase is critical for vitamin K epoxidation. *Biochemistry* 38, 9517-9523 (1999).
23. Pearson, D. L., Reimonenq, R. D. & Pollard, K. M. Expression and purification of recombinant mouse fibrillarin. *Protein Expression Purif.* 17, 49-56 (1999).
24. Schmitt, J., Hess, H. & Stunnenberg, H. G. Affinity purification of histidine-tagged Proteins. *Mol. Biol. Rep.* 18, 223-230 (1993).
25. Hochuli, E. Large-scale chromatography of recombinant proteins. *J. Chromatogr.* 444, 293-302 (1988).
26. Hochuli, E. Purification of recombinant proteins with metal chelate adsorbent. *Genet. Eng.* 12, 87-98 (1990).
27. Bornhorst, J. A. & Falke, J. J. Purification of proteins using polyhistidine affinity tags. *Applications of Chimeric Genes and Hybrid Proteins, Pt A* 326, 245-254 (2000).
28. Kindermann, M., George, N., Johnsson, N. & Johnsson, K. Covalent and selective immobilization of fusion proteins. *J. Am. Chem. Soc.* 125, 7810-7811 (2003).
29. Kwon, Y., Han, Z., Karatan, E., Mrksich, M. & Kay, B. K. Antibody arrays prepared by cutinase-mediated immobilization on self-assembled monolayers. *Anal. Chem.* 76, 5713-5720 (2004).
30. Hodneland, C. D., Lee, Y. S., Min, D. H. & Mrksich, M. Selective immobilization of proteins to self-assembled monolayers presenting active site-directed capture ligands. *Proc. Natl. Acad. Sci. USA* 99, 5048-5052 (2002).
31. Porath, J., Carlsson, J., Olsson, I. & Belfrage, G. Metal chelate affinity chromatography, a new approach to protein fractionation. *Nature* 258, 598-599 (1975).
32. Arnold, F. H. *Metal-affinity protein separations* (Academic Press, San Diego, 1992).
33. Hochuli, E., Bannwarth, W., Döbeli, H., Gentz, R. & Stüber, D. Genetic approach to facilitate purification of novel recombinant proteins with a novel metal chelate adsorbent. *BioTechniques* 6, 1321-1325. (1988).
34. Nieba, L. et al. BIACORE analysis of histidine-tagged proteins using a chelating NTA sensor chip. *Anal. Biochem.* 252, 217-228 (1997).
35. Dorn, I. T., Neumaier, K. R. & Tampé, R. Molecular recognition of histidine-tagged molecules by metal-chelating lipids monitored by fluorescence energy transfer and correlation spectroscopy. *J. Am. Chem. Soc.* 120, 2753-2763 (1998).
36. Schmitt, L., Dietrich, C. & Tampé, R. Synthesis and characterization of chelator-lipids for reversible immobilization of engineered proteins at self-assembled lipid interfaces. *J. Am. Chem. Soc.* 116, 8485-8491 (1994).
37. Shnek, D. R., Pack, D. W., Sasaki, D. Y. & Arnold, F. H. Specific protein attachment to artificial membranes via coordination to lipid-bound Copper(II). *Langmuir* 10, 2382-2388 (1994).

38. Dorn, I. T., Pawlitschko, K., Pettinger, S. C. & Tampé, R. Orientation and two-dimensional organization of proteins at chelator lipid interfaces. *Biol. Chem.* 379, 1151-1159 (1998).
39. Dorn, I. T., Eschrich, R., Seemüller, E., Guckenberger, R. & Tampé, R. High-resolution AFM-imaging and mechanistic analysis of the 20 S proteasome. *J. Mol. Biol.* 288, 1027-1036 (1999).
40. Thess, A. et al. Specific orientation and two-dimensional crystallization of the proteasome at metal-chelating lipid interfaces. *J. Biol. Chem.* 277, 36321-36328 (2002).
41. Meyers, D. *Surfaces, Interfaces, and Colloids: Principles and Applications*, Second Edition. John Wiley & Sons, Inc. (1999).
42. Singer, S. J. & Nicolson, G. L. Fluid mosaic model of structure of cell-membranes. *Science* 175, 720-731 (1972).
43. Engelman, D. M. Membranes are more mosaic than fluid. *Nature* 438, 578-580 (2005).
44. Winter, R. & Noll, F. *Methoden der Biophysikalischen Chemie*. Teubner Verlag (1998).
45. Andersen, O. S., Koeppe, R. E. & Roux, B. Gramicidin channels. *IEEE T. Nanobioscience* 4, 10-20 (2005).
46. Schmitt, L. & Tampé, R. Structure and mechanism of ABC transporters. *Curr. Opin. Struct. Biol.* 12, 754-760 (2002).
47. Lodish, H. et al. *Molecular Cell Biology*. New York: W. H. Freeman & Co (2000).
48. Neher, E. & Sakmann, B. Single-channel currents recorded from membrane of denervated frog muscle fibres. *Nature* 260, 799-802 (1976).
49. Fertig, N., Blick, R. H. & Behrends, J. C. Whole cell patch clamp recording performed on a planar glass chip. *Biophys. J.* 82, 3056-3062 (2002).
50. Mueller, P., Rudin, D. O., Tien, H. T. & Wescott, W. C. Reconstitution of cell membrane structure in vitro and its transformation into an excitable system. *Nature* 194, 979-980 (1962).
51. Ide, T. & Yanagida, T. An artificial lipid bilayer formed on an agarose-coated glass for simultaneous electrical and optical measurement of single ion channels. *Biochem. Biophys. Res. Commun.* 265, 595-599 (1999).
52. Dietrich, C. & Tampe, R. Charge determination of membrane molecules in polymer-supported lipid layers. *Biochim. Biophys. Acta* 1238, 183-191 (1995).
53. Rädler, U., Mack, J., Persike, N., Jung, G. & Tampé, R. Design of supported membranes tethered via metal-affinity ligand-receptor pairs. *Biophys. J.* 79, 3144-3152 (2000).
54. Fertig, N. et al. Stable integration of isolated cell membrane patches in a nanomachined aperture. *Appl. Phys. Lett.* 77, 1218-1220 (2000).
55. Schmidt, C., Mayer, M. & Vogel, H. A chip-based biosensor for the functional analysis of single ion channels. *Angew. Chem. Int. Ed. Engl.* 39, 3137-3140 (2000).
56. Römer, W. & Steinem, C. Impedance analysis and single-channel recordings on nano-black lipid membranes based on porous alumina. *Biophys. J.* 86, 955-965 (2004).
57. Malmstadt, N., Nash, M. A., Purnell, R. F. & Schmidt, J. J. Automated formation of lipid-bilayer membranes in a microfluidic device. *Nano Lett.* 6, 1961-1965 (2006).

58. Schmitt, E. K., Vrouenraets, M. & Steinem, C. Channel activity of OmpF monitored in nano-BLMs. *Biophys. J.* 91, 2163-2171 (2006).
59. Steltenkamp, S. et al. Mechanical properties of pore-spanning lipid bilayers probed by atomic force microscopy. *Biophys. J.* 91, 217-226 (2006).
60. Danelon, C., Perez, J. B., Santschi, C., Brugger, J. & Vogel, H. Cell membranes suspended across nanoaperture arrays. *Langmuir* 22, 22-25 (2006).
61. Purrucker, O., Hillebrandt, H., Adlkofer, K. & Tanaka, M. Deposition of highly resistive lipid bilayer on silicon-silicon dioxide electrode and incorporation of gramicidin studied by ac impedance spectroscopy. *Electrochim. Acta* 47, 791-798 (2001).
62. Jiang, Y., Ruta, V., Chen, J., Lee, A. & MacKinnon, R. The principle of gating charge movement in a voltage-dependent K⁺ channel. *Nature* 423, 42-48 (2003).
63. Mannuzzu, L. M., Moronne, M. M. & Isacoff, E. Y. Direct physical measure of conformational rearrangement underlying potassium channel gating. *Science* 271, 213-216 (1996).
64. Cha, A. & Bezanilla, F. Characterizing voltage-dependent conformational changes in the Shaker K⁺ channel with fluorescence. *Neuron* 19, 1127-1140 (1997).
65. Mueller, P., Wescott, W. C., Rudin, D. O. & Tien, H. T. Methods for formation of single bimolecular lipid membranes in aqueous solution. *J. Phys. Chem.* 67, 534-538 (1963).
66. Henn, F. A. & Thompson, T. E. Synthetic lipid bilayer membranes. *Annu. Rev. Biochem.* 38, 241-262 (1969).
67. Ogier, S. D. et al. Suspended planar phospholipid bilayers on micromachined supports. *Langmuir* 16, 5696-5701 (2000).
68. McConnell, H. M., Watts, T. H., Weis, R. M. & Brian, A. A. Supported planar membranes in studies of cell-cell recognition in the immune system. *Biochim. Biophys. Acta* 864, 95-106 (1986).
69. Barenholz, Y. et al. A simple method for the preparation of homogeneous phospholipid vesicles. *Biochemistry* 16, 2806-2810 (1977).
70. Groves, J. T., Ulman, N. & Boxer, S. G. Micropatterning fluid lipid bilayers on solid supports. *Science* 275, 651-653 (1997).
71. Orth, R. N. et al. Creating biological membranes on the micron scale: forming patterned lipid bilayers using a polymer lift-off technique. *Biophys. J.* 85, 3066-3073 (2003).
72. Yoshina-Ishii, C. & Boxer, S. G. Controlling two-dimensional tethered vesicle motion using an electric field: interplay of electrophoresis and electro-osmosis. *Langmuir* 22, 2384-2391 (2006).
73. Perez, T. D., Nelson, W. J., Boxer, S. G. & Kam, L. E-cadherin tethered to micropatterned supported lipid bilayers as a model for cell adhesion. *Langmuir* 21, 11963-11968 (2005).
74. Groves, J. T. & Boxer, S. G. Micropattern formation in supported lipid membranes. *Acc. Chem. Res.* 35, 149-157 (2002).
75. Lenz, P., Ajo-Franklin, C. M. & Boxer, S. G. Patterned supported lipid bilayers and monolayers on poly(dimethylsiloxane). *Langmuir* 20, 11092-11099 (2004).

76. Moran-Mirabal, J. M. et al. Micrometer-sized supported lipid bilayer arrays for bacterial toxin binding studies through total internal reflection fluorescence microscopy. *Biophys. J.* 89, 296-305 (2005).
77. Groves, J. T. & Boxer, S. G. Electric field-induced concentration gradients in planar supported bilayers. *Biophys. J.* 69, 1972-1975 (1995).
78. Groves, J. T., Boxer, S. G. & McConnell, H. M. Electric field-induced reorganization of two-component supported bilayer membranes. *Proc. Natl. Acad. Sci. USA* 94, 13390-13395 (1997).
79. Groves, J. T., Boxer, S. G. & McConnell, H. M. Electric field-induced critical demixing in lipid bilayer membranes. *Proc. Natl. Acad. Sci. USA* 95, 935-938 (1998).
80. Milhiet, P. E. et al. High-resolution AFM of membrane proteins directly incorporated at high density in planar lipid bilayer. *Biophys. J.* 91, 3268-3275 (2006).
81. Ulman, A. Formation and structure of self-assembled monolayers. *Chem. Rev.* 96, 1533-1554 (1996).
82. Schwartz, D. K. Mechanisms and kinetics of self-assembled monolayer formation. *Annu. Rev. Phys. Chem.* 52, 107-137 (2001).
83. Bigelow, W. C., Pickett, D. L. & Zisman, W. A. Oleophobic monolayers: I. Films adsorbed from solution in non-polar liquids. *J. Coll. Sci.* 1, 513-538 (1946).
84. Nuzzo, R. G. & Allara, D. L. Adsorption of bifunctional organic disulfides on gold surfaces. *J. Am. Chem. Soc.* 105, 4481-4483 (1983).
85. Love, J. C., Estroff, L. A., Kriebel, J. K., Nuzzo, R. G. & Whitesides, G. M. Self-assembled monolayers of thiolates on metals as a form of nanotechnology. *Chem. Rev.* 105, 1103-1169 (2005).
86. Fenter, P., Eberhardt, A. & Eisenberger, P. Self-assembly of n-alkyl thiols as disulfides on Au(111). *Science* 266, 1216-1218 (1994).
87. Delamarche, E., Michel, B., Kang, H. & Gerber, C. Thermal stability of self-assembled monolayers. *Langmuir* 10, 4103-4108 (1994).
88. Atre, S. V., Liedberg, B. & Allara, D. L. Chain-length dependence of the structure and wetting properties in binary composition monolayers of OH-terminated and CH₃-terminated alkanethiolates on gold. *Langmuir* 11, 3882-3893 (1995).
89. Boncheva, M. & Whitesides, G. M. Making things by self-assembly. *MRS Bulletin* 30, 736-742 (2005).
90. Fersht, A. *Structure and Mechanism in Protein Science. Guide to Enzyme Catalysis and Protein Folding.* W. H. Freeman & Co Ltd. (1999).
91. Lehn, J. M. Supramolecular chemistry - scope and perspectives, molecules, supermolecules, and molecular devices (Nobel Lecture). *Angew. Chem. Int. Ed. Engl.* 27, 89-112 (1988).
92. Mirkin, C. A., Letsinger, R. L., Mucic, R. C. & Storhoff, J. J. A DNA-based method for rationally assembling nanoparticles into macroscopic materials. *Nature* 382, 607-609 (1996).
93. van Blaaderen, A., Ruel, R. & Wiltzius, P. Template-directed colloidal crystallization. *Nature* 385, 321-324 (1997).
94. Terfort, A., Bowden, N. & Whitesides, G. M. Three-dimensional self-assembly of millimetre-scale components. *Nature* 386, 162-164 (1997).
95. <http://www.ifm.liu.se/applphys/biomaterial/research/sam.html> (2000).

96. Whitesides, G. M., Kriebel, J. K. & Love, J. C. Molecular engineering of surfaces using self-assembled monolayers. *Science Progress* 88, 17-48 (2005).
97. Delamarche, E., Michel, B., Biebuyck, H. A. & Gerber, C. Golden interfaces: The surface of self-assembled monolayers. *Advanced Materials* 8, 719-729 (1996).
98. www.assemblon.com. Product Catalog. (2006).
99. Balzani, V., Credi, A. & Venturi, M. *Molecular Devices and Machines - A Journey into the Nano World*. WILEY-VCH Verlag GmbH & Co. KGaA, Weinheim (2003).
100. Mrksich, M. & Whitesides, G. M. Patterning self-assembled monolayers using microcontact printing - a new technology for biosensors. *Trends Biotechnol.* 13, 228-235 (1995).
101. Mrksich, M. & Whitesides, G. M. Using self-assembled monolayers to understand the interactions of man-made surfaces with proteins and cells. *Annu. Rev. Biophys. Biomol. Struct.* 25, 55-78 (1996).
102. Waldeck, D. H., Alivisatos, A. P. & Harris, C. B. Nonradiative damping of molecular electronic excited states by metal surfaces. *Surface Science* 158, 103-125 (1985).
103. Imahori, H. et al. Chain length effect on the structure and photoelectrochemical properties of self-assembled monolayers of porphyrins on gold electrodes. *J. Phys. Chem. B* 104, 1253-1260 (2000).
104. Ulman, A. *An Introduction to Ultrathin Organic Films*. Academic Press, San Diego, CA (1991).
105. Stevens, M. J. Thoughts on the structure of alkylsilane monolayers. *Langmuir* 15, 2773-2778 (1999).
106. Piehler, J., Brecht, A., Geckeler, K. E. & Gauglitz, G. Surface modification for direct immunoprobes. *Biosens. & Bioelectr.* 11, 579-590 (1996).
107. Piehler, J., Brecht, A., Hehl, K. & Gauglitz, G. Protein interactions in covalently attached dextran layers. *Coll. Surf. B* 13, 325-336 (1999).
108. Lee, J. H., Kopecek, J. & Andrade, J. D. Protein-resistant surfaces prepared by PEO-containing block copolymer surfactants. *J. Biomed. Mater. Res.* 23, 351-368 (1989).
109. Desai, N. P. & Hubbell, J. A. Biological responses to polyethylene oxide modified polyethylene terephthalate surfaces. *J. Biomed. Mater. Res.* 25, 829-843 (1991).
110. Mori, Y. et al. A new antithrombogenic material with long polyethyleneoxide chains. *T. Am. Soc. Art. Int. Org.* 28, 459-463 (1982).
111. Homberg, K., Bergström, K. & Stark, M.-B. Immobilization of proteins via PEG chains. In: Harris, J.M. (Ed.), *Poly(ethylene glycol) Chemistry: Biotechnical and Biomedical Applications*. Plenum Press, New York (1992).
112. Piehler, J., Brecht, A., Valiokas, R., Liedberg, B. & Gauglitz, G. A high-density poly(ethylene glycol) polymer brush for immobilization on glass-type surfaces. *Biosens. & Bioelectr.* 15, 473-481 (2000).
113. Lata, S. & Piehler, J. Stable and functional immobilization of histidine-tagged proteins via multivalent chelator headgroups on a molecular poly(ethylene glycol) brush. *Anal. Chem.* 77, 1096-1105 (2005).
114. Taniguchi, N. On the Basic Concept of "Nano-Technology". *Proc. Intl. Conf. Prod. Eng. Tokyo, Part II - Japan Society of Precision Engineering* (1974).
115. Moore, G. E. Cramming more components onto integrated circuits. *Electronics* 38, 114-117 (1965).

116. Whitesides, G. M. The "right" size in nanobiotechnology. *Nature Biotechnol.* 21, 1161-1165 (2003).
117. Edwards, S. A. *The Nanotech Pioneers - Where Are They Taking Us?* WILEY-VCH Verlag GmbH & Co. KGaA, Weinheim (2006).
118. *Einführung in die Lithographie.* Hanns Eggen KG Hannover (1968).
119. Febvre, L. & Martin, H.-J. *The Coming of the Book.* Verso, London (1997).
120. Abbott, N. L., Folkers, J. P. & Whitesides, G. M. Manipulation of the wettability of surfaces on the 0.1-to-1-micrometer scale through micromachining and molecular self-assembly. *Science* 257, 1380-1382 (1992).
121. Abbott, N. L., Kumar, A. & Whitesides, G. M. Using micromachining, molecular self-assembly and wet etching to fabricate 0.1 to 1 micrometer-scale structures of gold and silicon. *Chem. Mater.* 6, 596-602 (1994).
122. Bietsch, A. & Michel, B. Conformal contact and pattern stability of stamps used for soft lithography. *J. Appl. Phys.* 88, 4310-4318 (2000).
123. Kumar, A., Biebuyck, H. A. & Whitesides, G. M. Patterning self-assembled monolayers - applications in materials science. *Langmuir* 10, 1498-1511 (1994).
124. Bernard, A. et al. Printing patterns of proteins. *Langmuir* 14, 2225-2229 (1998).
125. Young, B. R., Pitt, W. G. & Cooper, S. L. Protein adsorption on polymeric biomaterials. *J. Coll. Interf. Sci.* 124, 28-43 (1988).
126. Andrade, J. D. & Hlady, V. Protein adsorption and materials biocompatibility - a tutorial review and suggested hypotheses. *Adv. Polym. Sci.* 79, 1-63 (1986).
127. Lu, H. B. et al. Protein contact printing for a surface plasmon resonance biosensor with on-chip referencing. *Sensors Actuat. B - Chem.* 74, 91-99 (2001).
128. Kung, L. A., Kam, L., Hovis, J. S. & Boxer, S. G. Patterning hybrid surfaces of proteins and supported lipid bilayers. *Langmuir* 16, 6773-6776 (2000).
129. Stamou, D., Duschl, C., Delamarche, E. & Vogel, H. Self-assembled microarrays of attoliter molecular vessels. *Angew. Chem. Int. Ed. Engl.* 42, 5580-5583 (2003).
130. Gates, B. D., Xu, Q. B., Love, J. C., Wolfe, D. B. & Whitesides, G. M. Unconventional nanofabrication. *Annu. Rev. Mat. Res.* 34, 339-372 (2004).
131. Götzhäuser, A. et al. Chemical nanolithography with electron beams. *Advanced Materials* 13, 806-809 (2001).
132. Eck, W. et al. Generation of surface amino groups on aromatic self-assembled monolayers by low energy electron beams - A first step towards chemical lithography. *Advanced Materials* 12, 805-808 (2000).
133. Geyer, W. et al. Electron-induced crosslinking of aromatic self-assembled monolayers: Negative resists for nanolithography. *Appl. Phys. Lett.* 75, 2401-2403 (1999).
134. Götzhäuser, A. et al. Nanoscale patterning of self-assembled monolayers with electrons. *J. Vac. Sci. Technol. B* 18, 3414-3418 (2000).
135. Küller, A., Eck, W., Stadler, V., Geyer, W. & Götzhäuser, A. Nanostructuring of silicon by electron beam lithography of self-assembled hydroxybiphenyl monolayers. *Appl. Phys. Lett.* 82, 3776-3778 (2003).
136. Eck, W., Küller, A., Grunze, M., Völkel, B. & Götzhäuser, A. Free-standing nanosheets from cross-linked biphenyl self-assembled monolayers. *Advanced Materials* 17, 2583-2587 (2005).

137. Biebricher, A., Paul, A., Tinnefeld, P., Götzhäuser, A. & Sauer, M. Controlled three-dimensional immobilization of biomolecules on chemically patterned surfaces. *J. Biotechnol.* 112, 97-107 (2004).
138. Schmelmer, U. et al. Surface-initiated polymerization on self-assembled monolayers: amplification of patterns on the micrometer and nanometer scale. *Angew. Chem. Int. Ed. Engl.* 42, 559-563 (2003).
139. Geyer, W. et al. Electron induced chemical nanolithography with self-assembled monolayers. *J. Vac. Sci. Technol. B* 19, 2732-2735 (2001).
140. Jaschke, M. & Butt, H.-J. Deposition of organic material by the tip of a scanning force microscope. *Langmuir* 11, 1061-1064 (1995).
141. Piner, R. D., Zhu, J., Xu, F., Hong, S. & Mirkin, C. A. "Dip-Pen" nanolithography. *Science* 283, 661-663 (1999).
142. Su, M. & Dravid, V. P. Colored ink dip-pen nanolithography. *Appl. Phys. Lett.* 80, 4434-4436 (2002).
143. McKendry, R. et al. Creating nanoscale patterns of dendrimers on silicon surfaces with dip-pen nanolithography. *Nano Lett.* 2, 713-716 (2002).
144. Schwartz, P. V. Molecular transport from an atomic force microscope tip: A comparative study of dip-pen nanolithography. *Langmuir* 18, 4041-4046 (2002).
145. Hong, S. H., Zhu, J. & Mirkin, C. A. Multiple ink nanolithography: Toward a multiple-pen nano-plotter. *Science* 286, 523-525 (1999).
146. Sheehan, P. E. & Whitman, L. J. Thiol diffusion and the role of humidity in "dip pen nanolithography". *Phys. Rev. Lett.* 88, 1561-1564 (2002).
147. Lee, K. B., Park, S. J., Mirkin, C. A., Smith, J. C. & Mirkin, M. Protein nanoarrays generated by dip-pen nanolithography. *Science* 295, 1702-1705 (2002).
148. Orme, C. Small Science gets to the heart of matter. *Science & Technology Review* (2001).
149. Wadu-Mesthrige, K., Xu, S., Amro, N. A. & Liu, G. Y. Fabrication and imaging of nanometer-sized protein patterns. *Langmuir* 15, 8580-8583 (1999).
150. Xu, S., Miller, S., Laibinis, P. E. & Liu, G. Y. Fabrication of nanometer scale patterns within self-assembled monolayers by nanografting. *Langmuir* 15, 7244-7251 (1999).
151. Wadu-Mesthrige, K., Amro, N. A., Garno, J. C., Xu, S. & Liu, G. Fabrication of nanometer-sized protein patterns using atomic force microscopy and selective immobilization. *Biophys. J.* 80, 1891-1899 (2001).
152. Nam, J. M. et al. Bioactive protein nanoarrays on nickel oxide surfaces formed by dip-pen nanolithography. *Angew. Chem. Int. Ed. Engl.* 43, 1246-1249 (2004).
153. Drexler, K. E. *Engines of Creation, The Coming Era of Nanotechnology.* Anchor Press, New York (1986).
154. Lim, J.-H. et al. Direct-write dip-pen nanolithography of proteins on modified silicon oxide surfaces. *Angew. Chem. Int. Ed. Engl.* 42, 2309-2312 (2003).
155. Niemeyer, C. & Mirkin, C. A. *Nanobiotechnology.* WILEY-VCH Verlag GmbH & Co. KGaA, Weinheim (2004).
156. Binnig, G., Quate, C. F. & Gerber, C. Atomic force microscope. *Phys. Rev. Lett.* 56, 930-933 (1986).
157. Hembacher, S., Giessibl, F. J. & Mannhart, J. Force microscopy with light-atom probes. *Science* 305, 380-383 (2004).

158. Zhong, Q., Inniss, D., Kjoller, K. & Elings, V. B. Fractured polymer silica fiber surface studied by tapping mode atomic force microscopy. *Surface Science* 290, L688-L692 (1993).
159. <http://web.media.mit.edu/~minsky/papers/ConfocalMemoir.html>. (2006).
160. Hutschenreiter, S. Charakterisierung des Prozessierungsmechanismus des 20S Proteasomskomplexes. Dissertation - Johann Wolfgang Goethe Universität (2004).
161. Valiokas, R. Interfacial Design and Characterization of Oligo(ethylene glycol) Self-Assembled Monolayers - Templates for Biomolecular Architectures. Dissertation - Linköpings University (2000).
162. Francis, S. A. & Ellison, A. H. Infrared spectra of monolayers on metal mirrors. *J. Opt. Soc. Am.* 49, 131-138 (1959).
163. Karas, M., Bachmann, D. & Hillenkamp, F. Influence of the wavelength in high-irradiance ultraviolet-laser desorption mass-spectrometry of organic-molecules. *Anal. Chem.* 57, 2935-2939 (1985).
164. Karas, M., Bachmann, D., Bahr, U. & Hillenkamp, F. Matrix-assisted ultraviolet-laser desorption of nonvolatile compounds. *Int. J. Mass Spectrom.* 78, 53-68 (1987).
165. Frisbie, C. D., Rozsnyai, L. F., Noy, A., Wrighton, M. S. & Lieber, C. M. Functional group imaging by chemical force microscopy. *Science* 265, 2071-2074 (1994).
166. Wong, S. S., Joselevich, E., Woolley, A. T., Cheung, C. L. & Lieber, C. M. Covalently functionalized nanotubes as nanometre-sized probes in chemistry and biology. *Nature* 394, 52-55 (1998).
167. Piehler, J. & Schreiber, G. Biophysical analysis of the interaction of human ifnar2 expressed in *E. coli* with IFN alpha 2. *J. Mol. Biol.* 289, 57-67 (1999).
168. Valiokas, R., Svedhem, S., Svensson, S. C. T. & Liedberg, B. Self-assembled monolayers of oligo(ethylene glycol)-terminated and amide group containing alkanethiolates on gold. *Langmuir* 15, 3390-3394 (1999).
169. Hegner, M., Wagner, P. & Semenza, G. Ultralarge atomically flat template-stripped Au surfaces for scanning probe microscopy. *Surface Science* 291, 39-46 (1993).
170. Butt, H.-J., Wang, D. N., Hansma, P. K. & Kühlbrandt, W. Effect of surface roughness of carbon support films on high-resolution electron diffraction of two-dimensional protein crystals. *Ultramicroscopy* 36, 307-318 (1991).
171. Butt, H.-J., Müller, T. & Gross, H. Immobilizing biomolecules for scanning force microscopy by embedding in carbon. *J. Struct. Biol.* 110, 127-132 (1993).
172. Zhou, Y., Valiokas, R. & Liedberg, B. Structural characterization of microcontact printed arrays of hexa(ethylene glycol)-terminated alkanethiols on gold. *Langmuir* 20, 6206-6215 (2004).
173. Delamarche, E. et al. Transport mechanisms of alkanethiols during microcontact printing on gold. *J. Phys. Chem. B* 102, 3324-3334 (1998).
174. Allara, D. L. & Nuzzo, R. G. Spontaneously organized molecular assemblies. Formation, dynamics, and physical properties of n-alkanoic acids adsorbed from solution on an oxidized aluminum surface. *Langmuir* 1, 45-52 (1985).
175. Bain, C. D. et al. Formation of monolayer films by the spontaneous assembly of organic thiols from solution onto gold. *J. Am. Chem. Soc.* 111, 321-335 (1989).
176. Porter, M. D., Bright, T. B., Allara, D. L. & Chidsey, C. E. D. Spontaneously organized molecular assemblies. Structural characterization of n-alkyl thiol

- monolayers on gold by optical ellipsometry, infrared spectroscopy, and electrochemistry. *J. Am. Chem. Soc.* 109, 3559-3568 (1987).
177. Shi, J., Hong, B., Parikh, A. N., Collins, R. W. & Allara, D. L. Optical characterization of electronic-transitions arising from the Au/S interface of self-assembled n-alkanethiolate monolayers. *Chem. Phys. Lett.* 246, 90-94 (1995).
178. Pale-Grosdemange, C., Simon, E. S., Prime, K. L. & Whitesides, G. M. Formation of self-assembled monolayers by chemisorption of derivatives of oligo(ethylene glycol) of structure HS(CH₂)₁₁(OCH₂CH₂)mOH on gold. *J. Am. Chem. Soc.* 113, 12-20 (1991).
179. Prime, K. L. & Whitesides, G. M. Self-assembled organic monolayers: model systems for studying adsorption of proteins at surfaces. *Science* 252, 1164-1167 (1991).
180. Mrksich, M. et al. Controlling cell attachment on contoured surfaces with self-assembled monolayers of alkanethiolates on gold. *Proc. Natl. Acad. Sci. USA* 93, 10775-10778 (1996).
181. Sigal, G. B., Bamdad, C., Barberis, A., Strominger, J. & Whitesides, G. M. A self-assembled monolayer for the binding and study of histidine tagged proteins by surface plasmon resonance. *Anal. Chem.* 68, 490-497 (1996).
182. Schmitt, L., Ludwig, M., Gaub, H. E. & Tampé, R. A metal-chelating microscopy tip as a new toolbox for single-molecule experiments by atomic force microscopy. *Biophys. J.* 78, 3275-3285 (2000).
183. Tinazli, A. et al. High-affinity chelator thiols for switchable and oriented immobilization of histidine-tagged proteins: a generic platform for protein chip technologies. *Chemistry* 11, 5249-5259 (2005).
184. Valiokas, R., Svedhem, S., Ostblom, M., Svensson, S. C. T. & Liedberg, B. Influence of specific intermolecular interactions on the self-assembly and phase behavior of oligo(ethylene glycol)-terminated alkanethiolates on gold. *J. Phys. Chem. B* 105, 5459-5469 (2001).
185. Harder, P., Grunze, M., Dahint, R., Whitesides, G. M. & Laibinis, P. E. Molecular conformation in oligo(ethylene glycol)-terminated self-assembled monolayers on gold and silver surfaces determines their ability to resist protein adsorption. *J. Phys. Chem. B* 102, 426-436 (1998).
186. Valiokas, R., Svedhem, S., Svensson, S. C. T. & Liedberg, B. Self-assembled monolayers of oligo(ethylene glycol)-terminated and amide group containing alkanethiolates on gold. *Langmuir* 15, 3390-3394 (1999).
187. Valiokas, R., Ostblom, M., Svedhem, S., Svensson, S. C. T. & Liedberg, B. Thermal stability of self-assembled monolayers: Influence of lateral hydrogen bonding. *J. Phys. Chem. B* 106, 10401-10409 (2002).
188. Malysheva, L., Klymenko, Y., Onipko, A., Valiokas, R. & Liedberg, B. Ab initio calculations of equilibrium geometries and vibrational excitations of helical ethylene-glycol oligomers: application to modeling of monolayer infrared spectra. *Chem. Phys. Lett.* 370, 451-459 (2003).
189. Nuzzo, R. G., Dubois, L. H. & Allara, D. L. Fundamental studies of microscopic wetting on organic surfaces. Formation and structural characterization of a self-consistent series of polyfunctional organic monolayers. *J. Am. Chem. Soc.* 112, 558-569 (1990).

190. Liley, M., Keller, T. A., Duschl, C. & Vogel, H. Direct observation of self-assembled monolayers, ion complexation, and protein conformation at the gold/water interface: An FTIR spectroscopic approach. *Langmuir* 13, 4190-4192 (1997).
191. Lee, J. K., Kim, Y. G., Chi, Y. S., Yun, W. S. & Choi, I. S. Grafting nitrilotriacetic groups onto carboxylic acid-terminated self-assembled monolayers on gold surfaces for immobilization of histidine-tagged proteins. *J. Phys. Chem. B* 108, 7665-7673 (2004).
192. Arnold, R., Azzam, W., Terfort, A. & Woll, C. Preparation, modification, and crystallinity of aliphatic and aromatic carboxylic acid terminated self-assembled monolayers. *Langmuir* 18, 3980-3992 (2002).
193. Piehler, J. & Schreiber, G. Fast transient cytokine-receptor interactions monitored in real time by reflectometric interference spectroscopy. *Anal. Biochem.* 289, 173-186 (2001).
194. Hart, S. R., Waterfield, M. D., Burlingame, A. L. & Cramer, R. Factors governing the solubilization of phosphopeptides retained on ferric NTA IMAC beads and their analysis by MALDI TOFMS. *J. Am. Soc. Mass. Spectrom.* 13, 1042-1051 (2002).
195. Ahn, Y. H. et al. Dynamic identification of phosphopeptides using immobilized metal ion affinity chromatography enrichment, subsequent partial beta-elimination/chemical tagging and matrix-assisted laser desorption/ionization mass spectrometric analysis. *Rapid Commun. Mass. Spectrom.* 18, 2495-2501 (2004).
196. Seemüller, E. et al. Proteasome from *Thermoplasma acidophilum* - a threonine protease. *Science* 268, 579-582 (1995).
197. Bochtler, M., Ditzel, L., Groll, M., Hartmann, C. & Huber, R. The proteasome. *Annu. Rev. Biophys. Biomol. Struct.* 28, 295-317 (1999).
198. Voges, D., Zwickl, P. & Baumeister, W. The 26S proteasome: A molecular machine designed for controlled proteolysis. *Annu. Rev. Biochem.* 68, 1015-1068 (1999).
199. Zwickl, P., Voges, D. & Baumeister, W. The proteasome: a macromolecular assembly designed for controlled proteolysis. *Philos. T. Roy. Soc. B* 354, 1501-1511 (1999).
200. Löwe, J. et al. Crystal structure of the 20S proteasome from the archaeon *T. acidophilum* at 3.4 Å resolution. *Science* 268, 533-539 (1995).
201. Allen, M. J. et al. Tip-radius-induced artifacts in AFM images of protamine-complexed DNA fibers. *Ultramicroscopy* 42-44 (Pt B), 1095-1100 (1992).
202. MacBeath, G. Protein microarrays and proteomics. *Nature Genetics* 32, 526-532 (2002).
203. Zhu, H. & Snyder, M. Protein chip technology. *Curr. Opin. Chem. Biol.* 7, 55-63 (2003).
204. Hutschenreiter, S., Tinazli, A., Model, K. & Tampé, R. Two-substrate association with the 20S proteasome at single-molecule level. *EMBO Journal* 23, 2488-2497 (2004).
205. Spurlino, J. C., Lu, G. Y. & Quiocho, F. A. The 2.3-Å resolution structure of the maltose- or maltodextrin-binding protein, a primary receptor of bacterial active transport and chemotaxis. *J. Biol. Chem.* 266, 5202-5219 (1991).
206. Lata, S., Reichel, A., Brock, R., Tampé, R. & Piehler, J. High-affinity adaptors for switchable recognition of histidine-tagged proteins. *J. Am. Chem. Soc.* 127, 10205-10215 (2005).
207. Sharma, S. et al. Silicon-on-insulator microfluidic device with monolithic sensor integration for /spl mu/TAS applications. *IEEE J. MEMS* 15, 308-313 (2006).

208. Reyes, D. R., Iossifidis, D., Auroux, P. A. & Manz, A. Micro total analysis systems. 1. Introduction, theory, and technology. *Anal. Chem.* 74, 2623-2636 (2002).
209. Auroux, P. A., Iossifidis, D., Reyes, D. R. & Manz, A. Micro total analysis systems. 2. Analytical standard operations and applications. *Anal. Chem.* 74, 2637-2652 (2002).
210. Buchholz, K. Microprocessing of silicon on insulator substrates and biofunctionalisation of silicon dioxide surfaces for sensing applications in fluids. Dissertation - Technical University Munich (2005).
211. Hughes, B. D., Pailthorpe, B. A., White, L. R. & Sawyer, W. H. Extraction of membrane microviscosity from translational and rotational diffusion coefficients. *Biophys. J.* 37, 673-676 (1982).
212. Sluch, M. I., Vitukhnovsky, A. G. & Petty, M. C. Anomalous distance dependence of fluorescence lifetime quenched by a semiconductor. *Phys. Lett. A* 200, 61-64 (1995).
213. Bras, M. et al. Optimisation of a silicon/silicon dioxide substrate for a fluorescence DNA microarray. *Biosens. & Bioelectron.* 20, 797-806 (2004).
214. Janshoff, A. & Steinem, C. Scanning force microscopy of artificial membranes. *ChemBioChem* 2, 798-808 (2001).
215. Song, L. et al. Structure of staphylococcal alpha-hemolysin, a heptameric transmembrane pore. *Science* 274, 1859-66 (1996).
216. Bayley, H. Designed membrane channels and pores. *Curr. Opin. Biotechnol.* 10, 94-103 (1999).
217. Beismann-Driemeyer, S. & Tampé, R. Function of the antigen transport complex TAP in cellular immunity. *Angew. Chem. Int. Ed. Engl.* 43, 4014-4031 (2004).
218. El-Ali, J., Sorger, P. K. & Jensen, K. F. Cells on chips. *Nature* 442, 403-411 (2006).

9 Curriculum Vitae

Persönliche Daten

Vor- und Zuname: Ali Tinazli
 Geburtsdatum: 20.02.1978
 Geburtsort: Bad Homburg v. d. H., Deutschland
 Nationalität: Türkisch
 Familienstand: Verheiratet, keine Kinder

Werdegang

Berufliche Position

10/2006 – heute „**Specialist Collaborations**“ bei Applied Biosystems,
 Applera Deutschland GmbH, Darmstadt/Überlingen (Deutschland)

Dissertation

08/2002 – 07/2007 Institut für Biochemie, Biozentrum, J. W. Goethe-Universität,
 Frankfurt am Main, Prof. Dr. Robert Tampé in Zusammenarbeit mit der
 Universität Linköping (Schweden) und dem Max-Planck-Institut für
 Biochemie in Martinsried (Deutschland), Note: „**summa cum laude**“

Studium

10/1997 – 03/2002 **Biochemie**, J. W. Goethe-Universität, Frankfurt am Main,
 Spezialisierung: Biophysik, Entwicklungsbiologie, Molekularbiologie
Vordiplom, J. W. Goethe-Universität, Frankfurt am Main,
 Note: „**sehr gut**“
Diplomarbeit „*Alternsabhängige Transkriptionsprofile kupfer-
 regulierter Gene des Ascomyceten Podospora anserina*“, Institut für
 Molekulare Biowissenschaften, Biozentrum, J. W. Goethe-Universität,
 Frankfurt am Main, Prof. Dr. Heinz D. Osiewacz
 Abschluss: **Diplom-Biochemiker**, J. W. Goethe-Universität,
 Frankfurt am Main, Note: „**sehr gut mit Auszeichnung**“
 Mit dem *Procter & Gamble-Förderpreis 2002* für die beste
 Diplomarbeit ausgezeichnet.

Schule

08/1988 – 07/1997 **Abitur**, Burggymnasium, Friedberg, Note „**sehr gut**“